Reduced Order Modeling and Scale-up of an Entrained Flow Gasifier

by

Mohammad Hossein Sahraei

A thesis

presented to the University of Waterloo

in fulfillment of the

thesis requirement for the degree of

Doctor of Philosophy

in

Chemical Engineering

Waterloo, Ontario, Canada, 2017

AUTHOR'S DECLARATION

I hereby declare that I am the sole author of this thesis.

This is a true copy of the thesis, including any required final revisions, as accepted by my examiners.

I understand that my thesis may be made electronically available to the public.

Abstract

Climate change has increased attention towards reduction of carbon dioxide (CO_2) emissions and other heat-trapping gases to the atmosphere. This has affected the operation of process industries, particularly solid fuel power plants which are responsible for almost a third of the total CO_2 emissions. Among the choices for power generation from solid fuels, gasification-based power plants have been accepted as one of the most efficient means of generating electricity from solid fuels, when a CO_2 capture unit is considered in the plant's layout. However, improvements in the cost and availability of gasifiers are still required to make this technology competitive with combustors. In recent years, a new class of compact gasifiers, also known as short-residence time gasifiers, has been proposed to reduce the cost of power generation. To speed up the development of this technology, insights regarding the operability, efficiency and feasibility of these gasifiers are required through a mathematical modelling analysis. This research aims to develop a computationally efficient dynamic reduced order model (ROM) that considers the essential features of a short-residence time gasifier.

The ROM was initially validated for steady-state simulation of the pilot-scale gasifier by using data obtained from computational fluid dynamic (CFD) simulations and experimental tests. Although the framework of the ROM was fixed and developed based on CFD simulation generated at a base-case condition, the results showed reasonable agreement between the two models under different operating conditions and kinetic parameters. In addition, the ROM predicted the experimental observations for conversion in the range of 48-90%. The proposed ROM has shown to be computationally attractive as it reduces the computation time by two orders of magnitude when compared to CFD simulations. The attractive computational costs of the ROM has allowed the evaluation of the gasifier's performance through sensitivity analysis, uncertainty quantification, parameter estimation, dynamic simulation and process scale-up. The results of a sensitivity analysis indicated that the recirculation ratio and oxygen flowrate have a greater effect on the process compared to model geometry and kinetic parameters. An uncertainty quantification was performed to investigate the variability in the ROM's key outputs in the presence of uncertainty in parameters that affect the feedstock's properties and the mixing/laminar flows within different zones of the reactor network. The study revealed significant variability in the conversion, peak temperature and steam percentage in the syngas; while the dry syngas composition does not seem to be significantly affected by the uncertainty of the considered parameters. Since the recirculation ratio is

the most influential parameter in the ROM, and its true value is typically uncertain, a new semi-empirical correlation was proposed to estimate this parameter. The proposed correlation improved the well-known method of Thring and Newby for jet-flow recirculation by adding a term that takes into account the changes in the feed streams on the recirculation. This feature enhances the prediction capabilities of the reactor network, especially in dynamic simulations where the inlet flowrates may change over time, e.g., for load-following power plants. The dynamic simulation of the gasifier was then performed by implementing this correlation. Accordingly, the operability of the pilot-scale gasifier based on the responses the dry syngas composition, temperature distribution, cold gas efficiency, slag thickness and flowrate were studied under sinusoidal changes in the feed, load-following and co-firing scenarios. Furthermore, the ROM was scaled-up to perform the steady-state simulation of a 3,000 TPD commercial-scale short-residence time gasifier which uses a multi-element injector feed system with 36 nozzles. The performance of the gasifier was then examined under changes in the operating pressure, number of injectors and fuel distribution among injection tubes. The results provided valuable insights regarding the suitability of design parameters and the operational conditions which may damage the gasifier's refractory and injectors.

Based on the simulations performed through this research, a systematically developed ROM that captures the streamlines of the multiphase flow, can predict the behaviour of a gasifier for a wide range of operating conditions with reasonable accuracy. Moreover, a ROM can provide valuable insights on the following objects: 1) the suitability of the design parameters and model assumptions; 2) identifying the critical operating conditions or demand scenarios that may impose a safety hazard or operational constraints; and 3) the flexibility of the system under the changes in fuel, load and failure of mechanical equipment.

Acknowledgements

First, I wish to thank my supervisor, Prof. Luis A. Ricardez-Sandoval for believing in my capabilities and providing continuous support and guidance during my graduate studies.

I wish to thank my PhD examination committee members Prof. Thomas Adams, Prof. Peter Douglas, Prof. William Anderson and Prof. John Wen, for their valuable comments. I'm also grateful for the feedback and technical support provided by CanmetENERGY. Special thanks go to Dr. Marc Duchesne and Dr. Robin Hughes who were integral to the process of my research.

I'm indebted to my parents for their love, care and encouragement. I would like to dedicate this thesis to mom and dad. I cannot thank enough to them for supporting me in all my endeavors. I also appreciate the help of my friends and colleagues in University of Waterloo: Elnaz Halakoo, Behrad Gharedaghloo, Sami Bahakim, Manoj Mathew and Navid Bizmark.

Lastly, I wish to acknowledge the financial assistance provided by Natural Resources Canada and University of Waterloo.

Table of Contents

List of Figures

List of Tables

Nomenclature

Symbols

A	Area (m^2)
A'	Pre-exponential factor
C	Concentration ($mole/m^3$)
c_p	Heat capacity (J/kg/K)
d	Diameter (m)
D	Diffusivity (m^2/s)
E	Activation energy
f	Friction factor
F'	Volumetric force (N/m^3)
g	Gravitational acceleration (m/s^2)
h	Convection coefficient ($W/m^2/K$)
H	Enthalpy (J/kg)
HS	Heat source
k	Thermal conductivity (W/m/K)
m	Mass (kg)
m'	Mass flux ($kg/m^2/s$)
M	Mass flow (kg/s)
N	Density of particle ($1/m^{-3}$)
Nu	Nusselt number
P	Pressure (Pa)
Pr	Prandtl number
Q'	Heat flux (W/m^2)
r	Radius (m)
R	Reactions
Re	Reynolds
S	Silica ratio
t	Time (s)
T	Temperature (K)
u	Velocity (m/s)
w	Weight fraction
x	Molar fraction
X	Conversion
z	Axial domain (m)

Greek symbols

α	Model parameter
β	Model parameter
ε	Volume fraction
δ	Slag thickness (m)
ρ	Density (kg/m^3)
μ	Viscosity (Pa·s)
σ	Stefan-Boltzmann constant
τ	Time constant (s)
γ	Recirculation ratio
λ	Thickness
ϑ	Conversion decay rate

Subscripts

conv	Convection
cs	Cross section
eff	Effective
g	gas
het	Heterogeneous reactions
hom	Homogeneous reactions
i	ith gas phase specie
p	particle
rad	Radiation
rxn	reaction

Abbreviations

ACM	Aspen Custom Modeler
CCS	Carbon capture and sequestration
CFD	Computational fluid dynamic
CGE	Cold gas efficiency
CSTR	Continuous stirred tank reactor
DSZ	Down-stream zone
ERZ	External recirculation zone
GE	General Electric
GTI	Gas Technology Institute
HHV	Higher heating value
IGCC	Integrated gasification combined cycle

IRZ	Internal recirculation zone
JEZ	Jet expansion zone
LHV	Lower heating value
MW	Mega watt
ODE	Ordinary differential equation
PDE	Partial differential equation
PDF	Probability density function
PFR	Plug flow reactor
ROM	Reduced Order model
RR	Recirculation ratio
TPD	Tonne per day

Chapter 1
Introduction

Market concerns regarding greenhouse gas emissions have slowed down the development of coal-fired power generation systems. It is predicted that clean natural gas will surpass coal as the fuel to fulfill the world's electricity demands by 2040; however, coal would still be used to produce one third of the world's power demands [1]. Recent efforts in electricity production have been directed towards reduced-carbon energy production from fossil fuels. Therefore, sustainable coal-fired power plants that reduce the environmental impacts such as carbon dioxide (CO_2) emissions are needed. The operation of the world's first commercial-scale CO_2 capture facility in SaskPower's Boundary Dam power plant, Canada, demonstrated a 20% reduction in the power plant's electricity generation [2]. As a result, more efficient power production technologies need to be developed to compensate for the expenses of CO_2 capture systems.

Currently, there are multiple advanced pulverized-coal technologies for power generation such as fluidized-bed combustion (coal is suspended in an air column as it burns), advanced combustion/heat engines (including pulverized coal combustors, slagging combustors and coal fired diesel engines) and integrated gasification combined cycle (IGCC) power plants [3]. Among the choices for generating electricity from coal, IGCC has been accepted as one of the most efficient power plant when a CO_2 capture technology is considered in the plant's layout [4]. Other key benefits of IGCC are reduced production of solid wastes, lower SO_x and NO_x emissions, less expensive gas-cleaning equipment and higher fuel flexibility. To become competitive, IGCC still requires improvement in terms of process economics, particularly in the capital expenses associated with the gasification unit [5].

The role of the gasification unit in IGCC power plants is to convert solid feedstocks (e.g. coal, petroleum coke, biomass and waste) into synthesis gas, also known as 'syngas', which is mainly composed of hydrogen (H_2) and carbon monoxide (CO). Development of efficient gasification units that can handle different feedstocks has gained recent attention as the fuel flexibility allows industry to adapt to changes in fuel costs and sustain a cost effective energy production scheme. Among different types of gasifier available in the market, entrained-flow gasifiers are the most common commercial-scale gasifiers for IGCC applications this is partly due to their high throughput and efficiency when compared to the other types of

gasifiers [6]. One of the long-term technologies that can potentially reduce the power production costs of IGCCs is an advanced type of entrained flow gasifier referred to as a short-residence time gasifier [7]. This type of entrained flow gasifier is more compact and applies rapid mixing of fuel and oxygen to obtain a high carbon conversion with residence times in the order of 0.2-0.5 seconds [8].

During the design of a gasification unit, many parameters such as the reactor's geometry, number of injectors, feed flowrates and operating conditions must be specified such that they accomplish an optimal performance for a given capital cost. Conducting experimental tests, and having access to sample measurements, are costly and in some cases prohibitive. Therefore, computational models need to be developed and used to assess the performance and economics of the gasification units at different operating conditions in steady-state and transient modes. To assess the performance of gasifier inside an IGCC and polygeneration systems, gasifier models that capture the main aspects of this process must be developed and integrated to the other unit operations. Due to the complexity associated with this process, gasifier models are usually implemented in CFD software. As a result, they are computationally expensive and cannot be integrated in an IGCC simulation. On the other hand, gasifier models developed by process simulators are simplified and do not account for the most important features of the process. In addition, some process simulators, such as Aspen®, are not capable of handling solid particles in dynamic mode [9]. As a result, reduced order models (ROMs) are required to overcome the limitations imposed by computationally intensive CFD and simplified (ideal) reactors in process simulators.

1.1 Objectives and contributions

The goal of this research is to perform a comprehensive modeling study on the state-of-the-art entrained-flow gasifier by means of using a ROM, and address the modeling analyses which are computationally and economically prohibitive to perform by CFD simulations and/or experimental tests. The specific objectives of the current study are as follows:

- Develop a ROM for a short-residence time gasifier based on the design of a 1 tonne per day (TPD) pilot-scale gasifier owned by CanmetENERGY, Natural Resources Canada. The results of the ROM is validated with the data gathered from CFD simulation and experimental test, provided by CanmetENERGY. The assumptions considered in the ROM affects the results beyond the nominal operating condition of gasifier at which the framework of the model was developed. Therefore, the

reliability and accuracy of the ROM over a range of operating conditions is discussed in detail.

- Perform sensitivity analysis and uncertainty quantification to evaluate the effect of feed and model's parameters on the gasifier's performance.
- Extend the prediction capabilities of the ROM to the transient domain; validate the model's response with respect to transient experimental data and study the dynamic performance of the gasifier under different scenarios.
- Develop a ROM for a commercial-scale short-residence time gasifier (3,000 TPD) based on the design proposed by Gas Technology Institute (GTI) using a multi-element injector feed system. Assess the performance of the gasifier under different scenarios.

Due to compact structure of a ROM, the prediction capabilities of this modeling approach for a wide range of operating condition in not known. The validity of available reduced order modeling studies on entrained-flow gasifiers are limited to single operating condition and are based on modeling assumptions which are not known with certainty. The present research considers a ROM based on a comprehensive set of data (design parameters, experimental tests, CFD simulation and specific kinetic parameters) which were specifically derived for petroleum-coke gasification in CanmetENERGY's pilot-scale gasifier. Therefore, this research provides key contributions regarding the confidence and validity of a systematically developed ROM for the gasification process in a wide range of operating conditions. Moreover, it explores the performance of a state-of-the-art gasifier under various scenarios such as uncertainty in the feed, transient changes in operating condition and process scale-up of the system.

1.2 Outline of the thesis

The remainder of this thesis is organized as follows:

- Chapter 2 reviews the literature related to state-of-the-art technologies in IGCC power plants with emphasis on entrained-flow gasifiers and the corresponding modeling approaches that have been proposed to simulate these systems. The challenges and limitations associated with the modeling of entrained flow gasifiers and the proposed approaches to tackle these obstacles are described at the end of this chapter.
- Chapter 3 explains the steps required to develop a ROM for an entrained-flow gasifier. The method

used to design the ROM's reactor network using the available CFD simulation is explained in detail. Moreover, the mathematical model and sub-models describing the physical and chemical processes within the gasifier are presented in this chapter.

- Chapter 4 presents the results of steady-state simulation for CanmetENERGY's gasifier. The results of the ROM is initially compared with the results of CFD simulation for the base case used to develop the reactor network. This work has been published in *Fuel* [10]. Moreover the accuracy of the ROM compared with CFD simulation for changes in oxygen flowrate and kinetic parameters is examined in this chapter. This work has been published in *Energy and Fuels* [11]. The validation of the ROM is discussed with respect to data gathered from experimental tests of petroleum coke gasification. This work has been published in *Industrial & Engineering Chemistry Research* [12].
- Chapter 5 presents the parametric analyses performed on the gasifier's inlets by using the ROM. The most important parameters on the ROM's accuracy and gasifier's operating conditions are initially determined through a sensitivity analysis. The effect of uncertain parameter as well as the feed characteristics on the performance of the gasifier is investigated through an uncertainty quantification analysis. In addition, a correlation to estimate the recirculation ratio as a function of inlet flowrate (which increases the accuracy of the ROM) is presented in this chapter. These works have been published in *Energy and Fuels* [11] and *Industrial & Engineering Chemistry Research* [12].
- Chapter 6 presents the results of dynamic simulation for CanmetENERGY's gasifier. The implementation methodology used to solve the rector network in dynamic mode is explained in this chapter. Moreover, the dynamic responses of temperature, syngas composition and flowrate, slag thickness and flow, cold gas efficiency and conversion are discussed through simulation of load-following and co-firing scenarios. This work has been submitted for publication [13].
- Chapter 7 presents the results of steady-state simulation for a commercial-scale gasifier with a multi-element injector based on the design proposed by GTI. The modeling assumptions, process constraints and heuristics used to develop the reactor network of the ROM is presented in this chapter. The performance of the gasifier is then examined through changes in the operating pressure, number of injector and non-uniform distribution of fuel among the nozzles. Furthermore, a sensitivity analysis is presented which discusses suitability of the reactor network and

assumptions made in the ROM. This work has been submitted for publication [14].

- Chapter 8 provides the conclusions and recommendations derived from this research.

Chapter 2
Background and Literature Review

Integrated Gasification Combined Cycle (IGCC) power plants are considered one of the most attractive means of producing power from solid fuels with low or near zero emissions. A wide range of research, development, and demonstration activities are currently being conducted to improve the power generation efficiency, availability and economics of IGCC systems [7]. The aim of this chapter is to discuss in depth the current developments for state-of-the-art technologies related to IGCC's unit operations with particular emphasis on entrained-flow gasifiers. The next section describes a typical IGCC power plant and reviews the development and challenges of these systems. Section 2.2 presents the details of the gasification process and reviews the available and future gasification technologies which could improve availability and efficiency of IGCCs. The different methodologies of modeling gasifiers and their benefits/limitations are discussed in Section 2.3.

2.1 IGCC Development and challenges

A basic process flowsheet of a typical IGCC plant with CO_2 capture is shown in Figure 2-1. In IGCC power plants, fuel, oxygen and steam are fed to the gasifier to produce raw syngas. Upon leaving the gasifier, syngas must be cooled in radiant/convective coolers or quench vessels prior to pollutant removal. Particulates and sulfur are separated and clean syngas is fed to the gas turbine with the products being sent to a heat recovery steam generator coupled with a steam turbine. In IGCC plants with CO_2 capture, the syngas is initially passed through a water-gas shift reactor (water reacts with CO to produce H_2 and CO_2) before the gas cleaning unit removes the carbon in the form of CO_2.

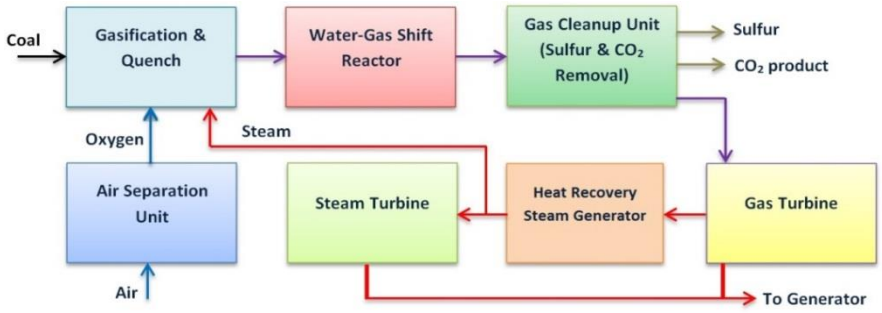

Figure 2-1. Process flowsheet of IGCC power plant with CO2 capture

Advanced IGCC pilot-scale and demonstration plants have shown potential for this technology to be implemented at the commercial-scale. However; it still requires improvement in terms of process economics to become fully competitive [5]. The plant's capital cost has been a concern for the global acceptance of IGCCs. The capital cost of a 600 MW IGCC plant without CO_2 capture is estimated to be 30% higher than conventional coal-based power plants even though IGCC plants can be 5% more efficient than conventional coal-based power plants [15]. Moreover, process reliability and availability have challenged the development and commercialization of IGCC power plants in terms of technology and equipment selection for different feedstocks [16]. Despite these challenges, in the past two decades, the viability of IGCC technology in power production has been demonstrated in developed countries. Table 2-1 presents most of the major existing commercial IGCC power plants with the potential to produce at least 150 MW. As shown in this Table, the new IGCC plants in Japan and the US have twice the power production size of the first IGCC plants installed in the Netherlands in the mid 1990's. This increase in power production has been achieved through the implementation of new technologies especially in syngas production and gas turbine systems.

Table 2-1. Major existing and planned IGCC commercial plants

Plant (location) Initial Year of Operation	Size (MW)	Feedstock	Plant efficiency without CCS
Buggenum (Netherlands) 1994	253	Bituminous coal and biomass	43%
Wabash river (USA) 1995	262	Bituminous coal and petroleum coke	40%
Tampa (USA) 1996	250	Coal and petroleum coke	38.2%
Pernis (Netherlands) 1997	155	Heavy oil residue	36.7%
Priolo Gargallo (Italy) 1998	532	Heavy fuel oil, tar	38%
Puertollano (Spain) 1998	335	Petroleum coke	40%
Sarlux (Italy) 2000	548	Residual oil, tar, bitumen	-
Negishi (Japan) 2003	342	Heavy oil, asphalt	36%
Vresova (Czech Republic) 2005	400	Brown coal	42.2%
Knox County (USA) 2013	618	Mid-western coal	-
Kemper County (USA) 2014	582	Lignite coal	-
Nakoso (Japan) 2014	500-600	Bituminous coal	42%

The lower heating value (LHV) efficiency of the commercial IGCC plants ranges between 36-42.2%. This difference is mostly due to factors such as the type of feedstock being used, which usually relies on the location of the plant and its conceptual design, e.g., whether process integration was considered or not at the process design stage.

IGCC is becoming a mature and more accepted process as the lessons learned from the early design of these plants have helped to improve the reliability, availability and efficiency of the future IGCC plants. A number of new IGCC projects are currently at different stages of development and may be in commercial operation by 2020 [7]. The next group of IGCC plants with carbon capture and sequestration (CCS) are expected to have larger sizes than the existing IGCC plants, co-firing of low cost fuels and state-of-the-art technologies for each process unit. In the next section, a review on the most current state-of-the-art technologies developed for gasification unit of IGCC power plants are presented. Since the focus of present research is on gasification, the recent developments on the rest of IGCC unit operations are not presented for brevity. Descriptions of advanced process technologies such as different types of air separation unit, application of membranes for CO_2 capture and new classes of gas turbines can be found in a review paper on IGCC state-of-the-art technologies published by Sahraei et al. [7].

2.2 Gasification technologies

Gasification involves the transformation of carbonaceous fuels (through thermal treatment) into a viable gaseous form typically referred to as *syngas*. The most important reactions taking place in this process are depicted in Figure 2-2. During gasification, the fuel is often mixed with steam and oxygen. Upon this mixing, the solid fuel is dried and decomposed to volatiles, ash and char. This process is referred to as *coal pyrolysis*. The amount of pyrolysis products are determined based on the properties of the fuel and the operating conditions of the system. Among the volatile products, combustible gases such as hydrogen, methane, ethane and carbon monoxide are produced. These species react with oxygen to produce heat. The heat emanated from these reactions provides the energy required by the heterogeneous char gasification reactions to produce the syngas. During the gasification reactions, the sulfur content within the fuel appears in the gas phase as hydrogen sulfide (H_2S) [17].

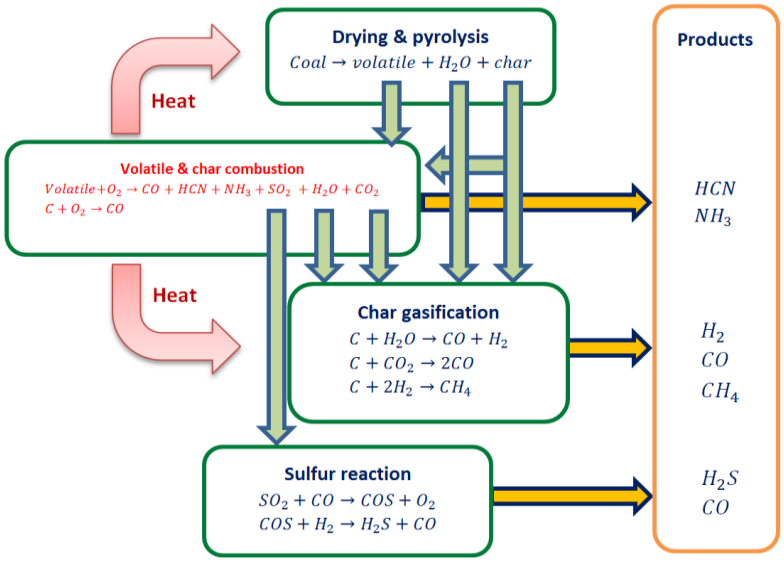

Figure 2-2. Reaction systems of gasification process

There are four types of gasifiers for solid fuels based on energy requirements, syngas heating value, purity and composition, operating conditions and feed availability. Details of these gasification systems and their technical aspects are shown in Table 2-2. Entrained-flow gasifiers are the most common commercial gasifier due its high throughput when compared to the other gasification technologies currently available in the market. The major challenges with entrained flow gasifiers are the associated capital cost and process availability. Most of the commercial-scale IGCC power plants use entrained-flow gasifiers developed by General Electric (GE) and Shell [7]. In their designs, the fuel is injected from a single nozzle as a slurry feed (GE) or dry feed (Shell). The residence time of particles in these gasifiers are up to approximately 3 (GE) and 4 seconds (Shell) [7], which results in higher size and capital cost of the system. In recent years, the Gas Technology Institute (GTI), previously as Aerojet Rocketdyne or Pratt and Whitney Rocketdyne, has been developing a compact gasifier with a multi-element feed injector which is capable of converting various solid fuels to syngas with a particle residence time of less than 0.5 seconds [18].

Table 2-2. Gasifier types for solid fuels, operating conditions and commercial examples

Gasifier	Advantages	Disadvantages	Commercial examples	
Fixed-bed	Less oxidant, low gas residence time simple construction, low pressure drop, high carbon conversion	High solid residence time, high methane content, poor temperature distribution control, caking coal issues	Lurgi slagging gasifier	
			Combustion zone T (°C)	1260-1370
			Residence time	10-15 min
			Lurgi dry ash gasifier	
			Gasification zone T (°C)	620-815
			Combustion zone T (°C)	980-1370 [19]
			Residence time	1 hour
			Wellman-Galusha gasifier	
			Combustion zone T (°C)	1315 [19]
			Residence time	4 hours
Fluidized-bed	Moderate reaction rate, moderate residence time for solid and gas, good mixing, good temperature distribution control, moderate oxygen/steam demand	No vitreous ash produced, moderate energy demand, higher pressure drop	Battelle ash agglomerating gasifier	
			Gasification zone T (°C)	870-980
			Combustion zone T (°C)	1100-1150 [19]
			Residence time	-
			Synthane gasifier	
			Gasification zone T (°C)	815-980 [19]
			Residence time	-
			Winkler gasifier	
			Gasification zone T (°C)	980-1150 [19]
			Residence time	20-30 min
			U-Gas	
			Gasification zone T (°C)	840-1100 [20]
			Residence time	-
Entrained-flow	Less technical complexity, suitable for all coal types, very short residence time (seconds or less)	Large oxidant requirement, high temperature, slagging operation	Koppers -Totzek gasifier	
			T (°C)	Max 1900 [21]
			Residence time	Less than 1 sec
			GE gasifier	
			Gasification zone T (°C)	1200-1480 [22]
			Residence time	3 sec [23]
			Shell coal gasifier	
			Flame T (°C)	1800–2000 [24]
			Residence time	0.5–4 sec
			GTI Rocketdyne	
			Outlet T (°C)	1297 – 1926 [25]
			Flat-flame T (°C)	3200 [26]
			Residence time	0.2-0.5 sec [25]
			Chicago Bridge and Iron E-STR	
			First stage T (°C)	1316-1427 [27]
			Second stage T (°C)	1010 [27]
			Residence time	-
			Siemens Gasifier	
			Gasification zone T (°C)	1300-1800 [28]
			Residence time	-
Molten-bath	Capable of both caking/non caking coals	High oxidation rate, carryover of alkalis, complicated regeneration system	Rockwell gasifier	
			Effluent gas T (°C)	980 [29]
			Melt bed T (°C)	980
			Residence time	-

An initial assessment of the potential effect of GTI Rocketdyne gasifier in IGCC applications compared to conventional single-stage entrained flow gasifiers is presented in Table 2-3. As shown in this table, the capital cost of IGCC power plants reduces by 14.5% when short-residence time gasifiers are used

[18]. In addition to the gasifier, the resulting decrease in capital cost is also realized for air separation unit as lower oxygen is required. Based on lifetime assessments for the GTI's gasifier, a considerable improvement in availability is predicted compared to typical availability in recent IGCC power plants. Overall, these benefits are expected to reduce the cost of electricity by 18.5% [18]. So far, GTI has completed risk reduction evaluations, feed system tests, 18 tonne per day (TPD) pilot plant testing and development of solids pump. They are now considered ready for demonstration at a 400 TPD scale system which can support advancement towards commercial-scale at 1000-3000 TPD [30]. The focus of this research is to assess the performance of short-residence time gasifiers in 1 TPD pilot and 3,000 TPD commercial-scales.

Table 2-3. Comparison of Rocketdyne gasifier in IGCC power plants with existing gasifier

	Rocketdyne	GE/Shell	Improvement
IGCC availability (%)	94%	85%	9 points
IGCC capital cost ($/kWe)	1297	1517	14.5%
Cost of electricity ($/MWh)	40.2	49.3	18.5%

To promote the implementation of a gasifier, insights regarding the design, geometry, number of injectors, feed flowrates, slag formation and operating conditions needed to ensure an efficient performance in different conditions. Since conducting experimental tests are costly, computational models are required to assess the performance and economics of the gasification units at different operating conditions. In the next section, a review of modeling methodologies used to simulate an entrained flow gasifier is presented.

2.3 Modeling of gasification process

In complex processes such as IGCC power plants, the responses of the gasifier and other equipment can cause undesired operational fluctuations to different load demands. The outcomes from a transient behaviour study is therefore essential to provide insights regarding the dynamic behaviour of the gasifier and potential control strategies that can be implemented to maintain its performance on target in the presence of external perturbations and uncertainty in the system's parameters. Dynamic studies can detect issues in the transient behaviour of start-up processes, set-point tracking and external disturbances (i.e. feed composition and load change) which are critical to maintain the plant's efficiency. These aspects, which are essential for the efficient operation of an IGCC plant and the development of effective control strategies,

cannot be detected while using steady state models. While multiple studies on air separation and CO_2 capture units have been performed to evaluate the dynamic behaviour of these systems in IGCC power plants studies providing insight on the dynamic performance of an IGCC's gasification unit are limited [7].

Three approaches can be employed to simulate the behaviour of the gasification process: CFD simulations, models developed by process simulators and ROMs. Due to the complexity associated with the gasification flows and mixing, gasifier models are often developed using CFD. In a CFD model, detailed multi-phase sub-models are often used to simulate the flow patterns and complex processes taking place inside the gasifier. Validated CFD models can provide insights on the locations of injectors, design of the gasification unit, optimization of experimental test matrices and investigation of commercial-scale gasifiers [31]. CFD models have been widely used to investigate biomass gasification [32], effects of coal particle density and size fraction in the process [33], feasibility of industrial-scale gasification systems [34], slag layer behaviour [35] and optimization [36]. CFD simulations are the most accurate models for gasifiers, however, they are usually computationally intensive. Therefore, their implementation to perform parametric analysis, co-simulation (models coupled with process simulation) and dynamic simulation may be limited or even prohibitive.

Previous works that have studied the dynamics of gasification units have employed models that are relatively simple and that only account for limited aspects of the gasification process. Aggarwal et al. [37] proposed an equilibrium-based gasifier model using Gibbs free energy minimization. In that study, only a limited number of reactions were considered which may lead to significant deviations with respect to the actual operation of the unit. Tan et al. [38] presented a gasifier model where only a few outputs such as gas calorific value, mass, gas pressure and gas temperature were reported. Robinson and Luyben [39] presented an alternative approach to simulate solid particles in Aspen® that lead to the development of a gasifier model in Aspen Dynamics®. That study assumed a high molecular weight hydrocarbon (available in the Aspen® library) as a pseudo fuel to represent coal. Although this model captures the macro-scale thermal, pressure, flow, and composition dynamics of the gasifier's outlet, it does not account for solid particles and other key features of the system, e.g., temperature and composition distribution inside the gasifier.

Recent studies have shown that the development of one-dimensional ROMs describing the essential features of the gasification process is a suitable and computationally attractive approach to study the transient performance of these systems [17], [40], [41], [42]. ROMs require lower computational effort

compared to CFD models, accounts for the most important features of gasification process and enabling the integration of gasifier models to process simulators. Some of the ROMs have used a single reactor to model the full gasification system [41], [42]. Although computationally attractive, these models may not provide accurate predictions since they may not precisely capture the multi-phase flow structure of the system.

In more comprehensive ROMs, the gasifier's behaviour is approximated by a reactor network based on the flow characteristics (mixing or laminar flows) and one-dimensional governing equations are solved for each zone to provide a distribution of different properties, i.e., mass, energy and momentum. Based on this modeling approach Monaghan et al. presented a comprehensive ROM for a range of entrained-flow gasifiers using Aspen Custom Modeler (ACM) [17]. They showed satisfactory ROM accuracy with the available data for the different gasifier designs [43]. Dynamic simulations of the ROM during start-up, fluxant removal, load following, feed change and feed co-firing were conducted by the same authors to evaluate the transient behaviour of the system [44]. Gazzani et al. presented a ROM to study the different operating conditions of a Shell–Prenflo gasifier [45]. Yang el al. used the ROM to investigate the performance of a membrane walled entrained-flow gasifier with two-stage oxygen supply [46]. The same authors developed a dynamic ROM to compare the transient response of a refractory wall gasifier against membrane wall gasifier [47]. The authors also presented a dynamic ROM for a two-stage entrained-flow gasifier to study its performance in controlling slag thickness with changes in feedstock [48]. Kong et al. performed a steady-state simulation for an industrial-scale Texaco gasifier by implementing a reactor network; and studied the effects of oxygen/coal ratio and coal slurry concentration on the gasifier's yield [49]. Li et al. presented a ROM for a commercial-scale opposed multi-burner gasifier and discussed the effect of particle size on the temperature and carbon conversion [50].

The outcomes of these studies confirm the acceptable level of details that can be incorporated in ROMs to simulate the important characteristics of an entrained-flow gasifier. Moreover, the model validation indicated reasonable accuracy in the ROMs' results with respect to experiments and higher order models. Lastly, the low computational time reported for the ROMs, makes this modeling approach suitable to be used to assess the performance of short-residence time gasifiers.

2.4 Chapter summary

In this chapter, a review of the available gasifiers and modeling approaches to simulate these systems was provided. Short residence time gasifier was introduced as one the state-of-the-art technologies that could improve the cost and efficiency of IGCC power plants. The needs for dynamic modeling of entrained-flow gasifiers and limitations in using CFD simulations were explained. Accordingly, development of computationally efficient model which accounts for physical and chemical processes within the gasifier is essential to assess the behaviour of a gasifier. The ROM of gasification process have been introduced as the main alternative for developing such models. These models have low computational time, can be used to perform analyses which are computationally expensive for CFD simulations, and can be integrated to other unit operations within IGCCs power plants. The next chapter presents the development of a reactor network for CanmetENERGY's gasifier, conservation equations of the multi-phase flow and the sub-model employed in the ROM.

Chapter 3
Reduced order modeling of gasifiers

This chapter presents the specification of CanmetENERGY's entrained-flow gasifier and the steps considered in the development of a ROM for this system. The next section describes CanmetENERGY's gasifier and the fuel used in this research. Section 3.2 presents the reactor network developed for the gasifier based on the streamlines of multi-phase flow. The conservation equations describing the momentum, heat and mass transfer inside the system are presented in Section 3.3. The sub-models implemented in the ROM for simulation of devolatilization, reactions, flow forces, heat transfer and slag model are presented in Sections 3.4 to 3.7

3.1 Gasification system and fuel

CanmetENERGY has a gasification facility that is used to develop state-of-the-art gasification technologies and related instrumentation. The gasifier is a pressurized, downward-fired entrained-flow gasifier that has been used to perform various experimental tests for different companies such as Pratt & Whitney Rocketdyne [51]. As shown in Figure 3-1, the gasifier's current configuration is for single-stage dry-fed gasification. It has diameter and length are 0.21 m and 2.2 m, respectively. The pilot gasifier is refractory-lined with a thickness of refractory and insulation materials, including mullite, Ziralcast ceramics and Kaowool board/paper, of 0.2 m. In this gasifier, oxygen is injected through the burner by eight jets that impinged on the fuel stream at high velocity. Steam, preheated up to 500 K, is passed through the outer burner annulus with a low velocity. A quench vessel beneath the gasifier is designed to allow for discharge of slag on a batch basis after test completion.

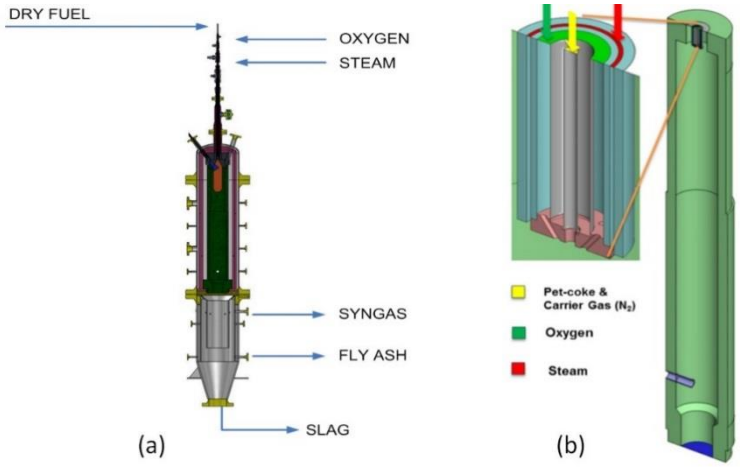

Figure 3-1. CanmetENERGY's entrained-flow gasifier: (a) Reaction zone and quench system; (b) inflow structure of the gasifier and feeds

This gasification unit has been the center of several studies in various areas of gasification such as behaviour of inorganic fuel components in the gasification process [52] - [53], waste classification of slag [54], CFD modeling of the gasifier [31] and dense-phase pneumatic conveying of pulverized fuel [55]. The system is capable of converting 1 tonne per day (TPD) of various solid fuels such as petroleum coke to syngas. Petroleum coke is a carbonaceous by-product of crude-oil refineries for heavy oil upgrading with thermal cracking processes. It is often more economical than coal and typically used as a source of energy in steam and power plants. On the other hand, it produces more carbon emissions than coal, i.e., on a per-unit of energy basis, petroleum coke emits 5-10% more CO_2 than coal [56]. In Canada, petroleum coke is primarily produced by oil sands upgraders. The proven oil sands reserves of Canada will yield roughly 5 billion tons of petroleum coke which is adequate to provide fuel for 111 U.S. coal power plants until 2050 [56]. Most of the existing modeling studies have focused on the gasification of coals and biomasses; less work has been reported on petroleum coke gasification [57]. It is predicted that almost 15% of planned gasification plants will be using petroleum coke as the feed [57]. Thus, the present study considers the gasification of petroleum coke in short-residence time entrained-flow gasifiers.

3.2 Reactor network

One of the challenges of modeling complex systems such as entrained-flow gasifier is the computational time of the model to reach convergence. To overcome the computational time, the order of differential equations can be reduced to certain domains and instead of solving the equations for a heavy mesh in the entire grid, some parts of the grid with low gradient of properties can be simplified to a single node. In the case of an entrained-flow gasifier, governing equations can be reduced to one-dimensional differential equation, describing the jet/plug-flow condition created by feed nozzle. However, part of the flow usually recirculates towards the feed nozzles and a recirculation zone may be formed. Due to mixing behaviour of the recirculation zones, uniform distribution of composition and temperature are often observed, therefore the meshes of these zones can be accounted as one node. Models developed based on these two techniques are referred to as reduced order models.

A ROM for entrained-flow gasifier requires a reactor network composed of plug flow reactors (PFRs) and continuous stirred tank reactors (CSTRs) to model the zones formed inside the gasifier. The zones with laminar jet/plug-flow and mixing condition are modeled as PFRs and CSTRs, respectively. The usage of reactor network to model complex reactors was initially proposed by Pedersen et al. [8]. In Pederson el al.'s approach, CFD simulation of a coal combustor is used to determine the flow fields, reactor network configuration, geometry, particle residence times and boundary conditions as well as model validation. As shown in Figure 3-2, Pederson et al. divided the combustor to four specific zones: internal recirculation zone (IRZ), jet expansion zone (JEZ), external recirculation zone (ERZ) and down-stream zone (DSZ).

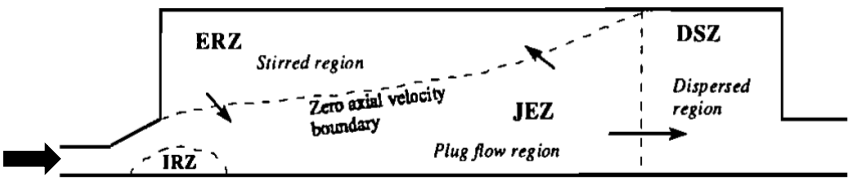

Figure 3-2. Characteristic regions of combustor *[6]*

The inlet streams fully mix with each other and with hot recirculate gas and particles in the front-end of the gasifier. All inlet streams are assumed to fully pass through this region called IRZ which is represented by a CSTR. JEZ refers to the areas where the sudden expansion at the inlet of the

gasifier causes the flow to spread out. JEZ is represented by a truncated conical PFR. As the flow approaches the walls of the gasifier, expanding jet splits into two streams. A portion of the flow detrains back towards the front-end of the gasifier (IRZ) through a recirculation region called ERZ, which is represented by a CSTR. The reminder of the flow leaving the JEZ proceeds to the reactor exit via DSZ which is modeled through a CSTR.

For the modeling of CanmetENERGY's gasifier, the approach proposed by Pedersen et al. to model a single-stage coal combustor has been adopted [8]. The reactor network configuration may vary depending on the type of gasifier, the number of firing stages, the position of the inlet streams and number of feed injectors. Thus, to develop a suitable reactor network, the flow fields and detailed design of the gasifier are required. In the present work, CFD simulations of CanmetENERGY's gasifier have been used to design a reactor network and determine related parameters such as reactor dimensions, inter-zone flows and the recirculation ratio. The modeling details of CFD simulation are presented in Appendix A. The streamlines of the CFD simulation for CanmetENERGY's gasifier are presented in Figure 3-3. As shown in that figure, fuel, oxygen and steam enter at the top of the gasifier. The oxygen nozzles are directed towards the fuel's inlet point to form a jet flow region while steam enters within a short distance of the created jet flow field. The two phases are suddenly expanded at the inlet of the gasifier which causes the flow to spread out. This region is referred as JEZ. As the flow reaches the walls of the gasifier, the flow splits into two streams. A portion of the stream recycles back to the top of the gasifier through the ERZ while the rest of the stream proceeds towards the end of the reaction via a one-dimensional flow jet region referred to as DSZ

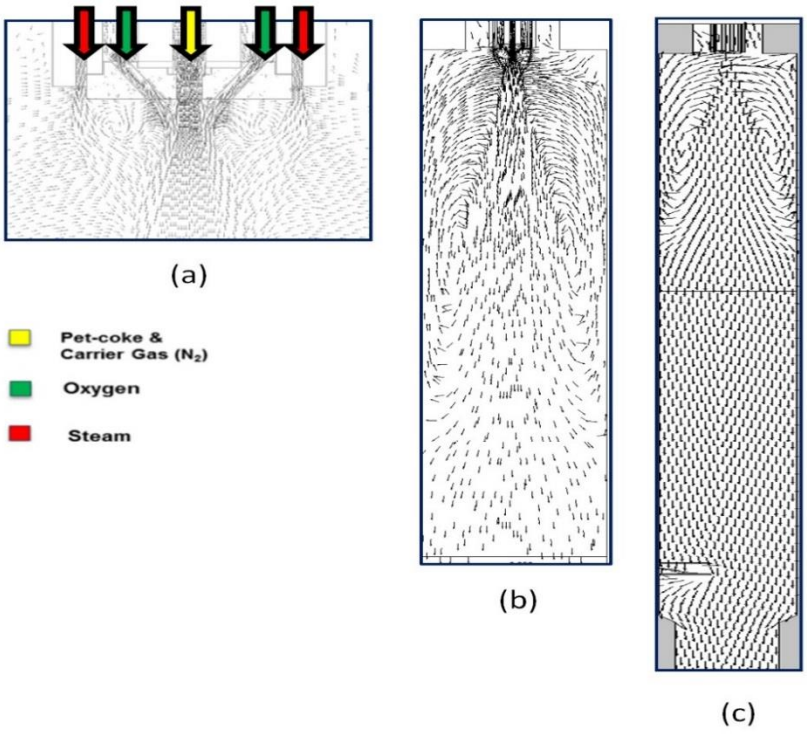

Figure 3-3. Characteristic regions of CanmetENERGY's gasifier: (a) near burner; (b) upper region; (c) full reactor level

As indicated in Figure 3-3, the positions of the steam's nozzles cause the steam to be fully mixed with the hot recirculated gases at the top of the gasifier prior to entering the JEZ. To account for the effect of this mixing zone, the jet expansion and external recirculation zones are divided into two sections, i.e., JEZ1and JEZ2, and ERZ1 and ERZ2. ERZ1 refers to the zone resulting from the mixing of steam and recirculated gases at the top-end of the gasifier, which merge with the flow jet through JEZ1. The corresponding configuration of the reactor network proposed in this work is presented in Figure 3-4. Due to extensive mixing in ERZ1 and ERZ2, these zones are modeled using CSTRs. JEZ1, JEZ2 and DSZ are modeled using PFRs. These regions are highly dependent on each other through the exchange of materials, momentum and energy.

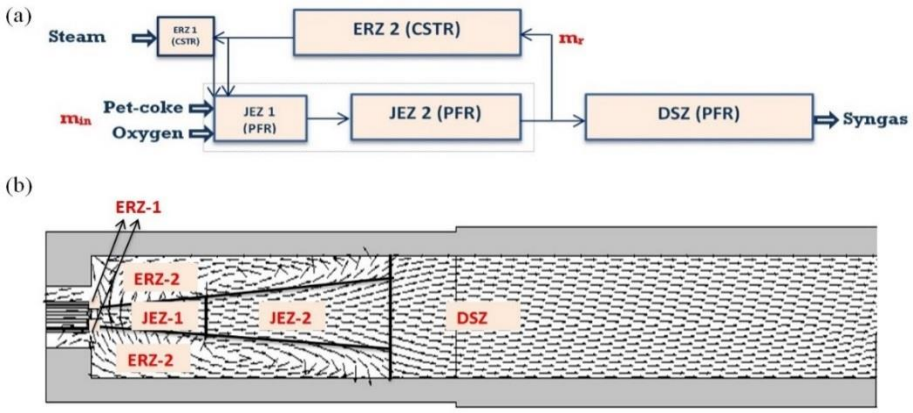

Figure 3-4. (a) the proposed reactor network of the gasifier; (b) corresponding regions of the reactor network inside the gasifier

The geometric parameters for the reactor network are presented in Table 3-1. These parameters were calculated based on the gasifier's dimensions, CFD simulations and the procedure presented by Pedersen et al. [8]. A recirculation ratio (α), which represents the molar flow ratio of the portion of the stream which flows from the outlet of JEZ2 to ERZ2 over the total inlet feed flow to JEZ1 ($\gamma = m_r/m_{in}$), of one was determined from CFD simulation and remains constant during the analysis. Mass flow rates obtained from CFD simulations were used to calculate this parameter, which is consistent with the calculated value using the widely known method of Thring and Newby [58].

Table 3-1. Geometry parameters of reactor network for pilot-scale gasifier

Zone	Length (m)	d_{inlet} (m)	d_{outlet} (m)	Volume (m^3)
JEZ1	0.20	0.02	0.05	1.20E-04
JEZ2	0.41	0.05	0.20	6.00E-03
ERZ1	0.02	0.02	0.02	8.42E-06
ERZ2	0.61	0.12	0.12	7.30E-03
DSZ	1.19	0.20	0.20	3.74E-02
Recirculation ratio (Molar)	1.0			
Jet angle	17 degrees			

The decision to separate the JEZ1 and JEZ2 was based on the respective reactions occurring inside each zone rather than the flow structure of the fields. The length of JEZ1 indicates the point within the gasifier where the peak temperature occurs, as determined by CFD simulation. The drying of fuel is

assumed to only take place in the JEZ1. The separation of the JEZ1 and JEZ2 also makes the ROM flexible for future adaptations, (e.g., simulation of a two-stage entrained flow gasifier).

3.3 Conservation equations

The sequentially divided zones along the gasifier length are highly dependent on each other through the exchange of materials, momentum and heat streams. Therefore, the governing equations must be solved simultaneously within each zone of the reactor network. The conservation equations can be reduced to zero-dimensional (for CSTR) and one-dimensional in the axial direction (for PFR) to decrease the computational costs. Table 3-2 presents partial differential equation used in the ROM. The equations are presented for PFRs and the same equations are applied to CSTRs with $\partial/\partial x$ terms replaced by $1/L_{CSTR}$. Each of the terms shown in the following equations has been defined in the nomenclature section.

Momentum conservation equations for gas and solids (Eq. 3-1 and 3-4) take into account accumulation, advection, momentum transfer, friction forces and gravity. Note that the gas phase momentum conservation equation also includes a pressure gradient term. The fundamental role of momentum conservation equations in the ROM is to establish the particle velocity profile that is the key to determine the residence time of particles in the gasifier. Mass balance equations (Eq. 3-2 and 3-5) consider the accumulation of mass inside the system, diffusion term of gases, advection term, reactions and particle mitigation to the walls of the gasifier. Note that a Peclet number of 1,000 has been used to calculate diffusion terms in the heat and mass transfer equations [44]. Note that high Peclet number are expected for short residence-time gasifiers where the feed are injected as jet with high velociy. Energy conservation equations for gas and solid phases (Eq. 3-3 and 3-6) account for accumulation, advection, heat transfer (via convection and/or conduction) and enthalpy addition/subtraction. The gas phase energy conservation equation also includes a diffusive term, which is the effective gas phase conductivity along the gasifier's axial domain. Also, in order to determine the volume fraction of the particles at each point in the gasifier, a conservation equation for the number of particles per unit of volume (N_p) is considered as shown in Eq. 3-7 of Table 3-2. High operating temperatures of entrained-flow gasifiers lead to melting of most of the fuel's ash that forms a liquid slag layer on the gasifier's refractory. This type of gasifiers is referred as slagging gasifier. To simulate the effect of slag formation, a single phase slag model is considered in the ROM. The slag mass transfer equation (Eq. 3-8) takes into account terms for accumulation, advection and

particle deposition rate on the gasifier's wall. The slag energy transfer equation (Eq. 3-9) considers accumulation, conduction and convection of heat through the slag layer, particle deposition, and convection terms for heat transfer between, gas, slag and the surroundings.

Table 3- 2. Mathematical model of the multi-phase flow inside the gasifier in the ROM

Gas phase		
Velocity	$\frac{\partial(A_{cs}\varepsilon_g\rho_g u_g)}{\partial t} = -\frac{\partial}{\partial z}(A_{cs}\varepsilon_g\rho_g u_g^2) + A_{cs}\left(-\frac{dP}{dz} + \varepsilon_g\rho_g g - F'_{g\to wall} - F'_{g\to p}\right)$	(3-1)
Molar composition	$\frac{\partial(A_{cs}\varepsilon_g C_{total}\, x_i)}{\partial t} = \frac{\partial}{\partial z}\left(A_{cs} D_{g,eff}\frac{\partial(\varepsilon_g C_{total}\, x_i)}{\partial z}\right) - \frac{\partial(A_{cs}\varepsilon_g u_g C_{total}\, x_i)}{\partial z} + A_{cs}(R_{hom} + R_{het})$	(3-2)
Temperature	$\frac{\partial(A_{cs}\varepsilon_g C_{total}\, c_{p_g} T_g)}{\partial t} = \frac{\partial}{\partial z}(A_{cs} k_{g,eff}\frac{\partial T_g}{\partial z}) - \frac{\partial(A_{cs}\varepsilon_g u_g C_{total}\, c_{p_g} T_g)}{\partial z} + A_{cs}(R_{hom} H_R) + Q'_{conv\ p\to g} - Q'_{conv\ g\to slag}$	(3-3)
Solid phases		
Velocity	$\frac{\partial(A_{cs}\varepsilon_p\rho_p u_p)}{\partial t} = -\frac{\partial}{\partial z}(A_{cs}\varepsilon_p\rho_p u_p^2) + A_{cs}(\varepsilon_p\rho_p g + F'_{g\to p})$	(3-4)
Mass flow rate	$\frac{\partial(M_{solid}/u_p)}{\partial t} = -\frac{\partial(M_{solid})}{\partial z} + A_{cs}(R_{het}) - m'_{slagging}$	(3-5)
Temperature	$\frac{\partial(A_{cs}\varepsilon_p\rho_{solid}\, c_{p_p} T_p)}{\partial t} = -\frac{\partial}{\partial z}(A_{cs}\varepsilon_p u_p\rho_p c_{p_p} T_p) + A_{cs}(R_{het} H_R) - Q'_{conv\ p\to g} - m'_{slagging}\, h_p - Q'_{rad\ p\to slag}$	(3-6)
Particle density	$\frac{\partial(A_{cs} N_p)}{\partial t} = \frac{\partial(A_{cs} N_p u_p)}{\partial z} + \frac{m'_{slagging}}{m_p}$	(3-7)
Liquid phase		
Slag mass	$2\pi r_{gasifier}\ \rho_{slag}\frac{\partial(\delta_{slag})}{\partial t} = -\frac{\partial m_{slag}}{\partial z} + m'_{slagging}$	(3-8)
Slag temperature	$2\pi r_{gasifier}\ \rho_{slag} C_{p_{slag}}\frac{\partial(T_{slag}\,\delta_{slag})}{\partial t} = 2\pi r_{gasifier}\ k_{slag}\frac{\partial}{\partial z}\left(\delta_{slag}\frac{\partial T_{slag}}{\partial z}\right) - \frac{\partial}{\partial z}\left(m_{slag} C_{p_{slag}} T_{slag}\right) + m'_{slagging}\ H_p + Q'_{rad\ p\to slag} + Q'_{conv\ g\to slag} - Q'_{conv\ slag\to surronding}$	(3-9)

3.4 Chemical reactions

There are several reactions taking place inside the gasification process, i.e., drying, devolatilization, combustion and gasification. These complex reactions and their kinetic rates are closely related to each other. In this section, each reaction system and the approaches used to model these reactions are described.

3.4.1 Drying and devolatilization

Inlet streams (solid fuel, steam and oxygen) mix vigorously with each other and the hot recirculation gases at the inlet of the gasifier. Upon this mixing, solid fuels face a sudden heating which

causes the moisture present in the particles to rapidly vaporize. Volatile components within the solid fuels also leave the particles in a process known as devolatilization or pyrolysis. The volatiles mainly consist of combustible gases such as hydrogen, tar, methane and ethane, which react with oxygen to provide the thermal energy required for subsequent reactions. The solid residue remaining after the devolatilization process is referred to as char with the primary components being carbon and ash. The devolatilization of solid fuels depends on a wide range of process variables, such as the gasifier's operating conditions, heating rate, particle size and volatile fraction within the fuel.

There are different approaches that can be used to predict the volatile products. In one approach, the volatile products are assumed to be a single component with averaged chemical and physical properties. Although this approach simplifies the analysis, the compositions of the final light gases and the volatile yield may not be well predicted using this method [59], [60]. In order to determine accurate compositions of syngas and the amount of char to be converted by the char gasification reactions, the volatiles may be considered as a multi-component gas based on the ultimate and proximate analysis of the solid fuel. Merrick proposed a method which assumes that, after devolatilization, the fuel is divided into ten species [61]. Although Merrick's model has been widely used in the literature [17], [62], it is most suitable for low pressures. For development of the ROM, PC Coal Lab® software was used to model the devolatilization process at higher operating pressures. PC Coal Lab® is a virtual laboratory which provides a breakdown of the devolatilization process, tar decomposition and kinetic parameters for char reactions based on the fuel's composition and the gasifier's operating conditions. Breakdown compositions for the volatiles considered in the present study are presented in Table 3-3. Note that the tar composition in the petroleum coke is 94.1% carbon, 3.24% sulfur, 1.84% nitrogen and 0.82 oxygen.

Table 3- 3. Devolatilization breakdown of petroleum coke

Component	Wt. %	Component	Wt. %	Component	Wt.%
Tar	8.2	C_3H_8	0	C_2H_6	0.24
H_2	3.5	CO	2.2	C_3H_6	0.23
CH_4	0.6	CO_2	0.1	H_2S	1.92
C_2H_2	0	H_2O	0	Char	82.6
C_2H_4	0.23	HCN	0.18		

3.4.2 Homogeneous reactions

In the gasification process, the combustion of volatiles occurs by homogeneous oxidations. These reactions are responsible for providing the thermal energy required to propagate the char reactions. Fourteen homogeneous reactions, presented in Table 3-4, are considered in this study. These reactions account for volatile combustion as well as the water-gas shift reaction (which is one of the primary determinants of syngas composition) and nitrogenous and sulfurous pollutant formation. No global kinetic expressions were found for sulfur reactions; therefore, rate expressions with extremely high constants are used as suggested in previous work [6]. The kinetics of the homogeneous reactions and the respective heats of reactions were adopted from the available literature [62], [6].

Table 3- 4. Homogeneous reactions

R_1	$H_2 + 1/2\ O_2 \overset{k_1}{\rightarrow} H_2O$	R_8	$Tar + O_2 \overset{k_8}{\rightarrow} CO + SO_2 + N_2$
R_2	$CH_4 + 1/2\ O_2 \overset{k_2}{\rightarrow} CO + 2H_2$	R_9	$C_3H_6 + 1.5O_2 \overset{k_9}{\rightarrow} 3CO + 3H_2$
R_3	$CO + 1/2\ O_2 \overset{k_3}{\rightarrow} CO_2$	R_{10}	$SO_2 + CO \overset{k_{10}}{\rightarrow} COS + O_2$
R_4	$C_2H_6 + O_2 \overset{k_4}{\rightarrow} 2CO + 3H_2$	R_{11}	$COS + H_2 \overset{k_{11}}{\rightarrow} H_2S + CO$
R_5	$C_2H_4 + O_2 \overset{k_5}{\rightarrow} 2CO + 2H_2$	R_{12}	$HCN + 1/2O_2 \overset{k_{12}}{\rightarrow} CNO + 1/2H_2$
R_6	$CO + H_2O \overset{k_6}{\rightarrow} CO_2 + H_2$	R_{13}	$CNO + 1/2O_2 \overset{k_{13}}{\rightarrow} NO + CO$
R_7	$CH_4 + H_2O \overset{k_7}{\rightarrow} CO + 3H_2$	R_{14}	$CNO + NO \overset{k_{14}}{\rightarrow} N_2 + CO + 1/2O_2$

3.4.3 Heterogeneous reactions

The carbon in the residual char takes part in four heterogeneous reactions listed in Table 3-5. Partial combustion of char is an exothermic reaction and provides thermal energy for steam gasification and the Boudouard reactions, which are endothermic reactions. There are nth-order rate laws presented in the literature for partial combustion of char (in the same format which is used in homogeneous reactions) [43]. However, such expressions are only capable of predicting the initial oxidation reactivity and cannot consider the influences of pore evolution and intrinsic chemistry [6]. As a result, they cannot satisfy a broad range of operating conditions for the heterogeneous reactions. In order to account for physical structure evolution, modified nth-order reaction kinetics are implemented by using PC Coal Lab®. In the rate laws of heterogeneous reactions, all parameters are adjustable constants that change with pressure, particle size, gas

compositions, temperature and fuel type**.** Note that the char has the following weight percentages: 92.7% carbon, 4.88% sulfur, 1.88% nitrogen, 0.4% hydrogen and 0.14% oxygen.

Table 3-5. Heterogeneous reactions

Combustion	$Char + 0.485\,O_2 \rightarrow 0.918\,CO + 0.0161\,NO + 0.0182\,SO_2 + 0.0236\,H_2$
Steam gasification	$Char + 0.969\,H_2O \rightarrow 0.918\,CO + 0.0161\,NO + 0.0182\,SO_2 + 0.993\,H_2$
Boudouard reaction	$Char + 0.969\,CO_2 \rightarrow 1.89\,CO + 0.0161\,NO + 0.0182\,SO_2 + 0.0236\,H_2$
Methane formation	$Char + 3.672\,H_2 \rightarrow 0.918\,CH_4 + 0.0161\,NO + 0.0182\,SO_2 + 0.0236\,H_2$

The format of reaction terms for heterogeneous char reactions is as follows:

$$R_i = \vartheta A'_i \exp\left(-\frac{E_i}{RT}\right) P_{i,s}^{n_i} \quad (3\text{-}10)$$

$$\vartheta = (-2E-08)X_{char}^5 + (5E-06)X_{char}^4 - 0.0005X_{char}^3 + 0.0244X_{char}^2 - 0.5849X_{char} + 6.7283 \quad (3\text{-}11)$$

where R_i is the char consumption rate based on the external particle surface; ϑ represents a decay parameter which slows down the char reaction rate with conversion (X_{char}), A_i' is the pre-exponential factor; $E_i$is the activation energy; n_i is the reaction order and $P_{i,s}$ is the partial pressure (in atm) of the gas component on the particle surface. As the solid fuel converts to syngas, the rate of gasification reactions decreases. A portion of the rate reduction is associated with the physical structure of the solid particles, which are considered through the decay parameter within the heterogeneous reactions rates. The decay rate coefficients have been calculated by fitting the product of the annealing factor, surface area factor of the random pore model, and char density factor. The kinetic parameters of heterogeneous reactions for the specific solid fuel used in the ROM and CFD simulation are listed in Table 3-6. Heats of reaction values for the heterogeneous reactions were taken from the literature [62]. For simplicity and numerical stability of the CFD model, the reaction of char with H_2 has been omitted and the inhibition of the char gasification reactions by CO and H_2 has been neglected. The formation of NO and SO_2 is based on the composition of char in order to balance the mass of the elements, and no other gas phase reactions associated with these compounds have been implemented in the CFD model.

Table 3-6. Kinetic parameters of heterogeneous reactions

Reactions	A	E (kcal/mol)	n
Partial combustion	75.4 g/(atm·cm^2·s)	47.2	1
Steam gasification	8.76×10^3 (atm·s)$^{-1}$	45.6	0.96
Boudouard reaction	3.53×10^5 (atm·s)$^{-1}$	64.4	0.88
Methane formation	4.47×10^{-3} (atm·s)$^{-1}$	43.5	0.78

3.5 Flow forces

Solid particles are suspended with a distinct velocity in the turbulent flow of the gas leading to interactions between the particles and the gas flow. Also, in turbulent wall-bounded flows, a friction force is established near wall regions. The following expressions are incorporated into the ROM to account for gas-particle [63] and gas-wall [64] viscous forces in the momentum conservation equations of the gas and solid phases:

$$F'_{g,p} = \frac{3\varepsilon_p C_D \rho_g \varepsilon_g^{-2.65}\left(u_{gas}^2 - u_{particle}^2\right)}{4d_p} \tag{3-12}$$

$$C_D = 24/Re_{d,p}\left(1 + 0.15\, Re_{d,p}^{0.687}\right) \tag{3-13}$$

$$F'_{g,w} = \frac{f\rho_g \varepsilon_g u_g^2}{16 r_{gasifier}} \tag{3-14}$$

$$\frac{1}{f^{0.5}} = -2\log\left(\frac{\Omega_{wall}}{7.4 r_{gasifier}} + \frac{2.51}{Re_{d,w} f^{0.5}}\right) \tag{3-15}$$

where $F'_{g,p}$ refers to the volumetric forces between gas and particles through the implementation of the drag coefficient (C_D); $F'_{g,w}$ refers to volumetric forces between gas and the gasifier's wall by using friction factor (f). The other symbols used in the above equations are defined in the nomenclature section of this article. These expressions are substituted in the general momentum balance equation shown in Table 3-2 for the reactor network considered in this analysis.

3.6 Heat transfer

As described earlier, the heat transfer terms considered in the energy conservation equations are convection sources for gas-to-particle, gas-to-wall and wall-to-surrounding, and a radiation source for particle-to-wall. Note that according to the CFD simulation data, gas-particle radiation can be neglected

when compared to particle-wall radiation. The ROM also considers the amount of heat released through the gasifier's wall. Effective heat transfer coefficients are implemented at the wall boundaries of ERZ2 and DSZ. Figure 3-5 shows the wall boundaries of the gasifier and the respective heat transfer coefficient and area of each section.

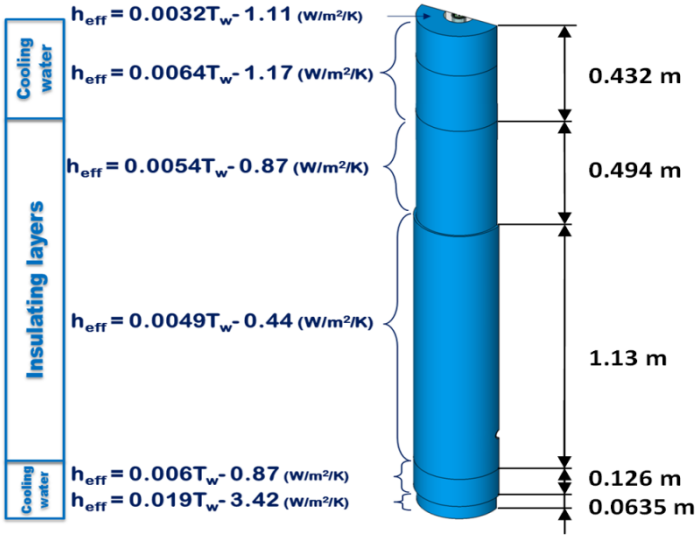

Figure 3-5. Effective heat transfer coefficients through the wall of the gasifier

The heat transfer is modeled through the innermost refractory layer, and the outer nozzle materials. Beyond the inner refractory layer, effective heat transfer coefficients are applied as boundary conditions to represent the remaining insulating layers of the gasifier, which are calculated from the sum of thermal resistances of the insulating layers. The thermal resistance of each conducting layer is calculated and arranged in series, while convective and radiative thermal resistances are arranged in parallel for the air gaps and heat transfer to the ambient air. The conductivities of the insulating layers are temperature dependent, so the effective heat transfer coefficient is a function of inner wall temperature. Therefore, a linear fit was calculated over a range of temperatures for each section of the gasifier. Furthermore, a correction factor was determined from experimental data of a gasifier run burning natural gas at atmospheric pressure, by matching thermocouple measurements with CFD predictions. The final effective heat transfer coefficients for each section of the gasifier are shown in Figure 3-5. Note that in the cooling water sections, there are refractory layers between the cooling water and the inner surface of the gasifier. The purpose of this cooling at the top section of the gasifier is for safety and protection of the outer layers, not to directly

cool the reacting zone. The main body of the pilot gasifier is refractory-lined to reduce heat loss as the pilot-scale has a much larger surface to volume ratio compared to commercial scales. The expressions used for the heat source terms per unit axial length that appear in the energy balance equations in Table 3-2 are as follows:

$$Q'_{conv,p\to g} = 4\pi\left(\frac{d_p}{2}\right)^2 N_p h_{pg}\left(T_p - T_g\right) \tag{3-16}$$

$$Q'_{convg\to slag} = \pi d_{gasifier} h_{gw}\left(T_g - T_{slag}\right) \tag{3-17}$$

$$Q'_{rad,p\to slag} = \pi d_{gasifier}\,\sigma\varepsilon_w\varepsilon_p\left(T_p^4 - T_{slag}^4\right) \tag{3-18}$$

$$Q'_{s\to surronding} = \pi d_{gasifier} h_{eff}\left(T_{slag} - T_{surronding}\right) \tag{3-19}$$

In the above equations, Q' is the heat flux between particles, gas, wall and surroundings, T stands for the respective temperature of each section, d is gasifier's diameter and h refers to convection heat transfer coefficients obtained by using Nusselt number correlations. The Nusselt number for gas-to-particle convection is calculated using the following expression [65]:

$$Nu_{d,p} = 1.32 Re_{p,d}^{\frac{1}{2}} Pr^{\frac{1}{3}} \tag{3-20}$$

The Nusselt number for gas-to-wall convection is calculated using Petukhov's equation [66]:

$$Nu_{d,w} = \frac{\frac{f}{8} Re_{d,w} Pr}{1.07 + 12.7\left(\frac{f}{8}\right)^{0.5}\left(Pr^{\frac{2}{3}} - 1\right)} \tag{3-21}$$

3.7 Slag model

High operating temperatures of entrained-flow gasifiers lead to melting of most of the fuel's ash that forms a liquid slag layer on the gasifier's refractory or membrane wall. Accounting for slag behaviour is critical as changes in the slag can affect the gasifier's availability, e.g., a low temperature of slag (which increases the viscosity) may solidify the slag and block the slag tap. Moreover, slag with very low viscosity may increase heat loss and cause excessive wear of refractory [67]. Therefore, it has been recommended to maintain a slag viscosity above 2 Pa·s and below 25 Pa·s [67]. This can be achieved by controlling the gasifier's wall temperature and the injection of fluxant. A review of slag viscosity models is available in

[68]. In the present work, the model used by Seggiani was adopted for slag viscosity [69]. This model describes the viscosity as a function of the silica ratio of the slag and the temperature of the slag layer:

$$S = \frac{W_{SiO_2}}{W_{SiO_2}+W_{Fe_2O_3}+W_{CaO}+W_{MgO}} \tag{3-22}$$

$$\log(\mu_{slag}) = 4.468S^2 + 1.265\left(\frac{10^4}{T}\right) - 8.44 \tag{3-23}$$

where μ_{slag} is the slag's viscosity in Pa·s, S is its silica ratio, T is the slag layer temperature in K and W is the weight fraction of slag components. To model the slagging process, conservation equations (presented in Table 3-2) for the distribution of particles' mass and energy on the gasifier's refractory are implemented in the ROM. To calculate the convection term, the following expression used by Seggiani [69] is used for the slag mass flow:

$$M_{slag} = \frac{2\pi r_{gasifier}\delta_{slag}^3\rho_{slag}^2 g}{3\mu_{slag}} \tag{3-24}$$

where r represents the gasifier's radius, δ_{slag} is the slag layer's thickness and ρ_{slag} is the slag's density. The slag density has been calculated based on the ash's composition and partial molar volumes of the components. The specific heat capacity and conductivity of slag were taken from Seggiani [69]. In addition, slagging has other effects on the performance of the gasifier such as changes in the wall's emissivity, reduction in heat transfer through the gasifier's refractory, and internal gas volume reduction. To simplify the ROM, the slag emissivity term was neglected in the energy transfer equation. The reduction in heat loss can be simulated in the ROM by adjusting the effective heat transfer coefficients through the wall; however, due to the small thickness of slag for gasification of petroleum coke, the heat transfer coefficients of the refractory were used in this work. Furthermore, the reduction of volume was considered in the ROM by adjusting the diameters of ERZ-2 and DSZ in the reactor network depending on the changes in slag thickness.

3.8 Chapter summary

In this chapter, the proposed ROM for CanmetENERGY's gasifier has been presented. The proposed ROM is capable of simulating the steady-state and dynamic operation of entrained flow gasifiers. The ROM consists of a reactor network that represents the gasifier using a set of chemical reactors that are aimed to capture distinct flow zones of the system. The layout of chemical reactors proposed in this work is based on CFD simulations of the gasifier that accounted for the detailed gas and particle flows. The reactor network employs three PFRs and two CSTRs to capture the streamlines of multi-phase flow inside the gasifier. Moreover, the conservation equations of mass, heat and momentum required to simulate the gasifier has been discussed in this chapter. The ROM implements sub-models for the simulation of drying, devolatilization, homogeneous and heterogeneous reactions, viscous fluid-solid interactions, pollutant formation, heat transfer and slag formation. The next chapter presents the implementation methodology, assumptions and mathematical approach used to simulate steady-state response of CanmetENERGY's gasifier.

Chapter 4
Steady-state Results and Model Validation

This chapter discusses the capabilities and accuracy of the ROM with a fixed reactor network to predict the output of a CanmetENERGY's gasifier over a wide range of operating condition. The structure of this chapter is as follows: Section 4.1 describes the assumptions and implementation methodology used to solve the model. Steady-state result of the ROM for the base-case condition used to develop the reactor network is presented in Section 4.2. The prediction capabilities of the ROM to meet the results of CFD in operating conditions beyond the base-case is discussed in Section 4.3. The model validation with the results of experimental tests for petroleum coke gasification is presented in Section 4.4. The results presented in this chapter have been published in the following papers:

1) Sahraei MH, Duchesne MA, Yandon R, Majeski A, Hughes RW, Ricardez-Sandoval LA. Reduced order modeling of a short-residence time gasifier. Fuel 2015;161:222-232.
2) Sahraei MH, Duchesne MA, Hughes RW, Ricardez-Sandoval LA. Experimental assessment, model validation and uncertainty quantification of a pilot-scale gasifier. Ind Eng Che Res 2016;55:6961-6970.

4.1 Assumptions and implementation methodology

In order to implement the ROM, a code was developed in MATLAB. At every point within the reactor network, one-dimensional conservation equations for mass, energy, momentum and particle density were solved. In setting up the conservation equations for each zone, the following assumptions have been made:

- The accumulation terms are set to zero.
- All moisture leaves the petroleum coke during drying in JEZ1.
- The leftovers of char during devolatilization are carbon and ash.
- Devolatilization reactions are assumed to be instantaneous reactions (due to high temperatures within gasifier).
- An average gas density is considered for each reactor zone.
- No pressure drop is accounted for the solid particles.

- Gas-wall friction and heat loss only occur in the outer layers of the reactor network, i.e., ERZ2 and DSZ.
- Due to low percentage of ash in petroleum-coke, no slag formation is considered for the steady-state ROM.

The system of non-linear differential equations expressing the gasification process was solved using the finite difference method. The spatial derivatives are approximated on a spatial one-dimensional grid with non-uniformly distributed nodes. The sudden changes in temperature and composition mainly occur in the oxidation zone of the gasifier, i.e. JEZ1 and JEZ2. The changes of gradients required suitable node spacing in that zone to obtain accurate results. Unequal grid spacing allows the ROM to capture the steep gradients within the JEZ. The non-linear solver within MATLAB® (fsolve), which is based on Newton's method, has been used to solve the present model. This solver approximates the Jacobian matrix using finite differences, which is a time consuming task for large-scale systems of non-linear equations. In order to reduce the computational time, an analytical Jacobian for the present system was developed and introduced to the solver which reduces the convergence time by an order of magnitude.

4.2 Steady-state results

The test condition and fuel properties used to design the reactor network and perform steady-state modeling of CanmetENERGY's gasifier are listed in Table 4-1.

Table 4-1. Test condition and fuel specification

Test conditions		
Petroleum coke		50 kg/h
Carrier gas (Nitrogen)		13 kg/h
Oxygen		67.9 kg/h
Steam		10.5 kg/h
Operating pressure		16 bar
Petroleum coke composition		Mass fraction
Proximate analysis	Ash	0.028
	Volatiles	0.120
	Moisture	0.005
	Carbon	0.847
Ultimate analysis	Hydrogen	0.001
	Sulfur	0.038
	Nitrogen	0.008
	Oxygen	0.002
	Carbon	0.864

In order to obtain the steady-state results, the spatial domain was discretized for each of the JEZ and DSZ reactors. This grid size was selected based on a sensitivity analysis that was performed for different grid sizes of the JEZ and the DSZ. Due to the non-linearity of the system in the JEZ, the least number of nodes to achieve a feasible solution was 13. By increasing the number of nodes, the relative errors in the outputs were decreased and accordingly no significant changes in the temperature and molar fraction profiles were observed. Table 4-2 presents the convergence test of the JEZ's outlet results with respect to increase in the size of grid. Note that the mass and energy balance for the base-case condition was also tested to ensure numerical convergence of the ROM. Overall, a system of 774 non-linear equations is simultaneously solved by using 30 nodes, i.e. 20 for the JEZ and 10 for the DSZ. The momentum transport is solved first to calculate the pressure drop and the velocity of gases and particles at each grid point by assuming an average gas density in each zone of the gasifier. The resulting velocity profiles are considered as inputs to solve for the mass and heat transfer equations simultaneously at each grid point inside the gasifier.

Table 4-2. The relative error percentages of JEZ's outlet for different grid size

Grid size	Temperature (K)	Conversion	H_2 mole fraction	CO mole fraction
16	0.9%	1.9%	4.3%	3.8%
18	0.3%	1.3%	3.8 %	2.7%

20	0.1%	0.6%	1.8%	1.2%
22	0.001%	0	0	0

4.2.1 Particle and gas velocities

The axial velocity profiles of the gases and particles are presented in Figure 4-1.a. As shown in this figure, the particle-gas flow expands in the JEZ and the velocity decreases quickly at the top end of the gasifier. However, the injected particles reach a peak velocity at the beginning of the expansion zone due to a higher velocity of the gas. At the end of the JEZ, which is at 0.61 m along the gasifier, the solids and the gas velocity profiles match. The residence time of particles is a function of the axial velocity profile in the gasifier. The calculated residence time is 0.4 seconds, which is in good agreement with the residence-time range reported from CFD simulation of the present system, 0.3-0.5 seconds. As shown in Figure 4-1.b, the pressure drop in the gasifier is less than 0.02 bar, which is consistent with the pressure drop experimentally observed for the present short-residence time gasifier, i.e., approximately less than 0.1 bar.

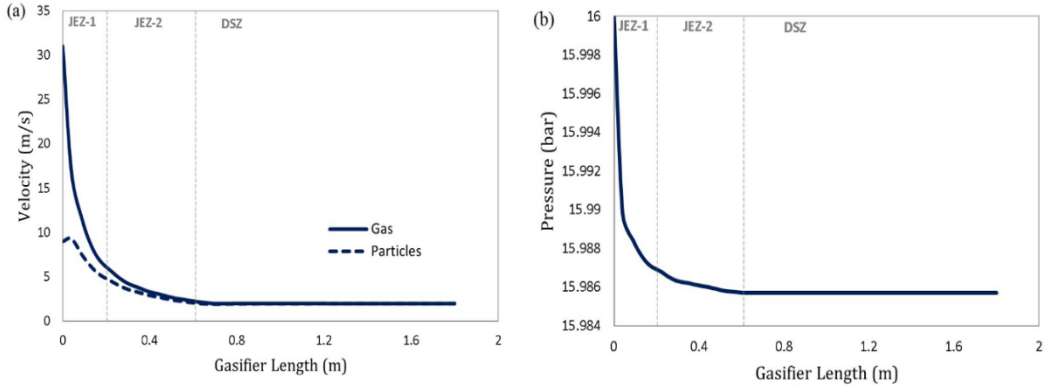

Figure 4-1. a) Axial velocity profiles; b) axial pressure profile

4.2.2 Syngas temperature and wall heat flux

The axial temperature profile and the wall heat flux inside the gasifier are presented in Figure 4-2. As shown in Figure 4-2.a, the temperature increases sharply at the beginning of the reactor (JEZ1) due to the combustion of volatiles and recirculation of gas. Also, the heat transferred by the recirculation gases to the expansion zone causes the temperature to rise and provides the energy required to ignite the solid particles and run the heterogeneous reactions. The char oxidation reactions cause the temperature to reach a peak value, also referred to as the flame temperature. This temperature is associated with the zones where

exothermic reactions occur. The ROM predicts a peak temperature of 2,878 K, which is in reasonable agreement with the peak temperature obtained from the CFD simulations, i.e., 2,800-2,900 K (presented in Figure 4-2.c.). An adiabatic flame temperature of 2841 K is calculated for the volatile gases. This value is also consistent with the peak temperature observed in the ROM and CFD simulations. By depletion of oxygen in the unit, endothermic reactions become dominant and the temperature decreases to 2,017 K at the reactor exit. In the DSZ, the particles and gas are in thermal equilibrium so the temperature reduces smoothly. The uniform temperature profile of recirculation zones is also shown in Figure 4-2.a. The temperature profile of the ERZ2 is lower than the average temperature of recirculated gases as endothermic reactions are the governing reactions in the recirculation zones. To simplify the analysis, the mass and energy balance equations for the ERZ1 are considered as a part of the ERZ2 since the length of the ERZ1 reactor is relatively small (i.e. less than 1 cm) and it also presents short residence times. Accordingly, the temperature of the ERZ1 is the same as in the ERZ2.

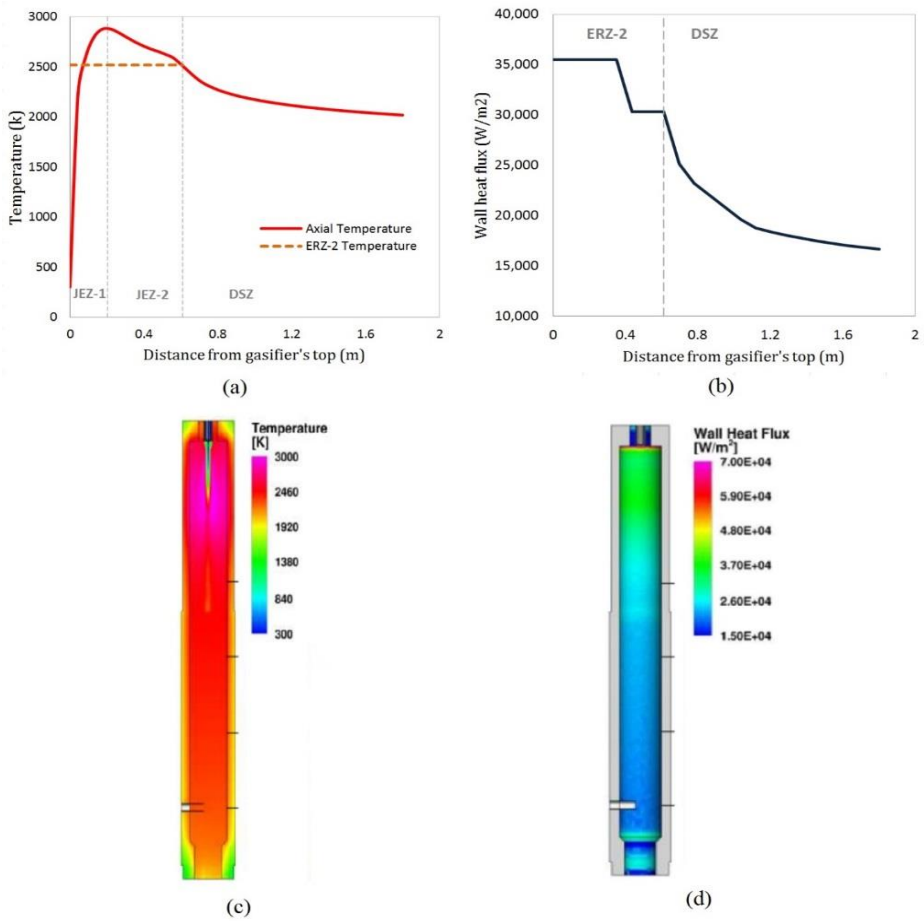

Figure 4-2. a) Temperature profile; b) Axial heat flux profile through the gasifier wall; and contour plots from the CFD model: c) Temperature; d) Wall heat flux

As shown in Figure 4-2.c, the CFD model predicts a temperature of 2,299 K at the outlet of the gasifier which is due high oxygen/fuel ratio. The CFD model assumes a single-component for the modeling of the volatiles. However, the present study adopted a multi-component approach to model the volatile species (see Section 3.3.1). This may potentially affect the homogeneous reactions taking place inside the gasifier thus causing changes in the heat distribution inside the system. As shown in Figure 4-2.c, the peak temperature predicted by CFD simulations is observed at 0.3 to 0.4 m down the gasifier; however, the ROM predicts the peak temperature at 0.21 m i.e., the end of the JEZ1. In the CFD model, the recirculation streams continuously pass into the expansion zone across the entire length of the JEZ. However in the proposed reactor network, the recirculation streams join the feeds at the beginning of the gasifier into the expansion

zone. As a result, more combustible materials are in contact with oxygen in a small volume which leads to faster oxidation at the end of the JEZ1 compared to the JEZ2.

Based on the effective heat transfer coefficients, the wall heat flux profile is presented in Figure 4-2.b for the ERZ2 and DSZ. The heat fluxes in the top section of the gasifier's wall (next to the combustion zone) are higher (35,500 W/m^2) due to the heat transferred to the cooling water system. The heat fluxes are reduced to 30,300 W/m^2 in the ERZ2 as the gas-particle flow reaches the insulation layers. Note that as ERZ2 is modeled using a CSTR reactor, a uniform temperature is calculated in that zone. Thus, the wall heat fluxes are constant in each sub-section of the ERZ2. However, as the gas-particle flow passes through the DSZ, the ROM considers temperature changes at the wall, which leads to a continuous reduction of the heat fluxes. The contour plot of the wall heat flux predicted by the CFD model is presented in Figure 4-2.d. Heat flux predicted by the ROM in the upper level of the gasifier is similar to CFD model predictions. The heat flux in the DSZ predicted by the ROM also matches the values predicted by the CFD model.

4.2.3 Syngas composition and conversion

The composition profiles of the main syngas components are presented in Figure 4-3.a. Based on this figure, oxygen is consumed quickly in the JEZ where volatile and char combustion take place. Hydrogen decreases initially as it reacts with oxidizing agents. As the gas-particle mixture leaves the combustion zone, CO_2 and H_2O starts to decrease due to char gasification and water-gas shift reactions, which causes an increase in the CO and H_2 molar fractions. The ROM is able to predict the compositions of H_2, CO, CO_2 and O_2 with a reasonable agreement to the data gathered from CFD simulation. The sudden and sustained changes of the species can be explained by the reaction rates of heterogeneous reactions, presented in Figure 4-3.b. At the top of the gasifier, all the heterogeneous reaction rates are almost zero due to the low temperature of the particles. As shown in Figure 4-3.b, steam gasification and Boudouard reactions are the dominant reactions inside the gasifier which determine the conversion of the char particles.

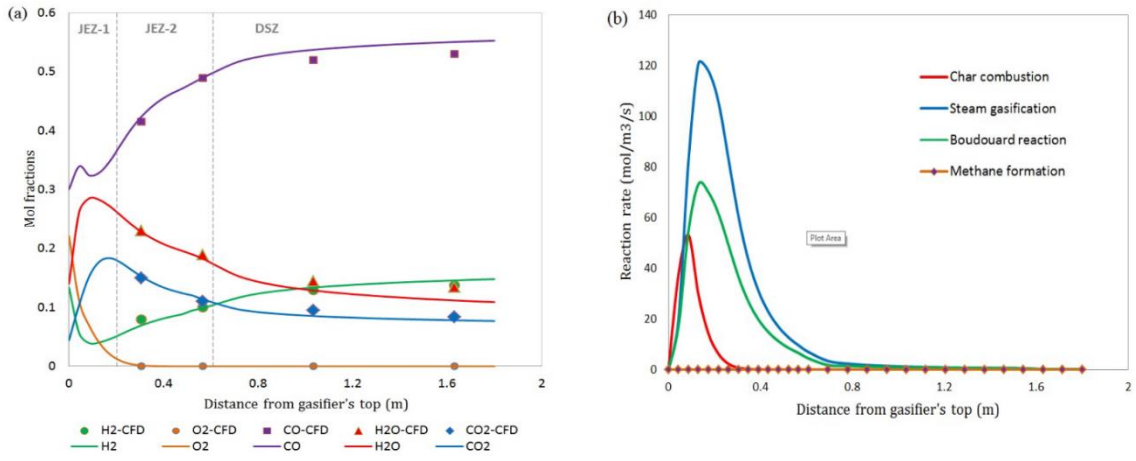

Figure 4-3. a) Gas composition profiles; b) profiles of reaction rates

According to the ROM results shown in Figure 4-4.a, almost complete conversion (99.6%) is achieved for the char particles, which is consistent with CFD results, i.e. 100% conversion of char. Note that for operating conditions beyond the base case condition where the oxygen flow rate is decreased, lower temperature profiles are established and accordingly higher residence time might be required. Figure 4-4.b shows the predicted concentration profiles of sulfurous and nitrogenous pollutants. One of the environmental benefits [70] of IGCC power plants is the capability to achieve extremely low sulfur emissions from burning solid feed stocks. The ROM predicts an H_2S mole fraction of 0.014 at the exit and a mole fraction of 0.009 for NO at the exit.

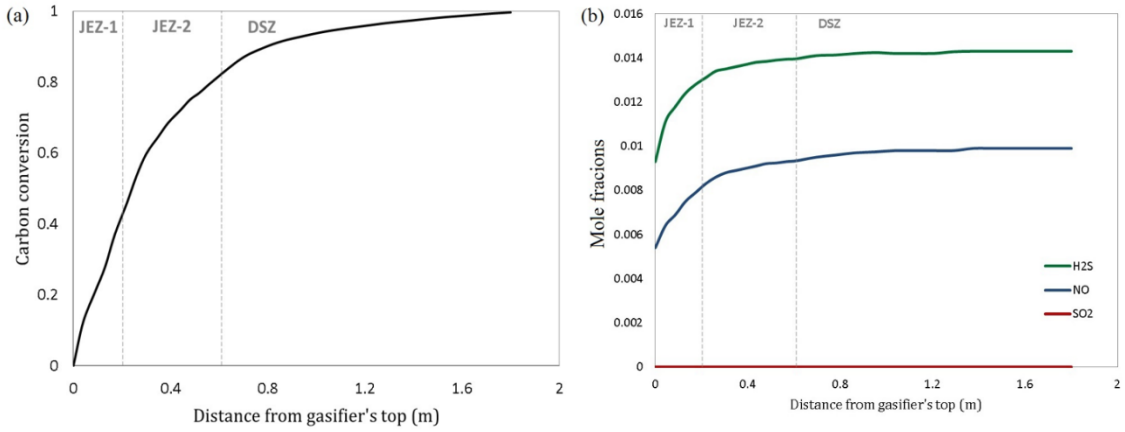

Figure 4-4. a) Carbon conversion profile; b) sulfurous and nitrogenous pollutant profiles

The required computation time to achieve results presented in this study with the proposed ROM was 2.5 minutes (Core i7, 3.4 GHz with 8 GB of RAM) compared to the computational time of a CFD simulation, i.e. 7-10 days. Therefore, the proposed ROM can be used to perform various analyses at low computational costs that can further validate the suitability of a short-residence time gasification unit as an attractive method for clean power production.

4.3 ROM vs CFD

The ROM framework was designed according to the flow patterns obtained from CFD simulations generated at the base-case operating conditions presented in Table 4-1. In order to assess the accuracy of the proposed ROM, the capability of the ROM's framework to predict the gasifier's behaviour needs to be investigated over a range of operating conditions. In the present work the accuracy of the ROM in predicting carbon conversion, temperature and composition profiles was examined by performing a sensitivity analysis on a test condition (oxygen flowrate) and a reactor network parameter (heterogeneous reaction kinetics). Note that the recirculation ratio of the base-case condition was increased by 10% in this section to match the value predicted by Thring and Newby and lower the dependence of the ROM to the CFD simulation.

4.3.1 Changes in oxygen flowrate

As indicated in Figure 4-5, no distinguishable changes were observed in the streamlines of CFD simulations when the oxygen flowrate was varied by +/-10%. Also, the recirculation zone ends at the same axial distance in all cases. Therefore, the ROM's framework was not adjusted for the changes in oxygen flowrate considered in this work.

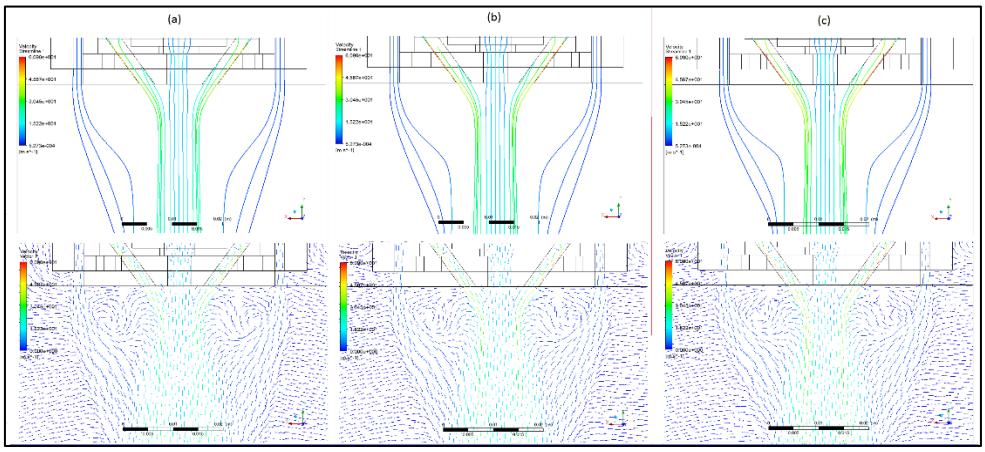

Figure 4-5. Streamlines and normalized velocity vectors of CFD simulation: a) -10% O2 flowrate; b) Base-case; c) +10% O2 flowrate

The temperature distribution predicted by the ROM and CFD simulation for three different oxygen flowrates are presented in Figure 4-6. As shown in this figure, the gas temperature is highest at the beginning of the reactor due to the combustion of volatiles for the three oxygen flowrates considered. The released heat provides the required energy to ignite the solid particles and run the gasification reactions. By depletion of oxygen, endothermic reactions which are dominant in the DSZ cause a drop in temperature. When the oxygen flowrate increases, more carbon particles are expected to react with oxygen; thus more energy is released causing a higher temperature distribution within the gasifier, as shown in Figure 4-6. The modeling results at the sampling probe are presented in Table 4-3. According to Figure 4-6 and Table 4-3, the ROM predicted a similar temperature distribution to that observed from CFD simulations; however, there is a temperature deviation of 70-120 K for the test conditions. The different approaches implemented in modeling of volatile species, homogeneous reactions and pollutant formation in the ROM, are the main expected causes for these deviations.

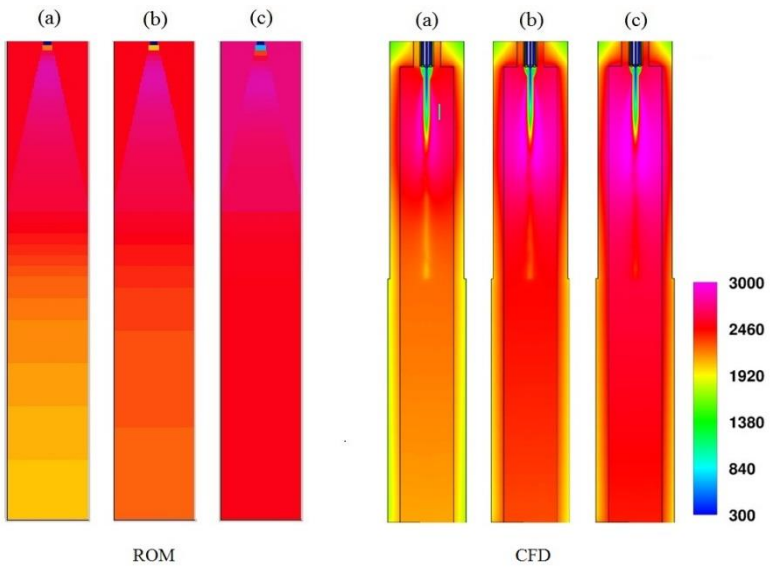

Figure 4-6. Temperature distribution in kelvins: a) -10% O2 flowrate; b) Base-case; c) +10% O2 flowrate

Furthermore as shown in Table 4-3, the proposed ROM predicted similar carbon conversions compared to CFD results. According to the results, high temperatures were attained in the gasifier in the gasifier. This increased the gasification reaction rates and resulted in high carbon conversion within a short residence time.

Table 4-3. Molar compositions of major species, temperature and char conversion at the sampling probe

	Base case		-10% oxygen flowrate		+10% oxygen flowrate		1/10 × kinetic parameters		10 × kinetic parameters	
	CFD	ROM	CFD	ROM	CFD	ROM	CFD	ROM	CFD	ROM
CO	0.520	0.552	0.535	0.558	0.485	0.541	0.473	0.503	0.522	0.565
H_2	0.148	0.141	0.173	0.165	0.104	0.097	0.117	0.111	0.137	0.139
CO_2	0.084	0.074	0.063	0.064	0.12	0.109	0.113	0.109	0.083	0.073
H_2O	0.143	0.112	0.111	0.097	0.188	0.152	0.182	0.160	0.140	0.111
T (K)	2299	2172	2099	1990	2395	2469	2329	2299	2301	2191
X_{char} (%)	99.2	98.5	95.8	94.9	99.7	99.2	89.5	91.4	99.9	98.7

The distributions of the molar compositions for CO and H_2 are presented in Figure 4-7 and 4-8, respectively. As shown in Figure 4-7 and Table 4-3, the composition of CO obtained from the CFD model decreased when more oxygen was injected into the system. The temperature profile increased proportionally with the oxygen flowrate. This expected behaviour shifted the water-gas shift reaction to the

right hand side which led to more CO converted to CO_2. Both the ROM and CFD simulations predicted this trend for the CO molar composition when oxygen flowrate was decreased. According to Figure 4-8, the ROM predictions in terms of the H_2 molar compositions are in agreement with those obtained from CFD simulations. At higher concentrations of oxygen, more H_2 is reacted to form H_2O; thus, in both models, H_2 molar composition at the outlet of the gasifier is decreased when more oxygen reacts with the fuel. Based on the results shown in Table 4-3, the proposed ROM was able to predict satisfactory results for CO_2 and H_2O molar fractions when compared to CFD simulation results. The major difference between the two models in predicting syngas composition was observed in the ERZ (the wall regions of the upper section of the gasifier). As shown in Figure 4-7 and 4-8, the molar compositions of CO and H_2 are higher in this zone of the ROM compared to CFD simulations. The ROM considers the recycle streams with the molar composition calculated from JEZ2 to enter ERZ where more CO and H_2 are already formed. In the CFD model however, these streams recirculate gradually into ERZ2. As a result, higher molar compositions are observed in ERZ2 sections of the ROM.

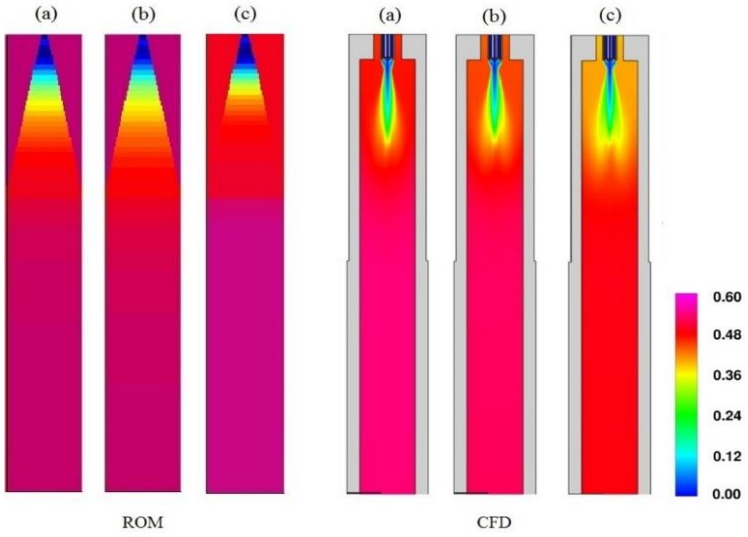

Figure 4-7. CO molar fraction: a) -10% O2 flowrate; b) Base-case; c) +10% O2 flowrate

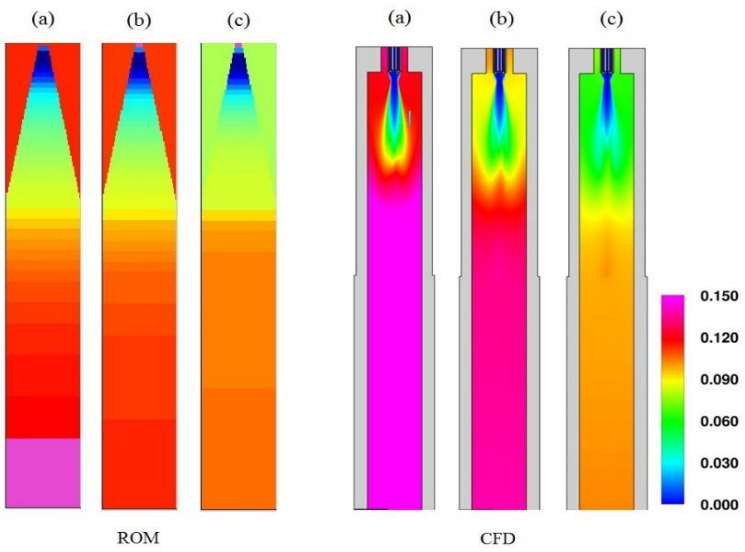

Figure 4-8. Hydrogen molar fraction: a) -10% O2 flowrate; b) Base-case; c) +10% O2 flowrate

4.3.2 Changes in kinetic parameters

In order to further examine the capabilities of the ROM, changes in the model parameters were performed by modifying the constant factor of the Arrhenius rate equations for the heterogeneous reactions. Two case-studies were considered: increasing and decreasing the Arrhenius constants by a factor of 10. As the kinetic parameters are reduced, the heterogeneous reactions become slower and less carbon conversion is expected within the gasification unit. According to Table 4-3, the carbon conversion is reduced to 91.4% when the kinetic parameters are decreased; however the carbon conversion did not change considerably for higher reaction rates as nearly complete carbon conversion was already achieved for the base-case condition. Thus, the results for the case study when the kinetic parameters are increased are expected to be similar to those obtained for the base-case condition. The ROM outputs for conversion, temperature and compositions of these case studies are in good agreement with the results of CFD simulation. The molar composition profiles of CO and H_2 are presented in Figure 4-9 and 4-10, respectively. The trend in the composition profiles is similar for the two models with the ROM predicting slightly higher CO composition for each case, i.e. 3-4%. The dominant reactions within the gasifier are the endothermic char gasification reactions rather than partial combustion of carbon. Therefore, the outlet temperature of the gasifier must increase for the case when the kinetic parameters are decreased. As shown in Table 4-3, both models predicted higher outlet temperatures for this case compared to the base-case operating condition.

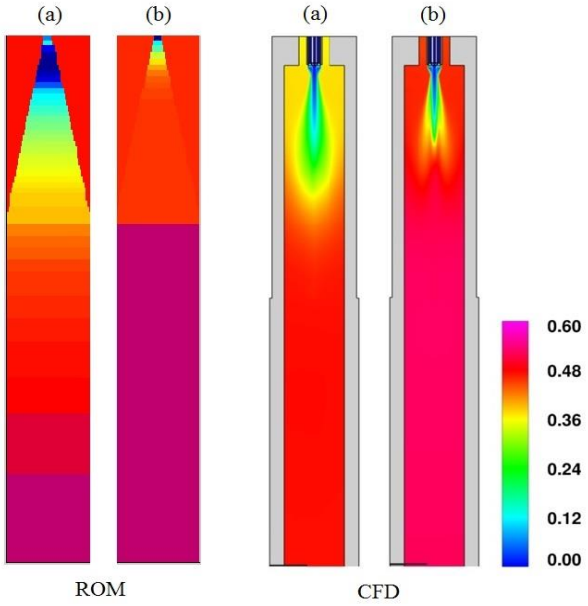

Figure 4-9. Carbon monoxide molar fraction: a) 1/10 × kinetic parameters; b) 10 × kinetic parameters

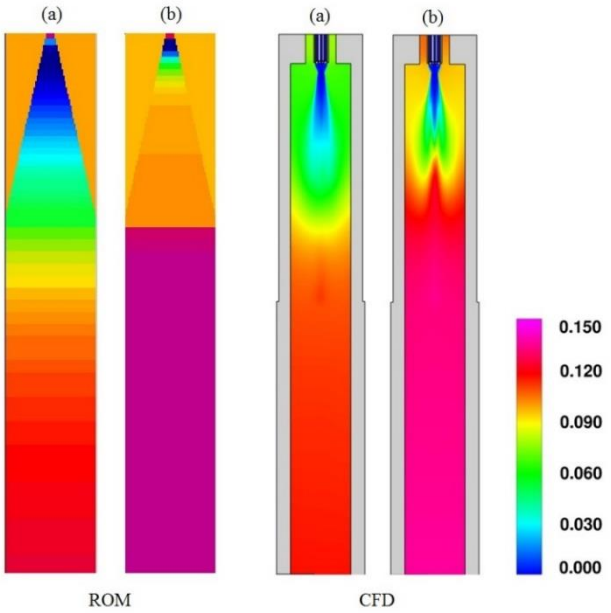

Figure 4-10. Hydrogen molar fraction: a) 1/10 × kinetic parameters; b) 10 × kinetic parameters

Overall, the ROM was capable of predicting the base-case results with more accuracy compared to the other four cases presented above. This is due to the fact that the ROM's geometry and framework was developed using the streamlines of the base-case CFD simulation. Although the ROM is only an approximation to the CFD model, the overall results (obtained over a range of operating conditions and

kinetic parameters) have demonstrated the prediction capabilities of the ROM as a computationally efficient alternative to describe the performance and operation of CanmetENERGY's gasification unit.

4.4 Model validation

This section presents ROM validation and investigates the capabilities and limitations of the model in predicting the results of experimental tests. These tests were performed using CanmetENERGY's pressurized entrained-flow slagging gasifier for petroleum-coke. The experimental design of these tests is presented in Appendix A. The operating conditions of the experimental tests are presented in Table 4-4. As shown in this Table, these tests were conducted at different operating conditions, i.e., injected fuel flowrates vary from 41.2 to 52.3 kg/h, injected steam flowrates vary from 0 to 21.8 kg/h, and injected oxygen flowrates vary between 28.4 and 37.2 kg/h. A high operating pressure is often desired for these systems as it decreases the volume of the gasifier and reduces capital costs (larger reactor volume is not required) for a given throughput. Hence, the set of experimental tests was performed at 16 bar. Note that the modeling results indicated that the original base-case condition under which the ROM was developed would have caused operational difficulties. These difficulties were due to high temperature distribution (up to 2900 K) along the gasifier, which can seriously damage the gasifier's wall and measurement devices [10]. Hence, this test was not considered as part of the experimental design.

Table 4-4. Operating conditions of the experimental tests

	Test 1	Test 2	Test 3	Test 4
Fuel (kg/h)	47.1	50.7	41.2	52.3
Steam (kg/h)	9.9	21.8	10.7	0
Oxygen (kg/h)	28.4	34.2	37.2	30.4
Nitrogen (kg/h)	11.9	11.0	12.1	11.4
Pressure (bar)	16	16	16	16

The results from the experimental tests and the ROM are presented in Table 4-5. According to this table, test 3 has the highest oxygen to fuel mass ratio (0.9); therefore, the highest conversion was achieved for this test, i.e., 90%. The lowest conversion (48%) was achieved in Test 4 where steam was not used. As shown in Table 4-5, the ROM predicts well the conversion measured in the different experimental tests.

Table 4-5. Experimental and modeling results for conversion; dry gas molar flowrate and percentages

	Percentage of carbon conversion		Dry gas flowrate (kmol/h)		Dry molar percentages					
					CO_2		H_2S		N_2	
	Exp.	ROM	Exp.	ROM	Exp.	ROM	Exp.	ROM	Exp.	ROM
Test 1	60	59.8	3.53	3.27	6.4	5.4	1.83	1.69	12.8	12.4
Test 2	69	68.0	4.31	4.30	10.7	9.2	1.78	1.53	10.2	9.9
Test 3	90	91.0	4.12	4.18	6.4	5.3	1.34	1.57	11.0	10.8
Test 4	48	52.8	3.01	3.38	1.7	2.0	1.58	1.77	14.6	14.0

The results for some of the components, i.e. CO_2, H_2S and N_2 are presented in Table 4-5. During devolatilization and char gasification, sulfur is released in the form of hydrogen sulfide (H_2S). The H_2S formation mechanism is described elsewhere [17]. Note that in the reducing environment of the gasifier, sulfur is mostly present in the form of H2S rather than COS. As shown in Table 4-5, the experimental dry syngas H_2S molar fractions deviate from ROM predictions by 0.14 to 0.25 percentage points. Also, according to this table, the predicted dry gas flowrates by the ROM were in reasonable agreement with experimental tests. In the case of CH_4; since the heterogeneous reaction of CH_4 formation implemented in the ROM has a slow rate, the ROM predicted lower CH_4 content (0.0006-0.001%) compared to the experimental tests (0.05-0.2%). Another reason for lower predictions of CH_4 concentration may be the lack of a devolatilization rate in the ROM. Due to high temperatures within the gasifier, devolatilization reactions are assumed to be instantaneous reactions. Accordingly, all the CH_4 released from the fuel is predicted to instantly react with oxygen near the injection point in the gasifier.

Figure 4-11 presents the dry CO and H_2 compositions obtained from the ROM and experimental tests at the sampling probe. The bars in this figure represent the relative measurement errors for gas composition ($\pm 5\%$) based on measurements with calibration gases. Although the ROM predicts slightly different CO (lower) and H_2 (higher) compositions, the results are in reasonable agreement with the experimental measurements. As shown in Figure 4-11, the highest CO mole fraction (0.546) was achieved for test 3 whereas the highest H_2 was reached in test 2, where the steam flowrate was high. For the latter test, higher CO_2 is produced when compared to the other tests, which can be due to the water-gas shift reaction and steam gasification.

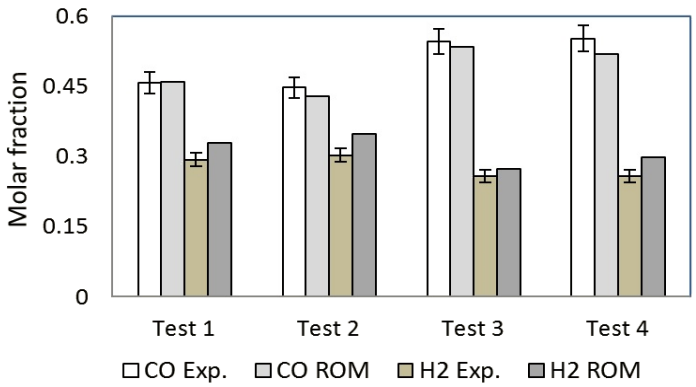

Figure 4-11. Dry syngas compositions of the experimental tests compared to ROM simulation results

In order to further demonstrate the distribution of the species along the gasifier's length, molar fraction profiles of the ROM for test 3 (which has the highest conversion) are presented in Figure 4-12. According to this figure, oxygen is consumed quickly at the inlet of the gasifier due to volatile and char combustion. During the conversion of fuel, molar fractions of CO, H_2 and H_2S gradually increase following the length of the gasifier. Furthermore, the molar fraction of CO_2 peaks at x=0.13 m (where oxygen is depleted) and decreases afterwards due to gasification reactions.

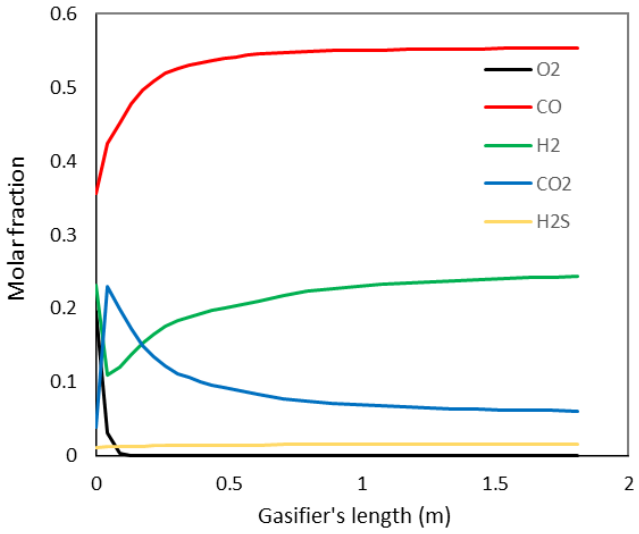

Figure 4-12. The trend of dry gas molar fractions along the gasifier's length for test 3

The temperature profiles obtained from the experiments and the ROM (centerline and wall) are presented in Figure 4-13. Near the burner, JEZ1 and JEZ2 in the ROM provide centerline temperature

predictions, while ERZ2 provides near-wall temperature predictions. Further from the burner, the ROM's DSZ provides both centerline and near-wall temperature predictions as the temperature is assumed to vary axially, but not radially. Based on thermocouple measurements, the temperature typically decreases along the gasifier's length. The temperature at the sampling probe is between 1,498 and 1,580 K for the test conditions. As shown in Figure 4-13, the centerline temperature increases sharply at the beginning of the reactor (JEZ1) reaching a peak value in this section, which is mostly due to the combustion of volatiles and recirculation of gases. Among the test conditions, Test 3 has the highest peak temperature (2,504 K) due to the highest oxygen to fuel ratio. By depletion of oxygen in the system, the heat required for endothermic reactions overcomes the heat released by exothermic reactions and the temperature decreases as the gases move toward the sampling probe. Based on these observations, the temperatures predicted by the ROM are in reasonable agreement with the experimental data.

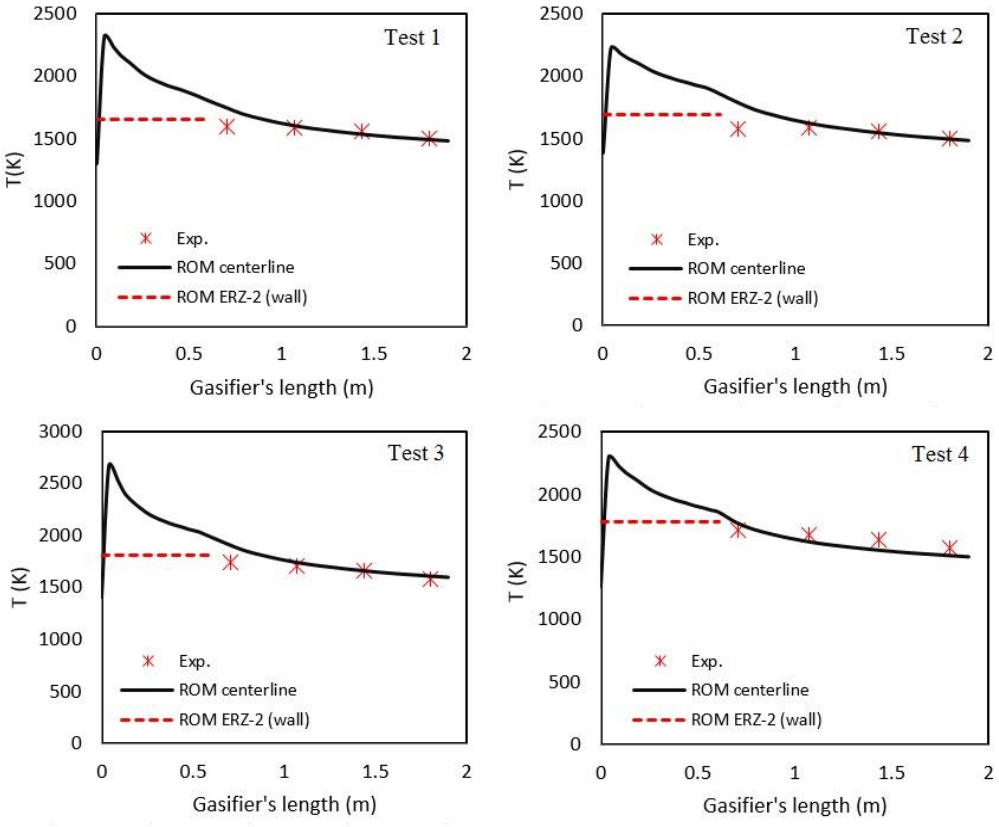

Figure 4-13. Temperature profile along the gasifier's length for the experimental tests

The results of conversion, temperature profile, dry gas flowrates and compositions from the model validation have demonstrated the capabilities of the ROM to describe the performance and operation of

CanmetENERGY's gasification unit at different operating conditions. Although the ROM was developed based on a CFD simulation with operating conditions different than the experimental conditions presented in this work, it was still capable of predicting the outputs with reasonable agreement with experimental results. Nevertheless, among the tests, the highest deviation between the ROM's output and experimental test result was observed for test 4 where the flowrate of steam was zero. Such deviation was expected since zero flowrate of the steam alters the streamlines of the multi-phase flow compared to the streamlines of the case under which the ROM was developed.

4.5 Chapter summary

The steady-state results of the ROM proposed for CanmetENERGY's gasifier have been presented in this chapter. In the first part, the results were compared with the CFD simulation data used to develop the ROM's reactor network. The predictions obtained by the ROM were in reasonable agreement with the CFD simulation data for axial temperature, heat flux, conversion and composition. Evaluation of the ROM in predicting the CFD results was further extended over a range of operating conditions. Although the ROM's framework was developed for the base-case test condition, the results showed satisfactory agreement with the CFD simulations for conversion, temperature and composition profiles under different operating conditions and kinetic parameters. The proposed ROM has shown to be computationally attractive as it reduces the computation time by several orders of magnitude when compared to CFD simulations. Furthermore, the prediction capabilities of the ROM were validated with the gasification tests. The ROM was able to predict the conversion, dry gas compositions and temperature distribution with satisfactory agreement when compared to experimental observations. According to the results, using a fixed framework in the reactor network to capture the streamlines of the multi-phase flow is sufficient to predict (with reasonable agreement) the outcome of gasification tests. The next chapter presents parametric analysis of the ROM to determine the sensitivity and variability of the gasifier's outlet, with respect to changes in feed and model parameters.

Chapter 5
Parameter Analysis

The low computational demands required to simulate the ROM enables the implementation of modeling analyses. The development of the ROM required the specification of parameters that were based on modeling assumptions that were not known with certainty and are subject to sensitivity. However, these parameters can take multiple values during operation depending on the operating conditions of the system and structure of the multi-phase flow patterns. Furthermore, the gasifier's feed streams may also experience variability in their operating conditions that cannot be readily measured online. This chapter presents a parametric analysis on the ROM's parameters through sensitivity and uncertainty analyses. The sensitivity analysis (presented in Section 5.1) aims to evaluate the impact of the model assumptions on ROM's accuracy and determines the influential parameters affecting the outlet of gasifier. The uncertainty quantification (presented in Section 5.2) aims to specify a range of variabilities for the gasifier's outputs based on combination in the realizations of the uncertain parameters in the inputs. One of the key concerns with a reactor network is the ability of the model to update its parameters during changes in the operating conditions. This chapter also presents a semi-empirical correlation to estimate the recirculation ratio, i.e. most influential parameter of the reactor network, as a function of gasifier's size and the operating flowrates by using the ROM and experimental data (Section 5.3). The results presented in this chapter have been published/submitted in the following papers:

1) Sahraei MH, Yandon R, Duchesne MA, Hughes RW, Ricardez-Sandoval LA. Parametric analysis using a reactor network model for petroleum coke gasification. Energy Fuels 2015;29:7681-7688.
2) Sahraei MH, Duchesne MA, Hughes RW, Ricardez-Sandoval LA. Experimental assessment, model validation and uncertainty quantification of a pilot-scale gasifier. Ind Eng Che Res 2016;55:6961-6970.
3) Sahraei MH, Duchesne MA, Hughes RW, Ricardez-Sandoval LA. Dynamic reduced order modeling of an entrained-flow slagging gasifier using a new recirculation ratio correlation. Fuel 2016 (submitted for publication).

5.1 Sensitivity analysis

A sensitivity analysis can provide insights into the effects of the design and reactor network parameters on the gasification behaviour and can therefore be used to increase the quality and prediction capabilities of the proposed ROM. Accordingly; a univariate sensitivity analysis of the ROM's inputs was conducted to identify the effect of key parameters on the simulation results. These parameters include reactor network parameters, i.e. the recirculation ratio, jet angle, steam gasification and Boudouard reaction rates; and design parameters, i.e. particle size, oxygen flowrate and steam flowrate. To perform the sensitivity analysis, all the input parameters were individually varied over a range of ±10% around their base-case values, which are listed in Table 1. The carbon conversion, H_2/CO ratio, and temperature profile obtained for each input change were recorded. The results of the sensitivity analysis are presented in Figure 5-1.

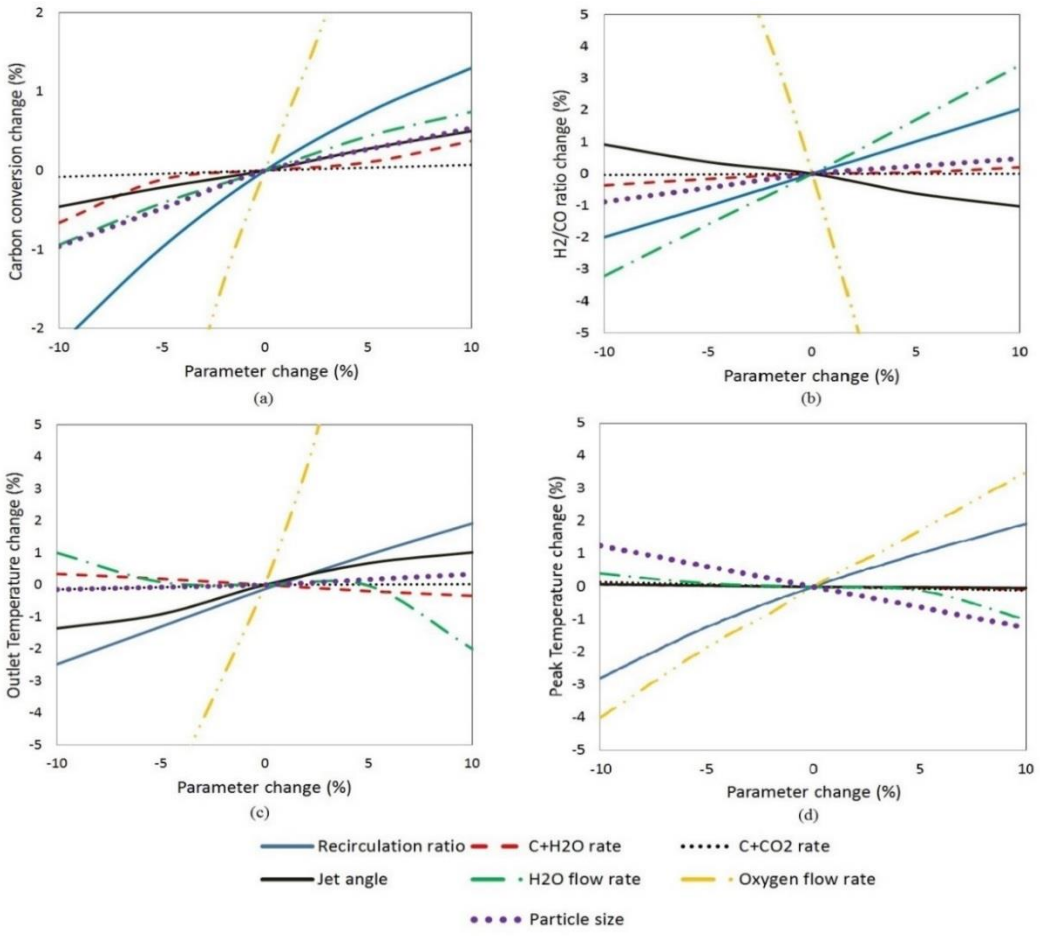

Figure 5-1. Sensitivity analysis of a) carbon conversion; b) of H2/CO ratio; c) outlet temperature; d) peak temperature

As indicated in Figure 5-1.a, carbon conversion is mostly influenced by the oxygen flowrate. In CanmetENERGY's gasifier design, the steam is injected at higher temperature than the other feeds, i.e. oxygen and fuel. Therefore, increasing the steam flowrate has a direct effect on the carbon conversion unlike slurry gasifier designs discussed by Monaghan and Ghoniem [43]. Among the reactor network parameters, the recirculation ratio has the highest effect on carbon conversion. As this parameter is increased, more particles are recirculated within the ERZ2, leading to higher residence time and carbon conversion. In addition, the jet angle and kinetic parameters have limited effect on carbon conversion. The input parameters considered in this analysis have almost the same effects on the H_2/CO ratio as they have on carbon conversion except for the $C+CO_2$ kinetic rate, oxygen flowrate and jet angle. As shown in Figure 5-1.b, more oxygen and an increased degree of the jet angle (which contributes to a larger expansion zone) decreased the H_2/CO ratio due to higher conversion of carbon to CO and H_2 to H_2O. The effect of changes on each individual parameter over the outlet temperature and peak temperature are presented in Figures 5-1.c and 5-1.d respectively. The oxygen flowrate and recirculation ratio are the most important parameters affecting these temperatures. During gasification, endothermic reactions were dominant; thus, larger particles decreased the peak temperature. However, the size of the particles has no significant effect on the outlet temperature. Other parameters such as the ERZ-1's diameter, particle-carrier flowrate, average gas density used for momentum equations, Peclet number and number of particles were also examined but they have no significant effects on the performance of the gasification unit.

5.2 Uncertainty quantification

The development of the ROM required the specification of parameters that were not known with certainty and were fixed to their expected (more likely) values. However, these parameters can take multiple values during operation depending on the operating conditions of the system and structure of the multi-phase flow patterns. Furthermore, the gasifier's feed streams may also experience uncertainties (variability) in their operating conditions that cannot be easily measured online. In the present study, fuel particle diameter, volatile matter percentages in fuel, angle of jet multi-phase flow and recirculation ratio of the reactor network are considered to be key uncertain parameters that affect the ROM's prediction capabilities in terms of conversion and syngas production.

As there is variation during operation in the size of particles, a distribution can be used to account for the fuel's particle size, rather than employing a single (averaged) particle size in the analysis. The volatile percentage of the fuel can also varies during gasifier operation by two mechanisms: 1) changes in the petroleum coke's composition and 2) changes in the volatility of petroleum coke components under different operating conditions, e.g. higher temperature increases the volatility of components. To study the effect of variability of volatiles in the gasifier, the volatile percentage of the fuel is considered as an uncertain parameter. Note that the volatile percentage of the fuel affects the proximate analysis as a whole. In this work, the uncertainty in the volatile percentage is also reflected in the carbon percentage of the proximate analysis, because there is low moisture and ash in petroleum coke. The inlet flowrates affect the geometry of the expansion and recirculation zones within the gasifier. Therefore, some model parameters such as jet angle and recirculation ratio are also considered as uncertain parameters since flowrates are prone to change during operation. The geometry of fuel and oxygen injectors forms a multi-phase flow which is dictated by an angle, typically referred to as the jet angle. Due to severe operating conditions inside the gasifier, it is often difficult to measure the jet angle. For the present ROM, this parameter was estimated based on the flow patterns of streamlines presented in our previous work. As mentioned above, the recirculation ratio is one of the sensitive parameters in the present ROM. In addition, the recirculation ratio is also sensitive to variations in the feed's flowrates; hence, it was considered as an uncertain parameter in the present analysis. Accounting for these uncertain parameters allows us to study the performance of CanmetENERGY's gasifier more thoroughly by using a ROM which considers parameters that are better described with probability density functions.

Application of mathematical techniques to evaluate the behaviour of models in the presence of uncertainty has been widely recognized in academia and industry [71], [72], [73]. To the authors' knowledge, only two studies have addressed parameter uncertainty in gasification models; however, none of these studies have used a ROM for this purpose. Gel et al. applied a non-intrusive uncertainty quantification method to study the variations of temperature, pressure and heating rate on the performance of a fluidized-bed gasifier [74]. In that study, a C3M-based computational coal kinetics model was employed to investigate the system's sensitivity and perform uncertainty quantification. Shastri and Diwekar used CFD simulations to study the effect of coal composition on a gasifier's operation [75]. Due to the computational costs of the CFD model, only 15 samples were employed in that study; accordingly,

the distributions provided are limited since they may not capture the actual distribution of the process outputs due to parameter uncertainty. As the computational costs of ROM are much lower than those needed for CFD simulations, a large number of samples can be employed for the uncertainty analysis. Accordingly, accurate distributions of ROM's outputs in the presence of model uncertainty can be used to quantify the potential financial risk associated with commercial performance of the technology. Decisions can then be made as to whether more research is needed or the level of certainty can be accepted and proceed with scale-up.

In this work, Monte Carlo (MC) sampling has been used as the uncertainty propagation method. MC sampling takes advantage of a large number of sample points chosen randomly from the distribution of uncertain parameters and a primary model to propagate uncertainty and therefore quantify output variability, typically represented as a probability distribution function (PDF). In the present study, normal (Gaussian) distributions in the uncertain parameters were considered as it is often regarded as an appropriate approximation in most engineering applications. The mean, standard deviation and basis of selection for the uncertain variables are presented in Table 5-1. The highest conversion was achieved for Test 3 of Table 4-4; therefore, this test was selected to perform the uncertainty quantification since it is expected that the gasifier will more likely operate at high conversion levels. In the present study, 2,500 MC samples that comply with the uncertainty descriptions provided in Table 5-1 were randomly generated for each uncertain parameter. Simulations of the ROM's gasifier were carried out for each combination in the realizations of the uncertain parameters obtained from the MC sampling technique. PDFs were generated from the MC simulation results to show the effect on output variability due to uncertainties in model parameters and the fuel's characteristics outlined in the previous section. Increasing the number of MC samples used in the present uncertainty analysis will not significantly improve the accuracy in the outputs' PDFs, i.e., the relative errors in the means and standard deviations are expected to be less than 1%; however, they will significantly increase the computational costs.

Table 5-1. Description of uncertain parameters

Parameter	Mean	Standard deviation	Observations
Volatile percentage	0.127	0.015	The mean value is taken from proximate analysis, while the standard deviation is assumed.
Particle diameter (μm)	79	10	Experimental data for particle size distribution of petroleum coke.
Recirculation ratio	1.1	0.2	CFD calculations and sensitivity analysis.
Jet angle (degrees)	17	1	Mean value is calculated from the flow patterns of a CFD simulation. Generally, a jet angle of 16-24^{O} exists in experimental and industrial investigations.

Based on the predicted distributions of outputs, upper and lower bounds evaluated at 10% confidence intervals, i.e., 95% and 5% respectively, are presented in Table 5-2.

Table 5-2. Probabilistic bounds evaluated at 10% confidence intervals

	Lower bound (5 %)	Upper bound (95 %)
Carbon conversion (%)	86.9	94.1
$T_{\text{sampling probe}}$ (K)	1,517	1,700
T_{peak} (K)	2,374	2,686
CO molar fraction	0.525	0.537
H_2 molar fraction	0.265	0.280
CO_2 molar fraction	0.047	0.063
H_2O molar fraction	0.069	0.115

According to this table and the distribution obtained for conversion (Figure 5-2), the average conversion is 90.7%, while there is a wide range of variability, i.e. from 86.9% to 94.1% (for the confidence interval of 10%), with a standard deviation of 2.3%. Higher volatiles in fuel, larger particle diameters and large recirculation ratios have direct effects on coal conversion.

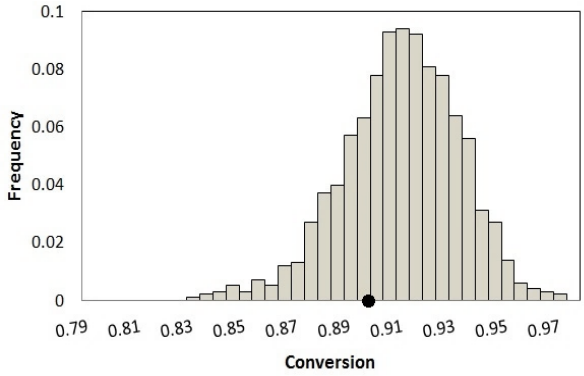

Figure 5-2: Carbon conversion distribution (the dot represents the experimental result)

Similarly, high variability was also observed for the temperature inside the gasifier at the sampling probe (the outlet) and at the position at which the highest (maximum) temperature was recorded (Figure 5-3). The average outlet (sampling probe) and peak temperatures obtained from the present uncertainty analysis are 1,604 K and 2,529 K, respectively.

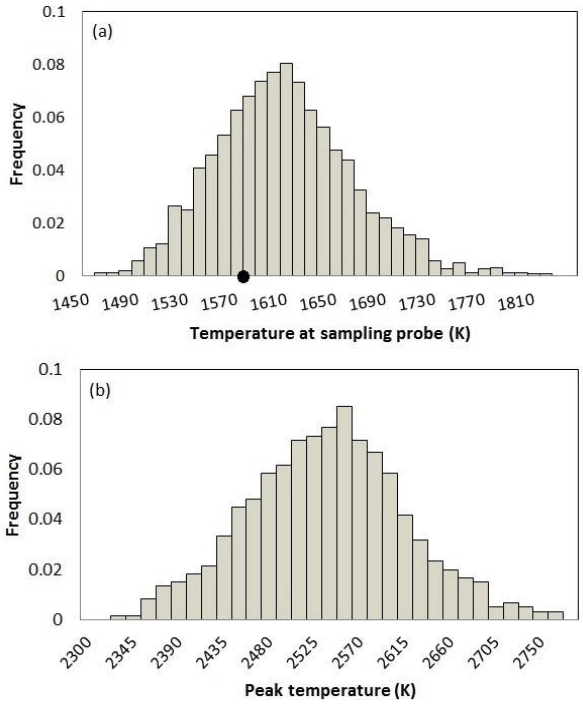

Figure 5-3. a) Distribution of temperature at the sampling probe (the dot represents the experimental result); b) distribution of peak temperature inside the gasifier

The main source of variability for the temperature distribution is expected to be directly correlated to the percentage of volatiles. As the volatile percentage increases, more hydrogen and hydrocarbons react with oxygen, causing higher peak temperatures inside the gasifier. According to the results shown in Figure 5-3, the standard deviation of sampling probe and peak temperatures are 56 K and 77 K, respectively. Note that the standard deviations in temperature for the other locations inside the gasifier (not shown here for brevity) are lower than that observed for the peak temperature. Temperature variability may cause safety concerns as it increases the risk of damaging the refractory. Note that the cooling water section installed at the top of the gasifier can potentially reduce the risk of such safety concern. On the other hand, a higher peak temperature leads to a higher temperature distribution inside the gasifier, which will improve conversion at the expense of increased risk.

The molar distributions of gas species are presented in Figure 5-4. Note that the presented values for the molar fraction of CO, CO_2 and H_2 are based on a dry gas composition. The mean values for CO and H_2 molar fractions are 0.532 and 0.273, respectively. The lowest variability was observed for the CO molar fraction with a standard deviation of 0.003 whereas the highest variability was obtained for the molar fraction of H_2O (standard deviation of 0.011). A narrow variability for the combined CO and CO_2 molar fractions (Figure 5-4) was expected since the standard deviation of volatile material has less impact on the total amount of carbon (above 80% of the petroleum coke is carbon). On the other hand, the considered volatile variability influences the major volatile components produced from the fuel, i.e. H_2. As there are several reactions that convert H_2 to H_2O and vice versa, the variability for the combined H_2 and H_2O molar fractions was expected to be greater than the variability of the combined CO and CO_2 molar fractions. The results shown in Figs. 5-4 indicate that the resulting distributions for the outputs analyzed in this study are non-normal, where the observed non-normality is higher for gas composition compared to temperature and conversion.

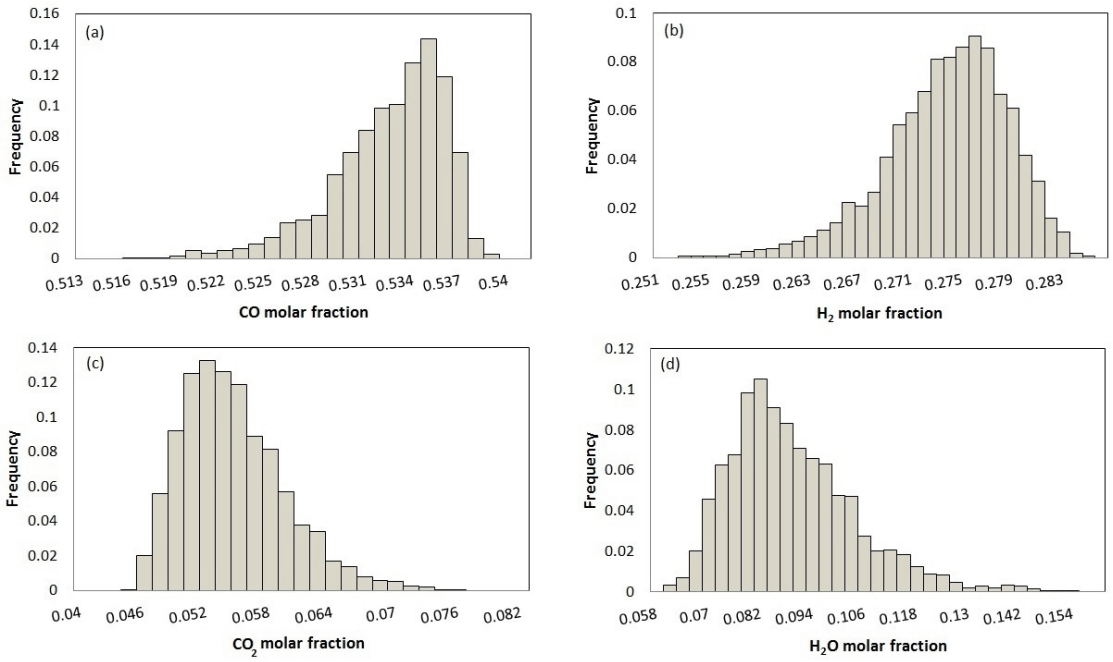

Figure 5-4. Molar fraction distributions of the major species inside the gasification unit (dry basis for H_2, CO and CO_2)

In order to perform the present uncertainty analysis, a total of 175.4 h of CPU time was required (Core i7, 3.4 GHz with 8 GB of RAM). Although the cost can still be considered significant, performing the same analysis using CFD simulations will result in prohibitive computational costs. Note that performing one realization of the uncertainty analysis using CFD model will roughly take 168 h (32 Cores, 2.9 GHz). Accordingly, the present uncertainty analysis cannot be performed using CFD or experimental tests due to prohibitive computational and economic costs. Therefore, the results of uncertainty analysis cannot be accessed using any other sources and therefore cannot be compared with CFD simulations. On the other hand, the proposed ROM is able to provide access to this information and can be used for example to evaluate the availability of the system under different operating conditions and in the presence of model parameter uncertainty.

5.3 Recirculation ratio correlation

Chemical reactors are often fed by two types of streams: primary jet flow and secondary flow which surrounds the primary jet (i.e., confined jet). If the momentum forces from secondary flow are not significant, part of the primary jet flow will recirculate towards the feed nozzles and a recirculation zone will be established [76]. Moreover, the size of the recirculation zone depends on the jet's expansion ratio

(jet and reactor diameters), turbulent fluid dynamics and the inlet flowrates. The most widely-used expression to estimate the mass recirculation flowrate is that proposed by Thring and Newby [77]; this correlation has been considered in the development of ROMs for different gasifiers [17], [49], [47]. Thring and Newby studied the flow behaviour within a furnace under the assumption of a free jet (i.e., no secondary flow) and proposed the following expression to calculate the mass recirculation ratio (γ):

$$\gamma = 0.47\left(\frac{d_{reactor}}{d_{jet}}\right)\left(\frac{\rho_{surrounding}}{\rho_{jet}}\right)^{0.5} - 0.5 \qquad (5\text{-}1)$$

where d_r and ρ represent the diameter and density, respectively. A review of similar expressions for mass recirculation ratios in chemical reactors is available in the literature [76]. While equation (5-1) provides reasonable estimates of the parameter, the correlation does not consider changes in the primary feed flowrates. Aaccording to mass balances from CFD simulations of CanmetENERGY's gasifier, the recirculation ratio varies as the inlet flowrates changes, e.g., increasing the oxygen feed flowrate by 10% resulted in a 6% increase in the recirculation ratio. A sensitivity analysis of the ROM's parameters has shown that the recirculation ratio is a sensitive model parameter in the ROM, i.e., a 10% increase in the recirculation ratio resulted in approximately a 1% change in carbon conversion and temperature [78]. Therefore, a correlation that provides an estimate for the recirculation ratio given the feed flowrate can increase the reliability of a ROM.

In the present work, the expression presented in (5-1) has been adapted to consider the transient changes in the individual flowrates of the jet and secondary flow, i.e. fuel, oxygen and steam. This has been done by adding an empirical term that accounts for the oxygen load, i.e., the ratio of oxygen mass flow to steam and fuel (without conveying gas) mass flows. Developing a general expression for the recirculation ratio as a function of the flowrates for different gasifiers is a challenging task due to the different types of gasifiers available and their wide range of operating conditions. Accordingly, the present study focused on the development of a correlation for the mass recirculation ratio for a dry-feed oxygen-blown gasifier. The following assumptions/considerations have been used to derive the proposed recirculation ratio correlation:

- The radial pressure gradient is neglected.
- The primary jet flow is comprised of fuel and oxygen whereas steam is introduced as secondary flow.

- Flowrates of fuel, oxygen and steam are greater than 0.
- Feed flowrates are introduced as a jet that results in similar flow patterns of streamlines to that presented in Figure 3-3.
- The operating flowrates are limited to oxygen loads of less than 1.

In the present analysis, the components of the jet flow (fuel and oxygen) have been considered separately since they have different effects on the recirculation ratio. It is likely that increasing the fuel flowrate will increase the density of the multi-phase jet at a fixed oxygen flowrate. Therefore, the fuel flowrate is considered to be inversely proportional to the recirculation ratio. However as mentioned above, the oxygen flowrate has the opposite effect on the jet density and it is considered as a proportional factor in the proposed correlation. Based on the nozzle configuration presented in Figure 3-3, the steam is injected far from the jet flow zone. Accordingly, the steam flow can act as a secondary flow and limits the recirculation of the multi-phase jet. Furthermore, it is assumed that the addition of steam also reduces the average temperature of the jet stream due to endothermic gasification reactions and therefore increases the jet stream's density which contributes to reduction of the recirculation ratio. Based on these heuristics, the following expression is proposed for the recirculation ratio:

$$\gamma = 0.47\left(\frac{d_{reactor}}{d_{jet}}\right)\left(\alpha\frac{M_{oxygen}}{M_{fuel}+M_{steam}}\right)^{\beta} - 0.5 \qquad (5\text{-}2)$$

where M_j is the mass flowrate of stream j. α and β are model parameters. Note that the recirculation ratio is an input to the reactor network in the ROM, therefore it must be expressed in terms of known variables. Since the density ratio of the jet (JEZ) and surroundings (ERZ-2) is not available *a priori*, previous ROMs for entrained-flow gasifiers implemented Thring and Newby's correlation assuming a density ratio of one [17], [49], [47]. This assumption is valid for non-reactive systems where the temperature and molecular weight of the jet and surrounding is similar. However, in reactive systems, such as a gasifier, a temperature and molecular weight difference exist between the jet and the surroundings thus resulting in a density ratio that is usually less than 1. Therefore, in the proposed correlation (equation 5-2), the effect of the density ratio has been indirectly accounted for by considering the changes in the inlet flowrates, as shown in the added term in equation (5-2). To obtain the model parameters, appropriate values for the recirculation ratio were initially estimated for various experimental tests by minimizing the integral squared errors (ISE) on

the outlet temperature and carbon conversion predicted by simulation. Once the most suitable recirculation ratios were obtained for each experimental test, the parameters α and β were calculated by using nonlinear least-squares to fit the proposed correlation to the estimated recirculation ratios. Note that a restricted range of recirculation ratios between 0.9-1.6 was chosen as γ is expected to vary near the value of the recirculation ratio predicted by Thring and Newby's method, (i.e., 1.1 in terms of molar flow or 1.2 in terms of mass flow [78]). The recirculation ratio predicted by Thring and Newby's method does not vary for the cases in this study since the nozzle configuration, geometry and expansion ratio of the gasifier are fixed.

To obtain the parameters of the proposed correlation for the recirculation ratio, a set of petroleum coke gasification tests have been used. The procedures implemented in experimental design and data collection of these tests have been previously described in [12]. In order to calculate the parameters (α and β) for the proposed recirculation ratio correlation (5-2), recirculation ratios for experimental tests were first estimated by performing simulations using the ROM. As shown in Table 5-3, these tests were conducted at a wide range of operating conditions, i.e., injected fuel flowrates vary from 41.2 to 59.7 kg/h, injected steam flowrates vary from 9.9 to 21.8 kg/h, and injected oxygen flowrates vary between 28.4 and 43.6 kg/h. The corresponding ranges of recirculation ratios for each of these tests are shown in Figure 5-5.a. These recirculation ratios correspond to the lowest ISE between the ROM and experimental tests in predicting outlet temperature and carbon conversion. Five of the tests (shown in Table 5-3) were used to estimate the parameters α and β whereas test 6 (also shown in Table 5-3) was used for validation of the correlation.

Table 5-3. Experimental test conditions and petroleum coke/coal properties

Test	1	2	3	4	5	6
Fuel (kg/h)	50.7	47.1	50.0	59.7	41.2	47.6
Oxygen (kg/h)	34.2	28.4	41.3	43.6	37.2	39.9
Steam (kg/h)	21.8	9.9	21.8	10.2	10.7	10.5
Oxygen load	0.47	0.50	0.57	0.62	0.72	0.69

The estimates for α and β, obtained from the least square method were 2.38 and 0.53, respectively. A statistical analysis on the correlation has indicated that both parameters contributed significantly in the proposed correlation for the recirculation ratio as the p-values reported for the model parameters α and β are 7.1e-6 and 1.3e-6, respectively. As shown in Figure 5-5.a, the proposed correlation can match the

recirculation ratios obtained by simulation at different oxygen loads. Moreover, the correlation was used to obtain the recirculation ratio for test 6 (γ=1.58); this value is close to that obtained from simulations of the dynamic ROM, i.e., 1.56.

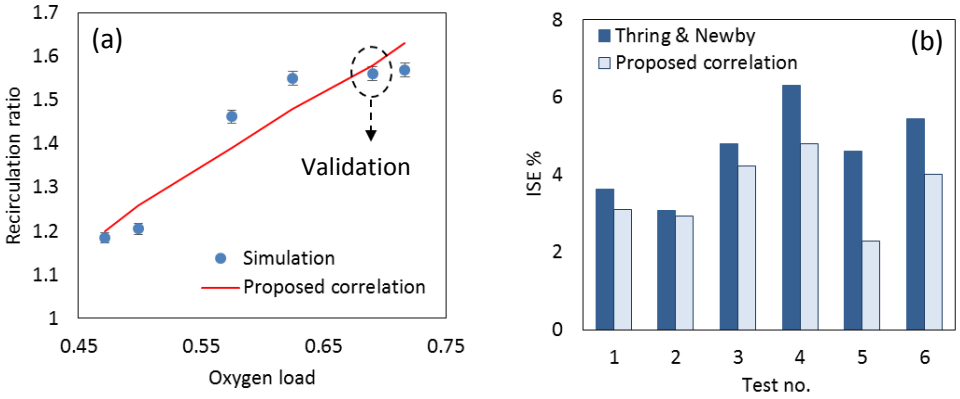

Figure 5-5. a) Estimates of the recirculation ratio for various oxygen loads; b) Comparison of ISE between the proposed correlation and Thring and Newby's correlation

According to Figure 5-5.b, the proposed correlation reduces the ISE of the ROM in predicating temperature and carbon conversion, compared to the case of using equation (5-2) that is based on a fixed recirculation ratio. The decreased percentages in ISE compared to Thring and Newby's method (Figure 5-5.b) correspond to 0.2-1.4 percentage points and 10-60 K of improvements in predicting carbon conversion and outlet temperature, respectively.

5.4 Chapter summary

A sensitivity analysis has been performed on the ROM to obtain insight regarding the impact of different inputs such as design (operational) variables and reactor network parameters on the ROM's performance. This analysis has shown that the major input parameters affecting the carbon conversion, H_2/CO ratio and temperature profile are the oxygen flowrate and the recirculation ratio. According to the results, other input or design parameters such as the jet angle, particle size and kinetic rates have been shown to have a secondary effect on the operation of the gasification unit studied in this work. Moreover, this chapter investigated the variability in the ROM's key outputs in the presence of uncertainty in the feed and model parameters, i.e., the volatile percentage of the fuel, solid particle diameters, angle of multi-phase flow jet and recirculation ratio. These parameters affect the feedstock's properties and the mixing/laminar flows within different zones of the gasifier. Insights gained from the uncertainty quantification study revealed significant variability in the conversion, peak temperature and steam molar percentage in the syngas; while the dry syngas composition does not seem to be significantly affected by the uncertainty of the parameters considered. The variability of peak temperature may result in unexpectedly high temperatures and stresses due to thermal cycling that can damage equipment with associated safety hazards in combustion zone of the gasifier. Furthermore, a new correlation for estimation of the recirculation ratio in the ROM's reactor network has been presented in this chapter. The proposed correlation improves the well-known method of Thring and Newby for jet-flow recirculation by adding a term that takes into account the changes in the feed streams (multi-phase jet and secondary flows) on the recirculation. The results indicated an improvement in the ROM's potential to predict experimental tests compared to a fixed recirculation ratio with the widely-used method of Thring and Newby. This feature enhances the prediction capabilities of the reactor network, especially in dynamic simulations where the inlet flowrates may change over time, e.g., for load-following power plants. The next chapter presents dynamic simulation of CanmetENERGY's pilot-scale gasifier using a ROM.

Chapter 6
Dynamic Simulation

The complexity and high integration of unit operations in Integrated Gasification Combined Cycle (IGCC) power plants render it challenging and expensive to make IGCC plants flexible [79]. The responses of an IGCC's unit operations to disturbances and the interactions between the units can lead to undesired fluctuations which may drastically affect the operability, availability and efficiency. It is therefore essential to study the dynamic performance of IGCCs as it provides insights that can lead to improvements in start-ups, set-point tracking and handling of disturbances, e.g., feed composition variability and load changes. The aim of this chapter is to extend the prediction capabilities of the ROM to consider the transient behaviour of the gasifier, assess its prediction capabilities with respect to experimental data, and study the dynamic performance of the gasifier under different scenarios. The structure of this chapter is as follows: Section 6.1 describes the assumptions and implementation methodology used to solve the model. Sections 6.2 and 6.3 presents the validation of dynamic ROM for steady-state and transient conditions, respectively. The performance of the gasifier during load following and co-firing are discussed through dynamic simulation of the gasifier in Sections 6.4 and 6.5, respectively. The results presented in this chapter have been submitted in the following paper:

> Sahraei MH, Duchesne MA, Hughes RW, Ricardez-Sandoval LA. Dynamic reduced order modeling of an entrained-flow slagging gasifier using a new recirculation ratio correlation (submitted for publication).

6.1 Assumptions and implementation methodology

In order to implement the dynamic ROM, the reactor network, partial differential equations (PDEs) and respective sub-models considered in the dynamic ROM were implemented in MATLAB®. In setting up the conservation equations for each zone, the following assumptions have been made:

- All moisture leaves the petroleum coke during drying.
- The leftovers of char during devolatilization are carbon and ash.
- Devolatilization reactions are assumed to be instantaneous reactions (due to high temperatures within gasifier).

- Particles are fully dried before leaving JEZ1.
- An average gas density is considered for each reactor zone.
- No pressure drop is accounted for in the solid particles.
- Gas-wall friction and heat loss only occur in the outer layers of the reactor network, i.e., ERZ2 and DSZ.
- Due to low amount of nitrogenous pollutants, the related reactions are neglected in dynamic ROM.
- The particle-wall radiation term is removed in dynamic ROM because of convergence difficulties.

The method of lines was used to solve the system of non-linear equations. Accordingly, the one-dimensional spatial domain was discretized using centered finite differences to transform the PDEs into a set of ordinary differential equations (ODEs). The ODE solvers available in MATLAB suitable for solving stiff problems have been employed in this work, i.e., *ode15s*. A step-by-step procedure has been used to integrate each zone of the reactor network in MATLAB. This procedure is as follows, with time denoted by the letter t: at $t = 0$, the multi-phase flow enters the JEZ-1; since the gasifier is assumed to be species-free at the initial condition, a time interval is needed for the materials to pass through the JEZs and circulate via the ERZ-2. To account for this, a time constant (τ) has been introduced to the reactor network in the dynamic mode. This parameter (which depends on the residence time of particles) is the time needed to have the effect of recirculation streams on the boundary conditions of the JEZ-1. In the present analysis, $\frac{\tau}{2}$ represents the time needed for the unreacted particles to pass through the JEZ-1 and JEZ-2. Therefore, the JEZ-1, JEZ-2 and ERZ-1 are the only zones of the reactor network integrated in the solver during $t < \frac{\tau}{2}$; consequently, ERZ-2 is integrated to the reactor network at $t = \frac{\tau}{2}$. Throughout $t < \tau$, it was assumed that there are no materials in the DSZ; thus, this zone in the reactor network is integrated when multi-phase flow exists at the top section of the gasifier, i.e., $t \geq \tau$. This procedure reduces the number of equations that need to be solved during $t < \tau$, which subsequently decreases the computational costs. Note that the step-by-step approach is only used for the time interval of $t = [0, \tau]$ to integrate zones of the reactor network in the ROM.

6.2 Steady-state results of dynamic ROM

To evaluate the response of the dynamic ROM when approaching a steady-state condition and assess the effect of the step-by-step approach in solving the model, the dynamic simulation of test 5 of Table 5-3 was considered. To perform the dynamic simulation, the following considerations have been made for the initial conditions: 1) the initial temperature along the gasifier was set to the start-up temperature following system pre-heating with natural gas, i.e., 1,000 K, 2) the initial composition along the gasifier's axial length was set to zero except for the boundary condition which has been calculated based on the inlet flowrates, and 3) the time constant parameter of the reactor network (τ) was set to 1 second.

The results obtained from the dynamic ROM for maximum and outlet temperatures, and molar compositions are presented in Figure 6-1. According to this figure, the behaviour of the dynamic model can be divided into two periods. Note that in the present analysis, peak temperature (T_{max}) is defined as the highest temperature inside the gasifier at steady-state. At $t< \tau$, the multi-phase flow coming from the ERZ-2 has no effect on the JEZ-1. Since the ratio of oxygen to volatiles is high, the temperature increased within the JEZ; therefore, the temperature at the end of the JEZ-2 was higher than the peak temperature at $t < \tau$ (Figure 6-1.a). At $t> \tau$, the recirculated gases influence the boundary conditions of the JEZ-1. As shown in Figure 6-1, the effect of the hot recirculated gas was immediately observed on the peak temperature (which is located at the beginning of the gasifier) compared to temperatures at the endpoints of the JEZ-2 and the DSZ (sampling probe). Furthermore, the results of dry gas molar composition at the DSZ's outlet (Figure 6-1.b) showed that the gas composition has a slower response to that observed for the temperature profile. Accordingly, the composition and temperature reached steady state (i.e., deviation of less than 1 K for temperature and 0.01 percentage points for composition) after 18 and 10 seconds, respectively.

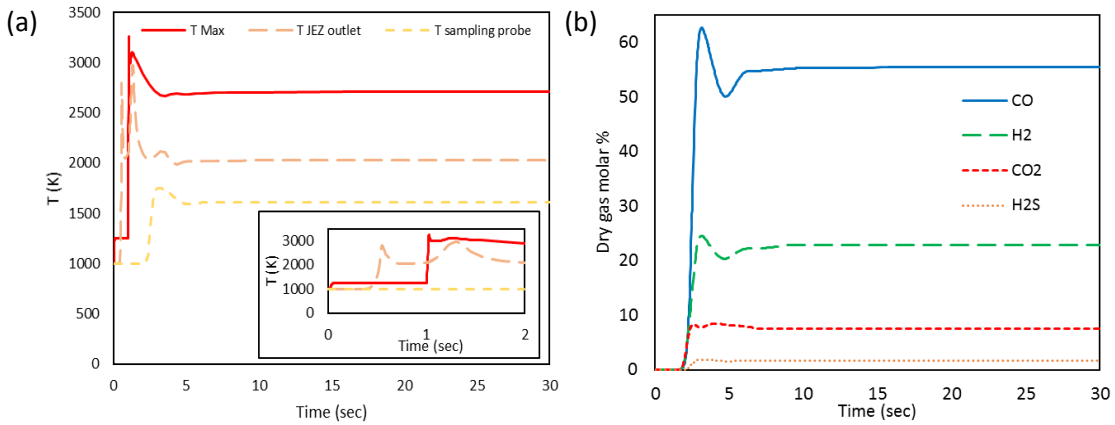

Figure 6-1. Transient responses for test 5 using the dynamic ROM: a) Gas temperature; b) Composition at the DSZ's outlet (gasifier sampling probe)

The results at the steady-state condition for the dynamic ROM and experimental test at the sampling probe are presented in Table 6-1. As shown in this Table, the dynamic ROM can predict the steady-state results of the experimental test. The required computational time to achieve steady-state results at t=30 seconds with the step by step approach was 6.5 minutes (Core i7, 3.4 GHz with 8 GB of RAM).

Table 6- 1. Experimental data and dynamic ROM simulation results test 3

	Outlet temperature (K)	Carbon conversion (%)	Dry gas molar fraction			
			CO	H_2	CO_2	H_2S
Exp. test	1580	90.0	55.65	25.77	6.42	1.34
ROM	1605	90.0	55.50	22.84	7.48	1.69

6. 3 Dynamic validation: sinusoidal changes in the feed

This case study examines the transient performance of the gasifier in the presence of changes in the feeds' flowrates. This is a typical scenario in power plants that occur during plant start-up, shutdown, or even during normal operation [80], [81]. This case-study considers transient experimental data of petroleum coke gasification, which will be used here to validate the dynamic response of the ROM. The respective flowrates of petroleum coke, oxygen and steam (used in dynamic simulation and experimental tests) are presented in Figure 6-2. The fuel's flowrate obtained from experimental measurements followed an oscillatory behaviour with considerable noise [82]. Therefore, a sinusoidal signal which fits the flowrate measurements for the fuel was used as the input for the dynamic ROM. Figure 6-2 also indicates that the

steam was increased by almost 10% in a ramp fashion while the oxygen flowrate was reduced by 5% during the experimental test. As the scatter level in the oxygen and steam flowrates is low, the experimental values reported for this test were directly used in the dynamic ROM for validation.

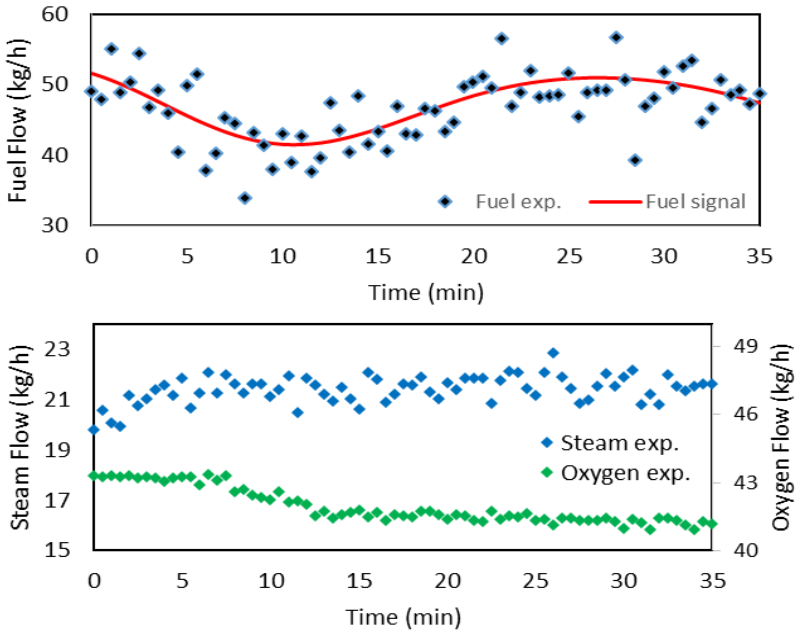

Figure 6-2. Experimental data and fuel feedstock signal for the dynamic validation of the ROM

The experimental data and results of the dynamic ROM are presented in Figures 6-3 and 6-4. As shown in Figure 6-3.a, the dry gas composition profiles of the key components in the ROM followed the experimental data in a sinusoidal fashion, which is due to the oscillatory changes considered in the fuel flowrate. The molar fractions predicted by the ROM for CO and CO_2 varied by -6.4% and +2.1% at the end of the test when compared to the initial operation. This is due to the addition of steam and the water-gas shift reaction. Furthermore, the results for the H_2 molar fraction presented a smaller deviation during the test (less than 1%). According to Figure 6-3.b, the maximum thickness of slag (at the sampling probe) fluctuated between 3 to 3.4 mm, while the slag flow was 1.9-5.0 g/s. Since the ash content of petroleum coke is low, 4.6 wt %, a thin layer is predicted by the ROM. Note that the slag thickness could not be measured during experiments since it is very thin, reacts with refractory and is porous.

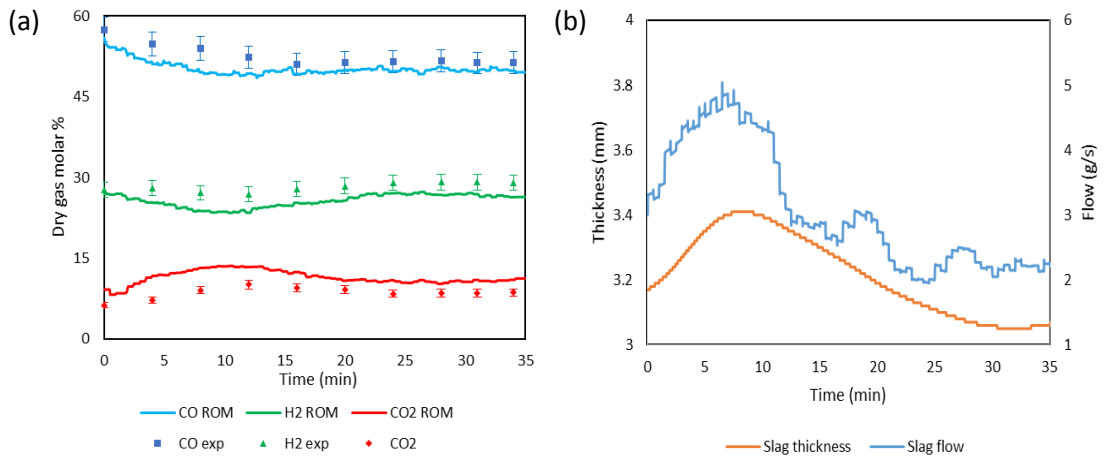

Figure 6-3. Dynamic validation of the ROM: a) Molar gas composition; b) Maximum slag thickness and slag flow

Figure 6-4 presents the thermocouple measurements at different locations on the gasifier's wall, as well as the ROM's predicted centerline and wall temperatures, over time. Based on this figure, the ROM predicts the changes in wall temperature with reasonable agreement (±0.01-3%) with respect to the measurements. The average carbon conversion based on the mass balance of experimental data and dynamic simulation with the ROM were 88.3% and 86.7%, respectively.

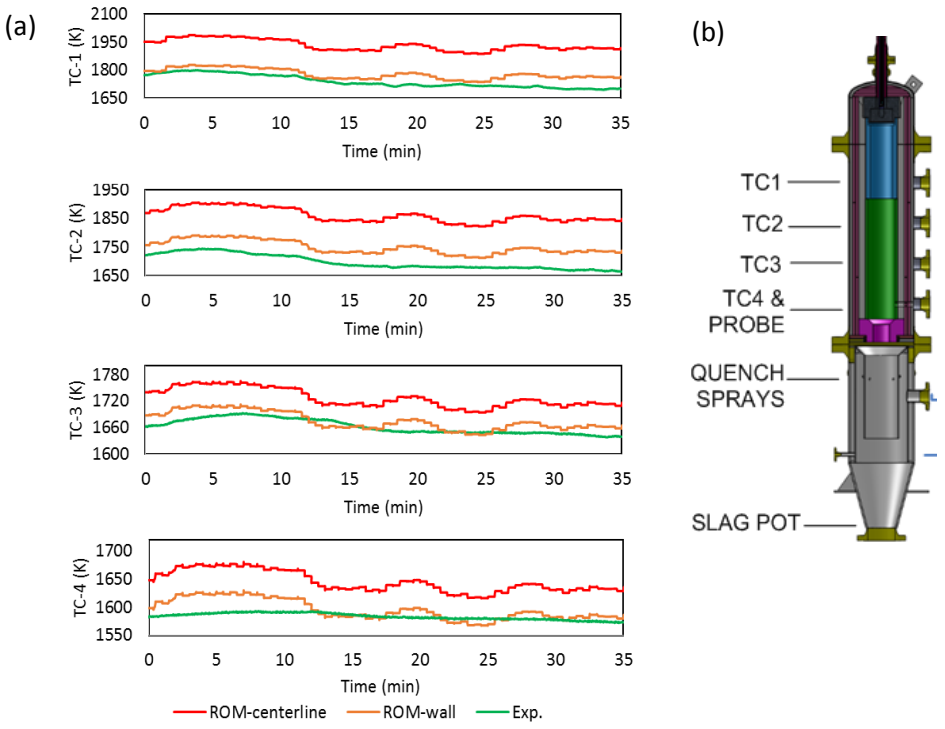

Figure 6-4. a) Dynamic validation of the ROM: wall thermocouple measurements and centerline/wall temperatures from ROM simulation; b) the location of thermocouples

6.4. Load following

Load-following power plants are designed so that they can adjust their power generation during operation based on the electricity demands and the variability of electricity supply from renewable energy sources [79]. Due to the high integration and operating cost of an IGCC power plant, the minimum partial load is restricted to 60-80% of the plant's capacity [83]. However, a combustion-based power plant can operate down to a minimum load of 10-30% [83]. Moreover, the ramping rate of an IGCC is also restricted to a maximum ramp of 5% per min [79] as the changes in the operating conditions and power cycling may limit the life span of IGCC facilities, particularly the refractory of the gasifier [83]. Based on the nature of the gasification process and the flexibility of the gas turbine, ramping up is generally slower than ramping down. In the present case study, the changes in the operating conditions of CanmetENERGY's gasifier are investigated during one cycle of load following, i.e., reduction of load from peak to 60% with a ramp rate of 5% per min and increasing it back to the peak value at a ramp rate of 3.3% per min.

The material used in the construction of CanmetENERGY's refractory is mullite which has a high temperature stability, strength and creep resistance with maximum temperature use of 1,973 K [84]. Accordingly, this temperature has been considered as an operational constraint within the present load-following scenario. To perform the simulation, the operating condition of test 3 shown in Table 4-4 is slightly modified to achieve a carbon conversion of 95%, i.e., this is the condition at which the gasifier is at its nearly full capacity to produce syngas. Note that increasing the oxygen and steam flowrates to achieve 99% carbon conversion resulted in temperatures above the refractory's maximum working temperature. Thus, during the load-following scenario, the O_2/C and H_2O/solid ratios were linearly adjusted to maintain the initial ratios and avoid having the refractory temperature exceed the thermal constraint. Since online measurements of the slag viscosity and thickness are not available, the CaO/ash weight ratio was fixed at 21% by hypothetical injection of a fluxant to keep the viscosity of the slag to less than 25 Pa·s. Note that in the present work, pure lime (CaO) was considered as a fluxant.

The results for the present scenario are depicted in Figure 6-5. Although oxygen and steam flowrates were adjusted during the load cycle, no significant changes were observed in the dry gas molar percentages (Figure 6-5.a); H_2 and CO molar percentages were changed by 0.49 and 0.78 percentage points, respectively. However, the temperature distribution varied during the load cycle. According to Figure 6-5.b, the temperature of the refractory in the ERZ-2 and at the DSZ outlet were reduced by 134 and 106 K during partial load, respectively. As expected, the dry gas flowrate decreased when the fuel's load was reduced. Accordingly, the average residence time of the solid particles increased from 1.6 to 2.7 seconds during the load reduction. This caused the carbon conversion to increase by roughly 1% though the reaction rates were reduced due to the reduction in temperature. This also resulted in a higher cold gas efficiency (+4.6%), based on the higher heating values (HHV), when the system operated at a lower load.

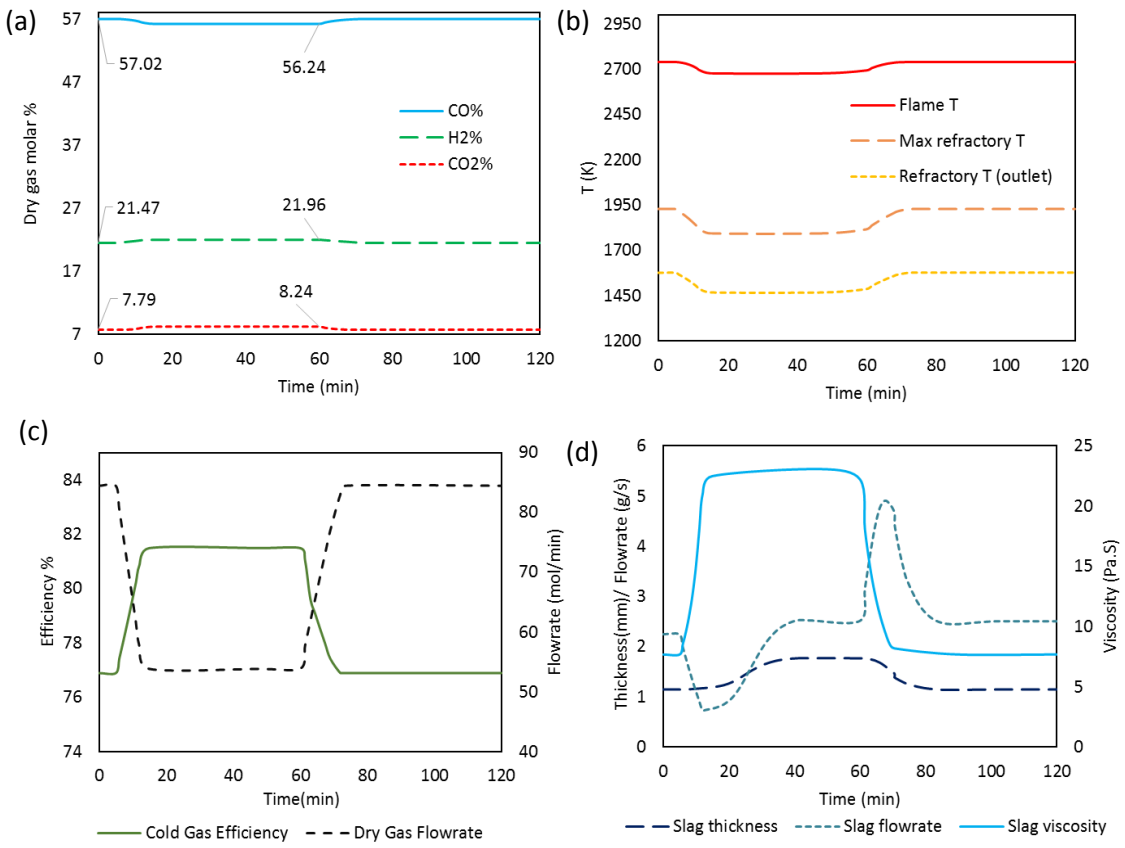

Figure 6-5. Load-following scenario: a) Dry gas composition; b) Temperatures; c) Cold gas efficiency and syngas flowrate; d) Slag response

The dynamic response of the slag at the outlet is illustrated in Figure 6-5.d. The slag viscosity was inversely proportional to the changes in the refractory temperature while it remained below 25 Pa·s during the lower load period. Moreover, thickness of the slag was increased during the lower load period as particles had higher viscosity in the gasifier, despite the deposition rate being reduced. Due to high viscous forces, the movement of slag on the refractory is slower than the gas and solid particles that do not stick to the refractory or slag layer. Therefore, the dynamics of slag flow and thickness were accompanied by a lag time. The response of slag flow can be explained by the changes in the viscosity and thickness. At the time of load change (t=5 min), the flow was substantially decreased as the viscosity was higher; however, it started to rise once the thickness increased (t=15 min). Although the transient changes of slag flow is significant, the flow was slightly increased during the lower load. Notably, the highest flow of slag was observed during the increase of load. For that reason, there may be a higher risk of blockage during the

transient phase from reduced load to peak load, particularly if the temperature drops or the fluxant rate is reduced.

6.5 Co-firing

Co-firing of different solid fuels can be used to maintain continuous operation of an IGCC power plant during peak load. Co-firing increases the availability of the fuel and may also be used to adjust the efficiency of the plant, production costs and environmental impacts. To assess the performance of the gasifier during co-firing, mixing Alberta petroleum coke and Genesee coal was considered in this case-study during the peak load of the system. The feedstock was linearly changed in a ramp fashion (3.33% per min) from petroleum coke feed to a 60:40 blended feed of petroleum coke and coal. The rest of the operating conditions were the same as that described for the load-following scenario, including linear adjustment of the O_2/C and H_2O/solid ratios to maintain the initial ratios.

The results of co-firing obtained from the dynamic ROM are presented in Figure 6-6. In order to obtain a suitable fluxant flowrate that maintains the viscosity of the unit below 25 Pa·s, this case study was first performed at different weight percentages of CaO by injection of fluxant, i.e., 10 to 20%, with respect to the mixing blend of fuel. According to the results shown in Figure 6-6.a, 20 wt.% CaO is suitable for co-firing of the 60:40 blend of petroleum coke and coal to maintain a slag viscosity below 25 Pa·s at the sampling probe's temperature, i.e., 1545 K, and was therefore used for the analysis that follows. Figure 6-6.b shows the changes in dry gas molar percentages of the syngas in the DSZ outlet. Since the coal has less fixed carbon and more volatiles than the petroleum coke, addition of coal increased the H_2 content by 7.15% while the CO was reduced by 7.7%. Similarly, the temperature inside the gasifier was reduced during co-firing as the heating value of coal is lower than the heating value of petroleum coke. As shown in Figure 6-6.c, the flame temperature decreased by 135 K even though the O_2/C ratio was kept constant during the test. The refractory temperature at the outlet of the DSZ (i.e., the gasifier sampling probe) was reduced from 1,600 K to 1,545 K, while the maximum refractory temperature (1,952 K) remained below mullite's temperature limit (1,973 K) during the test.

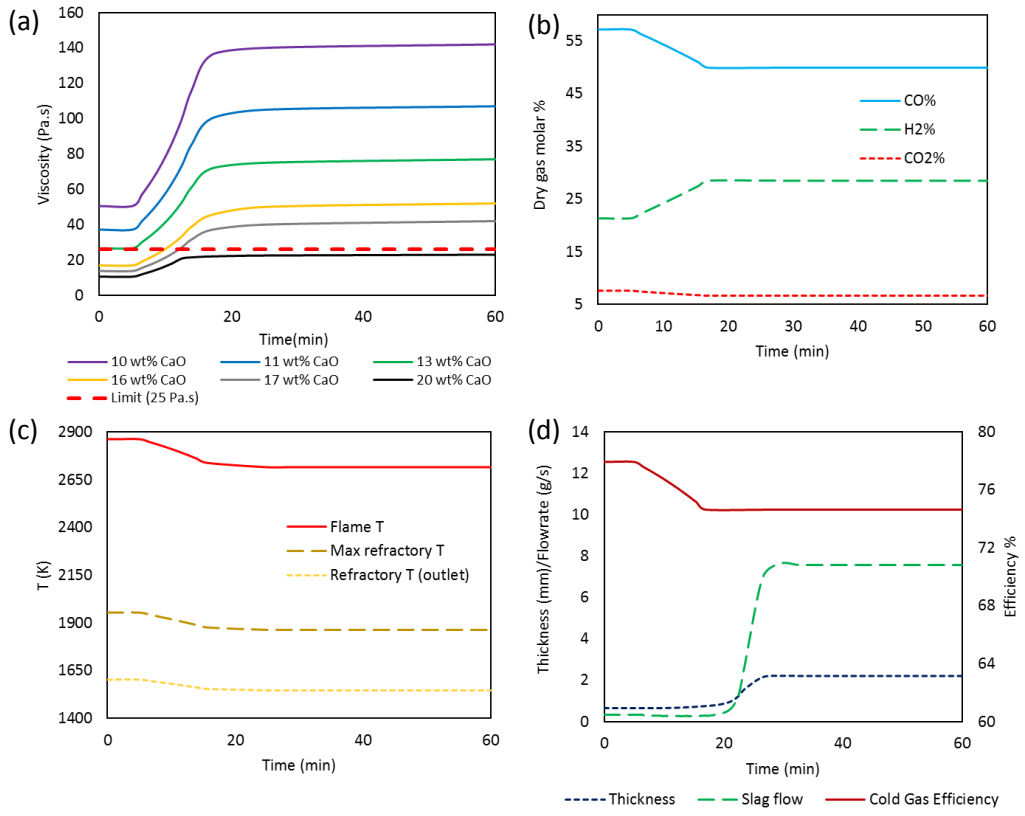

Figure 6-6. Co-firing scenario: a) Viscosity with different wt. % of CaO in the ash, b) Dry gas composition; c) Temperatures and d) Cold gas efficiency; slag response (b, c and d are with 20 wt.% CaO in the ash)

Figure 6-6.d illustrates the changes in the cold gas efficiency (based on HHV) of gasifier during co-firing. Despite the fact that the heating value of dry syngas composition was increased, due to increase in hydrogen content of dry syngas, the cold gas efficiency of the gasifier was decreased by 3.3 percentage points. The factors affecting the drop of cold gas efficiency are: 1) reduction of carbon conversion from 95% to 93.6%, which led to a lower dry syngas flowrate at the outlet, and 2) increase of ash content during co-firing, which decreased the available carbon for syngas production. Furthermore, the slag thickness and flowrate at the outlet exhibit significant lag times (Figure 6-6.d). The slag thickness was increased from 0.68 to 2.22 mm as the coal has a higher ash content. Changes in the temperature increased the slag viscosity and therefore resulted in a slight reduction of flow at the beginning of the transient phase (6 to 12 min). However, the slag flow was significantly increased (during the time interval of 20 to 30 min) when the slag thickness increased. Overall, the continuous flow of the slag and its low thickness on the refractory suggest that co-firing may not cause blockage in the gasifier.

6.6 Chapter summary

This chapter analyzed the dynamic response of CanmetENERGY's gasifier by means of using a dynamic ROM. According to the results, the proposed dynamic ROM is able to predict with relatively high accuracy the changes in temperature and syngas composition observed at the gasifier's sampling probe. The ROM was also tested during a cycle of load-following and co-firing. For these case-studies, fluxant was injected to maintain a slag viscosity below 25 Pa·s. The results indicated that the syngas composition varied little during load changes (0.49-0.78% for each component); however, significant changes in the syngas composition were observed during co-firing (i.e., approximately 7% for CO and H2). Furthermore, variations in the carbon conversion and residence time of particles affected the gasifier's cold gas efficiency during load reduction (+4.6%) and co-firing (-3.3%). The variability of slag flow was also investigated in both cases. Based on the results, the slag layer thickness increased during load reduction case and during the addition of coal in the co-firing case, but with a lag time. The slag flow only increased when increasing the coal content in the co-fired feed and remained almost unchanged during load-following case. Furthermore, the slag response demonstrated that the risk of slag blockage may be higher during load increments; thus, the system's temperature and fluxant flowrate must be accurately monitored during such events. The next Chapter presents scale-up modeling and the results of the steady-state for a commercial-scale gasifier with a multi-element feed system based on the design of GTI Rocketdyne gasifier.

Chapter 7 Scale-up modeling

To accelerate the development of compact multi-element injector gasifiers, insights regarding the design and operability of these systems are needed through mathematical models to ensure an adequate performance in different operating conditions. This chapter aims to propose a ROM for a compact commercial-scale gasifier with a multi-element injector feed system based on the insights and experiences gained through the reduced order modeling of CanmetENERGY's pilot-scale gasifier. The commercial-scale gasifier is not yet built and no detailed modeling/experimental study has been reported for this type of systems in the literature. This study intends to illustrate the performance, feasibility and operating limitations of the system under scenarios which are likely to occur for the gasifier. The ROM is initially used to investigate particle residence time, carbon conversion and cold gas efficiency. Next, the performance of the gasifier is explored with different operating pressures, various numbers of injectors and non-uniformity in fuel distribution among the nozzles. Finally, a sensitivity analysis is performed to identify the parameters which are most important to the accuracy of the model, and to indicate the effect of design parameters on the performance of the gasifier. The structure of this chapter is as follows: Section 7.1 describes the gasification system and the multi-element feed injector proposed by GTI. Section 7.2 describes the reactor network proposed for the gasifier based on CFD simulation of a coal combustor. The modelling assumptions and the approach used to implement the commercial-scale ROM is presented in Section 7.3. The results of the case-studies for operating pressure, number of injector and non-uniform fuel distribution are presented in Section 7.4. The results of sensitivity analysis is presented in Section 7.5. The results presented in this chapter have been submitted in the following paper:

> Sahraei MH, Duchesne MA, Boisvert PG, Hughes RW, Ricardez-Sandoval LA. Reduced order modeling of a commercial-scale gasifier using multi-element injector feed system (submitted for publication).

7.1 Gasification system

The compact gasification system modeled in this chapter is based on the system developed by GTI. It is a single-stage, pressurized, downward-fired entrained-flow gasifier (see Figure 7-1) that is anticipated to accommodate a range of solid fuels. According to a patent presented for a compact high efficiency gasifier and status update reports on GTI's compact gasifier development, the diameter and length of the

commercial-scale gasifier are expected to be 1 and 4.6 m, respectively [85], [86]. Some of the state-of-the-art design features of this type of gasifier include: 1) a high pressure solid pump and dense phase flow splitter which enables distribution of pulverized fuel particles to the gasifier at high pressure, 2) a rapid spray quenching that enables cooling up to 600 K prior to passing gas to a cyclone, 3) a ceramic matrix composite liner actively cooled by a membrane which increases the life of the gasifier's wall (shown in Figure 7-1) a rapid mix injector design that uses a multi-element injector to enable a high conversion of solid fuel in a short residence time. Note that the focus of the present work is on the feed system and the other design features are not considered in the ROM.

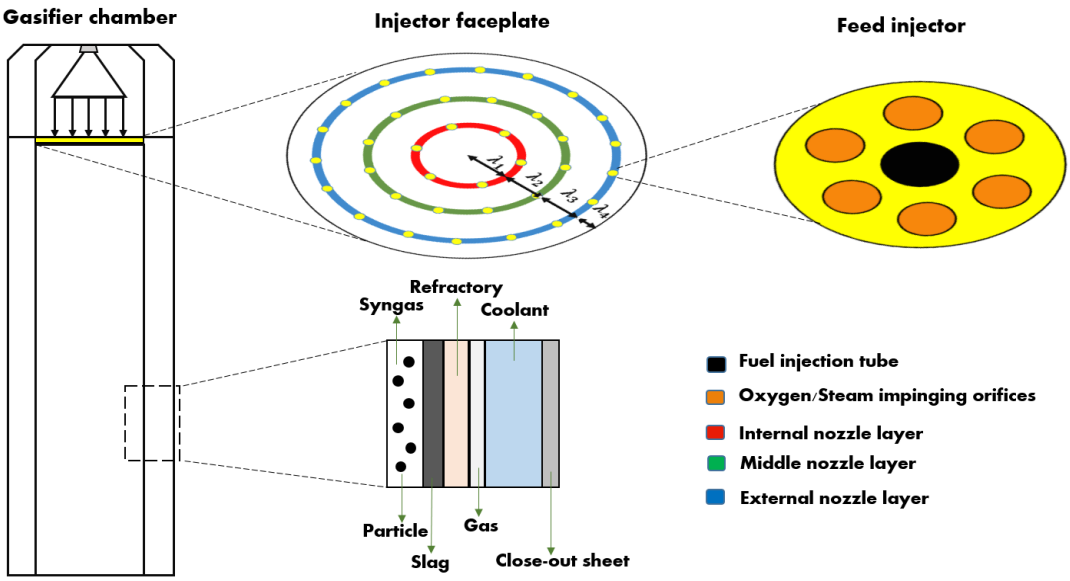

Figure 7- 1. Schematic of the gasifier system modeled in this study (with a 36-element injector)

A multi-element injector feed system rapidly mixes the fuel with oxygen/steam and quickly disperses the feed across the reactor's cross-section. This increases the mixing ratio of fuel and oxidizing agents (oxygen and stream) and reduces recirculation within the gasifier. The feed system for GTI's compact gasifier includes a solid pump which takes dried pulverized fuel from atmospheric pressure and delivers it to the multi-element injector at pressures up to 69 bar [87]. As shown in Figure 7-1, each feed nozzle has a fuel injection tube (surrounded by six oxygen/steam impinging orifices) that is sized to inject up-to 100 TPD of dry fuel to the gasifier [88]. Therefore, at commercial scale the gasifier requires 18 and 36 nozzles to inject fuel for the capacities of 1,200-1,500 TPD and 2,400-3,000 TPD, respectively [87].

Figure 7-1 illustrates the nozzle configuration proposed by PWR for a design with 36 injectors [87]. The nozzles are placed on three ring layers, where the thickness of each layer is a decisive parameter in the design of the injector. For instance, a small thickness results in a small distance between the nozzles which could increase the flame temperature and cause operational difficulties.

There is no experimental data available for this type of gasifier, however based on initial assessments in technology status update reports and the insights gained from the operation of similar systems, a set of operational constraints and limitations have been taken into account to avoid infeasible operational regimes. The following considerations have been considered in the present study:

- Momentum ratio of oxygen to fuel of 2-5 to promote high mixing.
- Particle residence time of 0.5 second [89].
- Maximum operating pressure of 69 bar [86].
- Maximum temperature near the water-cooled injectors of 1,470 K.
- Peak temperature (or flame temperature) of approximately 3,000 K [18].

7.2 Reactor network

A ROM for an entrained-flow gasifier requires a reactor network composed of PFRs and continuous CSTRs to model the zones formed inside the gasifier. As explained in Chapter 3, a method to design a reactor network is through CFD simulation since the streamlines, composition and temperature profiles of CFD can provide good approximations for the boundaries and geometric parameters. Currently, the authors do not have CFD simulation results for a gasifier with multiple feed nozzles. Therefore, CFD simulation result of a similar system, i.e., combustor with a multiple injection nozzles, was used to study the flow field created by multiple feed nozzles. The modeling details of CFD simulation are presented in Appendix A.

Velocity vectors obtained by multi-element injector combustor CFD simulation are presented in Figure 7-2. The combustor's flow field is divided into three sections, i.e., top, middle and bottom sections. As shown in Figure 7-2, the slurry fuel and oxygen were injected at the top of the combustor through 16 nozzles. Each nozzle consists of an inner fuel injection tube and outer concentric oxygen-enriched flue gas injection tube. 20% of the total injected gases are injected through the porous burner face as a cooling mechanism.

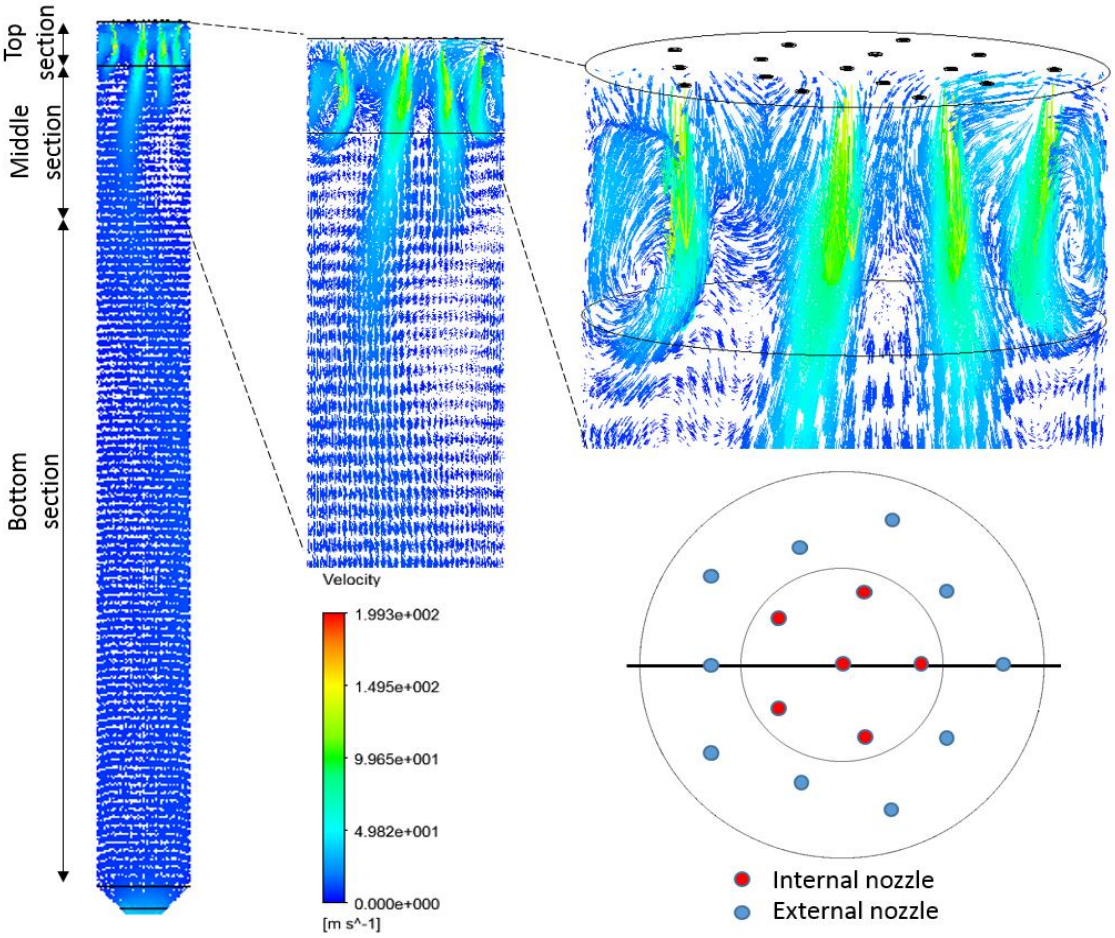

Figure 7-2. Streamlines at a cross-section inside the combustor, with the bottom right image showing the cross-section plane from above

The orifices around the fuel tube directed the oxygen towards fuel's inlet point. The multi-phase jets were then expanded into the combustor chamber through regions which are typically referred to as the jet expansion zone (JEZ). Due to high momentum of the jet and difference between the diameters of feed nozzle and burner, a portion of the flow coming from JEZ recycled back towards the feed nozzles, while the rest of the stream passed into the middle section of the system. This behaviour was observed for all of the nozzles (see Figure 7-2), however the recirculation flow of nozzles closer to the wall (external nozzles) was higher compared to nozzles closer to the centerline (internal nozzles) of the combustor. Accordingly, the recirculation regions were divided into the internal recirculation zone (IRZ) and external recirculation zone (ERZ). In the middle section, the jet flows coming from the top section were merged together and formed a larger jet stream. As the larger jet approached the wall, some parts of the flow recycled towards the intersection of the top and middle sections, while the rest proceeded towards the outlet of the combustor

through a laminar plug flow region in the bottom section. This region is typically referred to as down-stream zone (DSZ).

Due to similarities in the design of the feed system for the combustor simulated by CFD and the compact gasifier being modeled by the ROM, it was assumed that they have similar flow structures. A reactor network is proposed to account for the flow structures in each section of the gasifier (Figure 7-3).

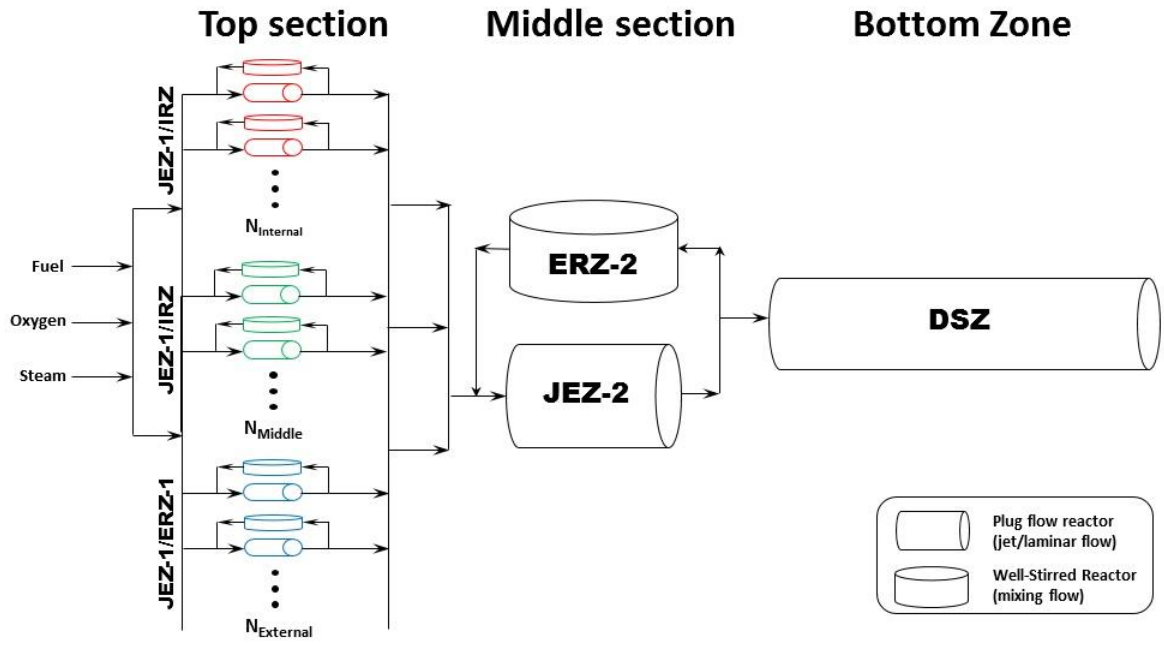

Figure 7-3. The proposed reactor network for the multi-element injector gasifier

As shown in this figure, the nozzles in the top section are classified into internal, middle and external nozzles. To account for the jet and mixing zones of each nozzle, two reactors are implemented for each nozzle: a conical PFR to simulate the JEZ (JEZ-1) and a CSTR to simulate the IRZ (IRZ) or ERZ (ERZ-1). The differences between the reactors associated to internal, middle and external nozzles are the jet angle, recirculation ratio, size of reactors and heat loss. Since a JEZ and ERZ are also expected in the middle section, two reactors are used to account for this section: a conical PFR for JEZ-2 and a CSTR for ERZ-2. Moreover, a PFR is used to simulate the plug-flow condition of the DSZ in the bottom section. Due to the uniform distribution of feed among the nozzles and high velocity jet flow in the top section of the gasifier, it is likely that no significant heat and mass are transferred among the recirculation zones of each nozzle. Therefore to simplify the analysis, transfer of mass and heat among the recirculation zones was not

considered in the ROM. The geometry parameters for the different zones of the gasifier (presented in Table 7-1) are calculated based the following procedure:

- The inlet diameter of the JEZ-1 is calculated based on the diameters of the fuel tube and oxygen orifices proposed in [88], i.e. 12.7 mm.
- The lengths of the top and middle section were assumed as 20% of the gasifier's length.
- The length of top section was assumed as half of the length of middle section
- The cross-sectional area of each JEZ-1 outlet is equal to its layer cross-sectional area divided by the number of nozzles in the layer.
- The jet angle of each nozzle was calculated based on the corresponding layer thickness and JEZ-1 length.
- The inlet diameter of the JEZ-2 is calculated by adding the outlet diameter of the JEZ-1s located in an axial plane at the outlet of the top section.
- The outlet diameter of the JEZ-2 and diameter of the DSZ are set to the gasifier's diameter.

One the most important parameters for a reactor network is the recirculation ratio. This parameter is defined as the mass flow entering an IRZ/ERZ over the mass flow entering the corresponding JEZ. This parameter is one of the most uncertain parameters in a reactor network and can only be accurately calculated through the mass balance of CFD simulation. According to the multi-element injector combustor CFD simulation, the recirculation ratio of external nozzles seems to be higher than internal nozzles. Therefore, different recirculation ratios were considered for each set of nozzles. As the flow stability was not observed in the CFD simulation of the combustor, it was not used to calculate an estimate for the recirculation ratio. The current author proposed an empirical correlation to calculate the recirculation ratio for a confined jet based on the flowrates of the feed [90] (chapter 5). The correlation was derived by minimizing the ROM's mismatch (in terms of conversion and temperature) with respect to the experimental data obtained with CanmetENERGY's pilot-scale gasifier which uses a single injector. The proposed correlation improved the ROM's accuracy with respect to experimental data, compared to the method proposed by Thring and Newby which uses a fixed recirculation ratio for different flowrates. Since no correlation for the recirculation ratio of confined multi-element injector is available in the literature, the proposed correlation was used to calculate the recirculation ratio for each nozzle (Table 7-1).

Table 7-1. Geometry parameters of the reactor network

	18 element injector			36 element injector			
Gasifier diameter (m)	0.7			1			
Gasifier length (m)	4.6			4.6			
Fuel nozzle diameter (m)	0.012			0.012			
Section	Top Int. (λ_1)	Top Ext. (λ_2)	Middle	Top Int. (λ_1)	Top Mid. (λ_2)	Top Ext. (λ_3)	Middle
Number of injector	6	12	NA	6	12	18	NA
Nozzle layer thickness (m)	0.35	0.28	NA	0.30	0.25	0.3	NA
Wall-space,λ_4 (m)	NA	0.07	NA	NA	NA	0.15	NA
Recirculation ratio	0.95	1.04	0.26	0.53	0.75	0.98	0.28
Jet angle (deg)	14.3	15.8	7.8	10.5	12.3	15.8	12.6
Length (m)	0.32	0.32	0.83	0.32	0.32	0.32	0.83
IRZ/ERZ-1 diameter (m)	0.10	0.14	0.28	0.08	0.09	0.16	0.42

7.3 Assumptions and implementation methodology

In setting up the conservation equations for each zone, the following assumptions have been made:

- The accumulation terms are set to zero.
- All moisture leaves the petroleum coke during drying.
- The leftovers of char during devolatilization are carbon and ash.
- Devolatilization reactions are assumed to be instantaneous reactions (due to high temperatures within gasifier).
- Particles are fully dried before leaving JEZ-1.
- An average gas density is considered for each reactor zone.
- No pressure drop is accounted for in the solid particles.
- Due to low percentage of ash in petroleum-coke, no slag formation is considered for the steady-state ROM.
- Gas-wall friction and heat loss only occur in the outer layers of the reactor network, i.e., ERZ-1, ERZ-2 and DSZ.

As shown in Figure 7-1, the cooling liner adapts a slag layer on its interior surface. The slag layer consists of two phases: flowing and immobile layers. The flowing slag often has viscosity of below 25 pa.s [91]. To simplify the analysis, a flowing slag layer with viscosity of 10 pa.s was assumed which exchanges

heat through convection and radiation terms with multi-phase flow. To obtain the slag temperature for the heat transfer terms, the slag model adapted by Seggiani [69] was used to determine the temperature, i.e. 1880 K.

The governing equations and sub-models stated in Chapter 3 were solved using the finite difference method. The spatial derivatives were estimated on a spatial one-dimensional grid. Accordingly, the momentum transport was solved initially to calculate the velocities and pressure drop at each grid point by assuming an average gas density in each zone of the gasifier. The resulting velocity profiles were passed as inputs to solve for the mass and heat transfer equations simultaneously at each grid point inside the gasifier. To obtain the steady-state results, the spatial domain was discretized for the JEZ-1, JEZ-2 and DSZ reactors. The grid sizes of each reactor were selected based on a sensitivity analysis that was performed with different numbers of nodes so that the relative error of the velocity, temperature and conversion are less than 0.1%. Accordingly, a non-uniformly distributed grid size was obtained in the axial domain: 20 nodes for each JEZ-1, 40 nodes for the JEZ-2 and 40 nodes for the DSZ.

7.4 Case studies

7.4.1 Operating pressure

Most gasifiers operate in the pressure range of 10 to 100 bar [92]. Gasifying under pressure reduces the equipment size and the compression energy required for downstream units. The energy required for feed pumping and syngas compression reduces by 78% when the gasification is performed on 50 bar compared to operating pressure of 5 bar [92]. Moreover, the operating pressure usually depends on upstream and downstream unit operations. The operating pressure of GTI's compact gasifier is reported to be 69 bar [85]; however the testing of its feed system was conducted for lower pressures, down to 46 bar. To evaluate the effect of pressure on the performance of a multi-element injector gasifier with a throughput of 3,000 TPD, and to illustrate the operational feasibility of such a system, simulation of petroleum coke gasification was performed under three operating pressures: 20, 40 and 69 bar. The operating conditions and fuel properties used to model the gasifier are listed in Table 7-2. Note that a uniform flow distribution among 36 nozzles was assumed in this case study.

Table 7-2. Operating conditions and fuel properties

Flowrate (TPD)	Case I	Case II
Fuel	3,000	1,500
Oxygen ratio	2,795	1397
Steam	779	389
Nitrogen	600	300
Proximate analysis of fuel (*as received*)		
Ash	0.046	
Volatiles	0.127	
Moisture	0.005	
Carbon	0.822	
Ultimate analysis of fuel (*dry, ash-free)*		
Hydrogen	0.042	
Sulfur	0.061	
Nitrogen	0.018	
Oxygen	0.015	
Carbon	0.864	

The temperature and molar fraction profiles of the top section are presented in Figure 7-4. As shown in Figure 7-4.a-c, within each individual JEZ-1, the temperature initially increased sharply due to the combustion of volatiles/carbon and recirculation of hot gases. By depletion of oxygen, the heat required for endothermic reactions overcame the heat released by exothermic reactions and the temperature decreased as the gases moved toward the gasifier's outlet. Furthermore, the temperatures at the jet expansion and recirculation zones of the external nozzles were lower than middle/external nozzles, due to heat loss through the gasifier's wall. The highest peak temperature was observed in the JEZ-1s of internal nozzles; which was 3,085, 2,987 and 2,934 K for operating pressures of 20, 40 and 69 bar, respectively. The obtained peak temperature at 69 bar is consistent with the initial data reported for the peak temperature of GTI's compact gasifier, i.e., 3,000 K [18]. In the present work, the average residence time of particles was estimated by using the particle's velocity profile in the axial domain. At lower pressures, the average residence time of particles was decreased (shown in Table 7-3) and the particles were moving faster. As a result, the peak temperature was shifted towards the end of the JEZ-1s.

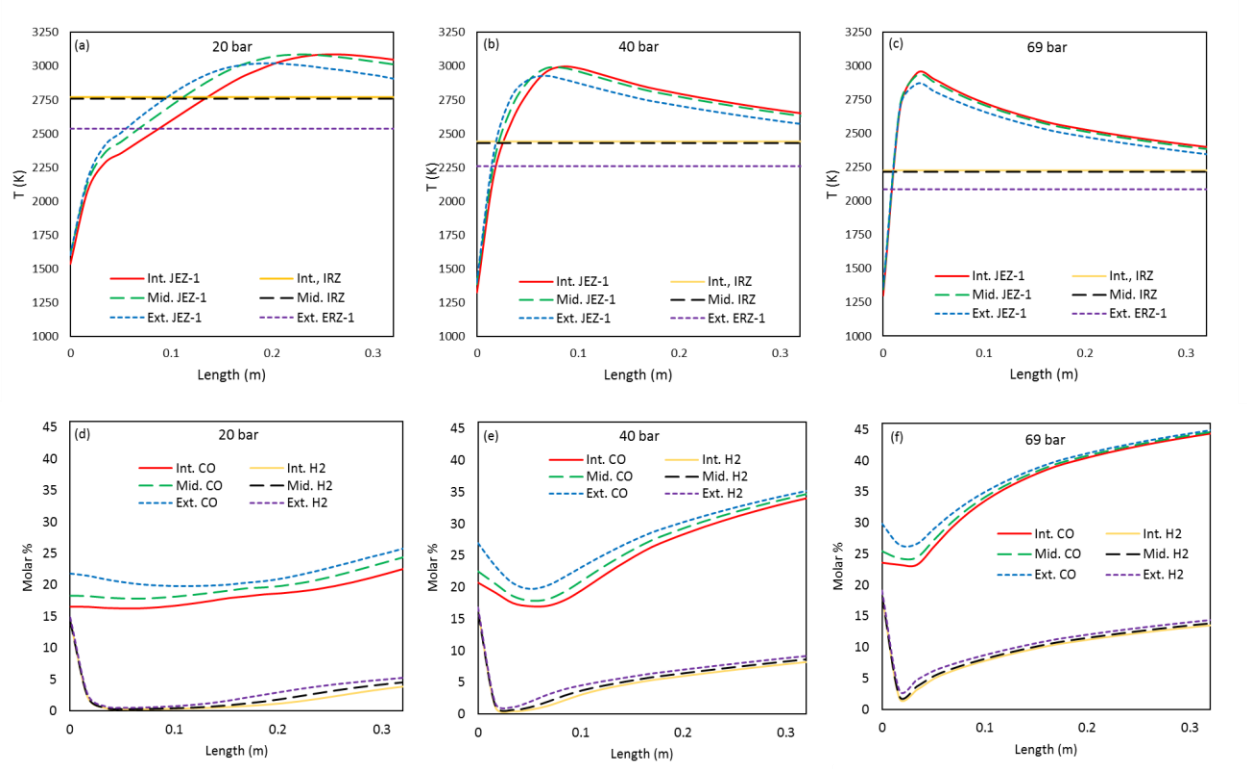

Figure 7-4 JEZ-1 results for simulations with different pressures: a-c) Temperature profiles;

The molar fraction profiles of CO and H_2 are presented in Figure 7-4.d-f. The concentration of these two species initially decreased at the beginning of JEZ-1s as they reacted with oxidizing agents (i.e., oxygen and steam) to produce H_2O and CO_2. After the particles passed through the combustion zone, the gasification reactions became dominant and the molar fractions of CO and H_2 increased as more syngas was produced. The size of PFRs used for JEZ-1s of external nozzle was higher than the internal/middle nozzles. Therefore, more carbon was converted to syngas in JEZ-1s of external nozzle. As a result, the molar fractions of these two species were higher in the JEZ-1s of external nozzles compared to the JEZ-1s of internal/middle nozzles. The temperature and molar fraction profiles for the middle and bottom sections are presented in Figure 7-5. Overall, at elevated pressure more fuel was converted to syngas as the partial pressures of reactants were higher and particles had longer residence times. As a result, the molar fractions of CO and H_2 were higher at the gasifier's outlet in the 69 bar scenario compared to the 15 and 40 bar scenarios.

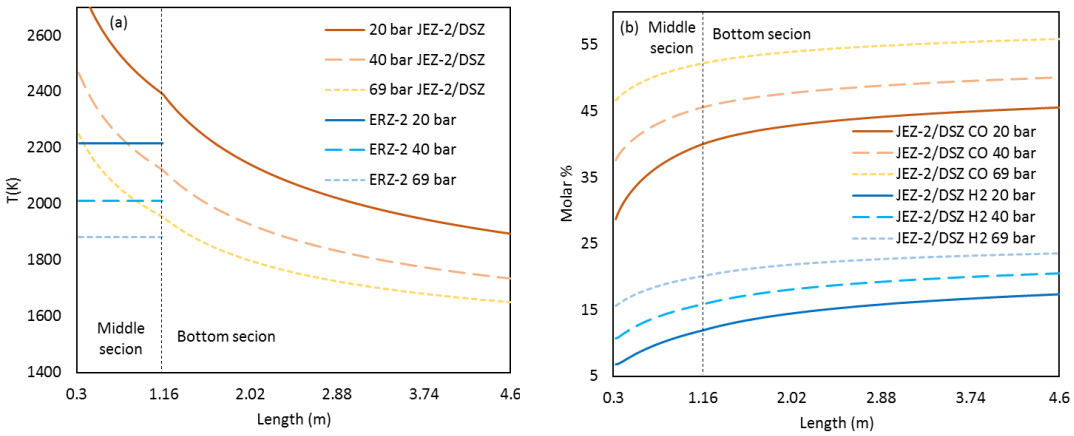

Figure 7-5. Middle and bottom section results for simulations with different pressures: a) Temperature profiles; b) Molar fraction profiles

A summary of the gasifier's performance with varied pressure is presented in Table 7-3. At 69 bar, a fuel conversion, cold gas efficiency (CGE) based on the higher heating values, and particle residence time of 99.7%, 83.7% and 0.52 s, respectively, were predicted by the ROM. These results are in agreement with the data reported for GTI's compact gasifier, i.e., a conversion of >99% and a CGE of 80-85% with a particle residence time of less than 0.5 s [18], [93].

As presented in Table 7-3, the residence time of particles was strongly affected by the operating pressure. With lower pressure, the gases were less compact and the particles moved faster. Therefore at 20 bar, the CGE was reduced to 61.2%. The temperature surrounding the injector at 20 bar exceeded the considered temperature limit, i.e., 1,470 K. Such high temperature may damage the injector. Moreover, the inlet velocity of the gas at 20 bar was increased by factor of 3.2 compared to the velocity at a pressure of 69 bar. As a result, the proposed feed ratio and design parameters (such as nozzle size) were not suitable for operation of the gasifier at 20 bar. It should be noted that the intent of performing this case study was to illustrate the capabilities of the ROM to predict such operational difficulties, not to optimize a gasifier design for various pressures. Moreover, inappropriate operating conditions for the given gasifier design also affected numerical convergence of the ROM. For example, the authors intended to examine the performance of the gasifier at pressure of 15 bar, i.e., the normal operating pressure of CanmetENERGY's pilot-scale gasifier, however low particle volume fractions (calculated based on the nozzle size and inlet flowrates) resulted in convergence difficulties.

Table 7-3. ROM results at different operating pressures

Capacity		3,000 TPD			1,500 TPD
Pressure (bar)		20	40	69	69
Conversion (%)		84.4	91.0	99.7	98.2
Cold gas efficiency (%)		61.2	71.2	83.7	79.3
Residence time of particles (s)		0.16	0.31	0.52	0.40
Near injector Max T (K)	Internal nozzle	1537	1327	1299	1178
	External nozzle	1601	1400	1364	1240

Based on the above results, the proposed ROM was able to predict reasonable results for the peak temperature, conversion, CGE and residence time of the gasifier at 69 bar. The required computation time of the ROM to achieve the results was approximately 17-30 minutes for each simulation (Core i7, 3.4 GHz with 8 GB of RAM).

7.4.2 Number of injectors

The GTI compact gasifier was designed to process 1,500 to 3,000 TPD of dried coal [87]. In this case study, the performance of a similar gasifier is compared at two fuel capacities: 1,500 (lower scale) and 3,000 (higher scale) TPD which requires 18 and 36 fuel injector nozzles, respectively [87]. The oxygen/fuel and steam/fuel ratios were kept constant for both gasifiers, with each nozzle capable of injecting 83.33 TPD of dried fuel to the gasification chamber at 69 bar. No design is available for the lower-scale gasifier. However, since the inlet flowrates for the lower-scale gasifier were decreased by 50%, the cross-sectional area of the large-scale gasifier was reduced by 50% and two layers of nozzles were considered. Accordingly, the reactor network was adjusted for two layers of nozzles. The geometry parameters for the two gasifiers are presented in Table 7.1.

Figure 7-6 presents the simulation results for the two gasifiers. As seen in Figure 7-6.a-b, the peak temperature in both gasifier were the same; however the outlet temperature of lower-scale gasifier was lesser by 25 K. This was due to higher heat-loss area per volume in the lower-scale gasifier. The molar fraction of CO was slightly higher in the higher-scale gasifier, however the molar fraction of H_2 was the same for both cases (Figure 7-6.c-d). Overall, the carbon conversion of the lower-scale gasifier was 98.4%, which was 1.3% less than the higher-scale gasifier, even though the particle residence time of lower-scale gasifier was slightly higher. Both of the gasifiers were able to maintain the near injector temperature less than the desired value of 1470 K. Based on the insights gained from this case study, the 50% reduction in

gasifier's cross-sectional area for lower-scale gasifier was reasonable to obtain high conversion and CGE. The proposed design can be passed to a more complex model such as CFD for further evaluation of the system.

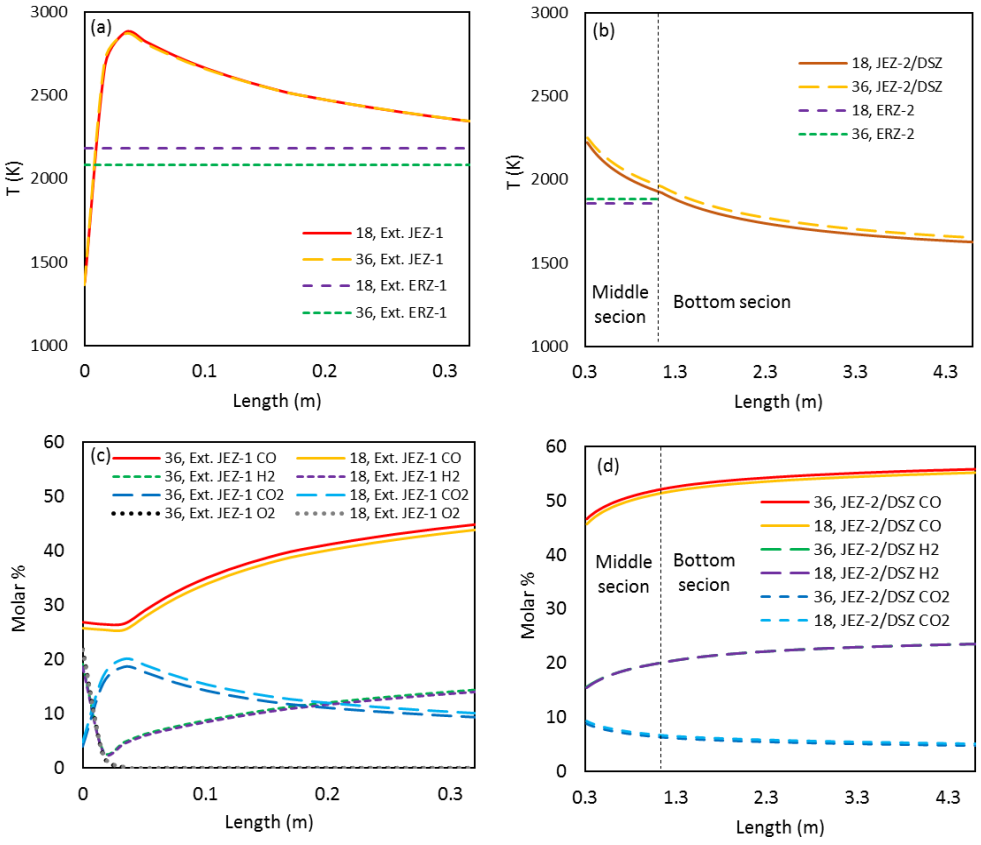

Figure 7- 6. Results of the ROM for gasifiers with 18 and 36 injector elements: a) Temperature profile in top section; b) Temperature profile in middle/bottom sections; c) Molar fraction profile in top section; d) Molar fraction profile in middle/bottom sections

7.4.3 Fuel distribution

To achieve high carbon conversion, uniform distribution of fuel is required within the elements of the injector to ensure that the solid particles are well mixed with steam and oxygen. As the residence time of the particles is short, poor mixing may create insufficient reaction environment and reduce the efficiency of the system. An initial design requirement for GTI's compact gasifier feed system was a relative standard deviation (RSD) of less than 2% for the fuel split non-uniformity [87]. However, testing of GTI's feed system indicated a RSD of 4.5% and 10% for 6 and 18 element injectors, respectively [94]. In addition to flow non-uniformity, plugging is another concern that may happen to fuel nozzles. In this case study, the

performance of a gasifier with 36 injector elements is investigated under flow non-uniformity and plugging conditions. In addition, the measurement of properties at the gasifier's outlet to indicate the presence of feed flow non-uniformity is discussed.

4.3.1 Flow non-uniformity in nozzles

The nominal flowrate of each fuel nozzle is 83.3 TPD, while they are designed to inject up to 100 TPD of dry coal to the gasifier. For the present case study, the maximum fuel flowrate within a nozzle is assumed to be 100 TPD. To assess the effect of flow non-uniformity, the flowrates through the nozzles of a given layer are assumed to be equal, however; flow non-uniformity between each layer of nozzles is considered through two scenarios. Note that flow non-uniformity was only considered for the fuel, while the oxygen/steam flowrates were at their nominal values. In the first scenario, the internal nozzles had higher flowrates compared to the external nozzles, while the middle nozzles operated with the nominal flowrate. Based on such a distribution of the flowrates, a maximum RSD of 20% was calculated. The results of this scenario are presented in Figure 7-7.

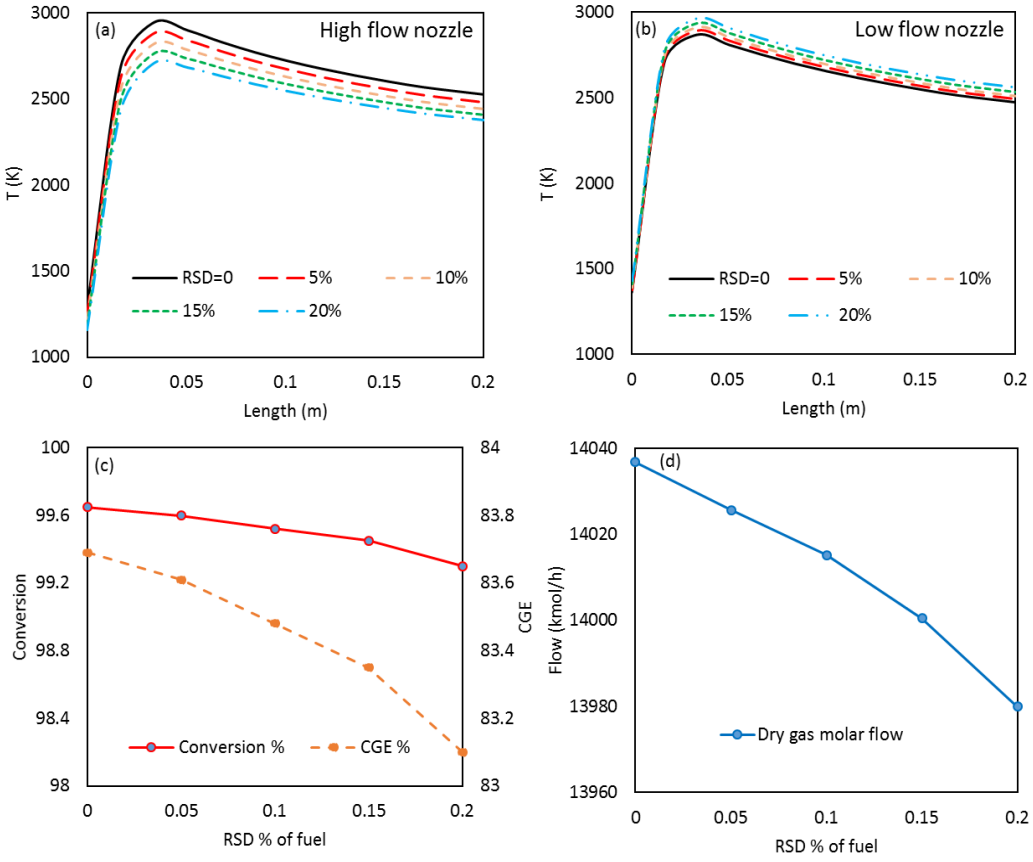

Figure 7-7. Simulation results with flow non-uniformity, Scenario 1: a) Temperature profile of the internal (high-flow) JEZ-1s; b) Temperature profiles of the external (low-flow) JEZ-1s; c) Carbon conversion with different relative standard deviations (RSDs) of fuel flow; d) Dry gas molar flow with different relative standard deviations (RSDs) of fuel flow

As shown in Figure 7-7.a, as the fuel flowrate increased in the internal nozzles, the oxygen/fuel ratio was reduced which led to a lower temperature profile. On the other hand, the temperature profile of low flow nozzles (Figure 7-7.b) was increased with greater feed flow non-uniformity. Since the number of external nozzles is higher than the number of internal nozzles, the effect of flow non-uniformity was more significant on the temperature profile of internal nozzles. Figure 7-7.c indicated that the carbon conversion and CGE of the gasifier were reduced by 0.4 and 0.5 percentage points, respectively with a feed flow RSD of 20%. The molar fraction of CO and H_2, and the temperature at the outlet did not change significantly with a feed flow RSD of 20% compared to the base case, i.e., 0.22 and 0.18 fraction points for CO and H_2, respectively, and 7 K for temperature. As a result, measurements of the temperature and composition may not indicate the presence of flow non-uniformity. Figure 7-7.d shows that the dry molar flowrate of gas exiting the reactor was decreased by 57 kmol/hr (15.8 mol/s) with a fuel feed RSD of 20% compared to

base case. Therefore, signals coming from flow measurement seems to be more efficient (in this scenario) to inform the operator of the presence of flow non-uniformity within the feed system.

The fuel distribution in the second scenario is the opposite of the first scenario, i.e., internal nozzles have a lower flowrate and external nozzles have a higher flowrate. Figure 7-8 demonstrates the trend of temperature profiles in higher/lower flowrate nozzles for feed flow RSDs of up to 20%.

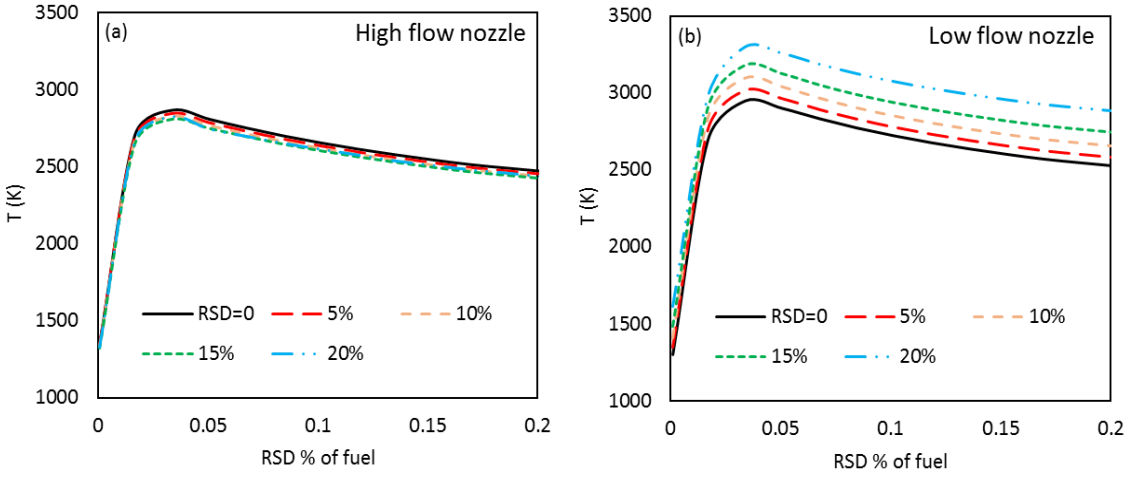

Figure 7- 8. Simulation results for flow non-uniformity, Scenario 2: a) Temperature profiles of external (high-flow) JEZ-1s; b) Temperature profiles of internal (low-flow) JEZ-1s

As shown in this figure, the peak temperature of internal JEZ-1s (which have lower fuel flowrates) increased significantly with higher feed flow RSDs. Accordingly, the peak temperature elevated by 350 K with a feed flow RSD of 20% compared to the base case. As the temperature increased within the internal JEZ-1s, there is less risk of wall damage in the gasifier. In this scenario, the carbon conversion increased to 100% for flow non-uniformity RSDs of 5% and greater. As a result, flow measurement will not indicate the presence of flow non-uniformity in this scenario. On the other hand, temperature measurement at the outlet seems to be more appropriate to detect the flow non-uniformity as the outlet temperature was increased by 40 K with a feed flow RSD of 20% compared to the base case.

Based on the above results, no significant changes were observed in the fuel conversion and CGE of the gasifier with flow non-uniformity RSD of up to 20%. It is expected that the effect of non-uniformity increases when the feed system has fewer nozzles. Furthermore, two potential risks could affect the

operation of the gasifier during flow non-uniformity, i.e., the temperatures surrounding the injector elements and the gasifier's wall could increase. Regarding temperature surrounding the injector elements, the maximum temperature surrounding the injector elements in the first scenario was 1,431 K which is lower than the considered constraint (1,470 K). Therefore, when the internal nozzles have higher flowrates, it is more likely that gasifier operation can continue. In the second scenario, the maximum temperature surrounding the injector was 1,480 K and 1,612 K for feed flow RSDs of 15% and 20%, respectively. Therefore, with feed flow RSDs higher than 15% (when the external nozzles have higher flowrates), injector elements may be damaged. Regarding temperature near the wall, since there are 16 nozzles in the external layer, the effect of non-uniformity on the temperature distribution of the JEZ-1s/ERZ-1s was minor and no significant risk was observed in both scenarios. However, if the RSD is not evenly distributed between the external nozzles, risk of wall damage will increase.

4.3.2 Plugging

Multi-element injectors have flow splitters to evenly distribute the feed flow. To assess the performance of the gasifier during plugging, failure of a splitter which provides flow to six nozzles is considered in the present case study. The six nozzles include one internal nozzle, two middle nozzles and three external nozzles. In this scenario it was assumed that the gasifier needs to convert the maximum amount of fuel to syngas. The maximum fuel flowrate which can be injected through a tube is 100 TPD. Therefore, during the failure of a splitter, the fuel flowrate of each injection tube was increased from 83.33 TPD to 100 TPD. Note that the plugging was only considered for the fuel injection nozzles, meaning the oxygen/steam impinging orifices of the failed nozzles were still in operation at their nominal values.

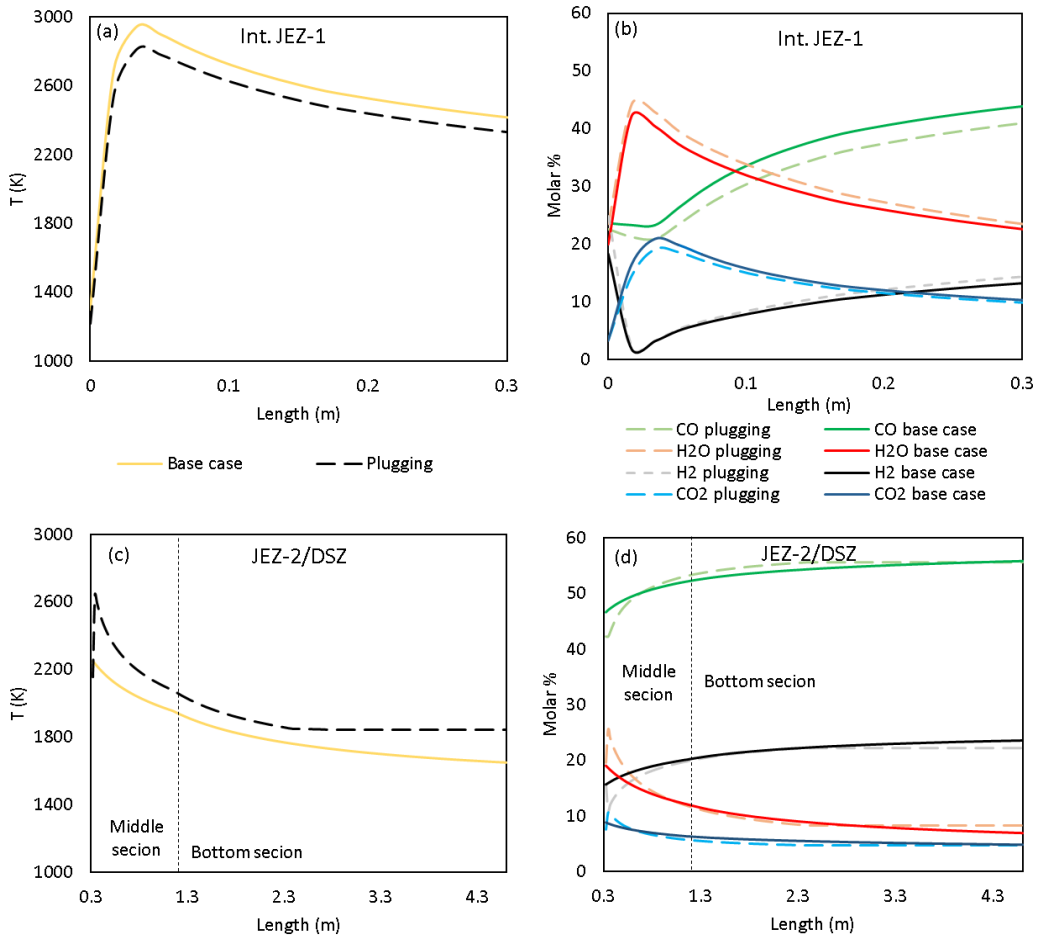

Figure 7- 9. Simulation results of the plugging scenario (data for non-plugged nozzles are shown): a) Temperature profiles in the top section; b) Molar percentage profiles in the top section; c) Temperature profiles in the middle/bottom sections; d) Molar percentage profiles in the middle/bottom sections

Figure 7-9 presents the simulation results of the plugging scenario. According to Figure 7-9.a, the temperature profiles of non-plugged nozzles at the top section of the gasifier were decreased, since the oxygen/fuel ratio was lower in those nozzles. Moreover, the molar fraction of CO was reduced (see Figure 7-9.b) compared to the base case, since less carbon was converted to syngas. On the other hand, the molar fraction of H_2 was slightly increased due to higher volatiles content coming to the system, even though less carbon was converted. Note that the results of middle and external nozzles followed the same trends as internal nozzles, and are not presented for brevity. One of the most important effects of plugging was observed in the middle section where the multi-phase flows coming from all nozzles merge together. At the beginning of this section, the unused oxygen (coming from the impinging orifices of the nozzles with dis-functioned fuel tubes) reacted with H_2, CO and carbon, resulting in a second peak temperature (Figure 7-

9.c). Accordingly, the rates of char gasification reactions were increased, which resulted in complete carbon conversion of fuel at 2.5 m from the gasifier's inlet. Therefore, the outlet molar fractions of gas species in the plugging scenario were almost the same as the base case (Figure 7-9.d). The CGE of the gasifier during plugging was 80.5%, i.e., 3.2 percentage points less than the CGE of the base case, while the dry gas flowrate was decreased by 3.5% compared to the base case. The peak temperature, now found in the middle section of the gasifier instead of the top section, reached 2,592 K. Depending on the physical forces inside the gasifier during plugging, this peak temperature is likely to be shifted towards the wall of gasifier, which could damage the refractory/membrane materials. If the corresponding oxygen/steam impinging orifices of the nozzles with plugged tubes do not inject any oxygen to the system, such a problem will not arise. However, according to the results obtained from the ROM, the conversion and CGE of the gasifier will be reduced to 74% and 62%, respectively, for such case if the oxygen/steam flowrates of the other nozzles stayed at their nominal values. Note that increasing the oxygen/steam flowrates of the non-plugged nozzles (which their injection tube is not plugged) may result in a high peak temperature which could damage the injectors and wall of the gasifier.

7.5. Sensitivity analysis

The proposed reactor network was based on assumptions that could not be verified. To improve the accuracy of the ROM, it is useful to identify the most influential parameters affecting the results. In this section, univariate sensitivity analyses of the following reactor network parameters are considered: the recirculation ratio (RR) of the internal, middle and external nozzles, and the length of the JEZ-1s and JEZ-2. To perform the sensitivity analyses, the input parameters were individually varied by up to ±20% relative to their base-case values.

Figure 7-10 presents the sensitivity of the carbon conversion, particle residence time, peak temperature and outlet temperature to changes to reactor network parameters. As seen in this figure, the selected ROM outputs were not significantly affected by the recirculation ratio of the nozzles. Since multiple feed nozzles reduced the recirculation flow in the system, the recirculation ratio is less impactful on the results compared to a gasifier with a single-element feed injector [43], [78]. As seen in Figure 7-10.b, the considered parameters did not significantly increase the average residence time of particles. Moreover, the length of JEZs is a critical parameter in the reactor network. In order to maintain a fixed

length of the gasifier, the length of the DSZ was adjusted based on the changes in the lengths of the JEZ-1s and JEZ-2. Increasing the length of JEZs has two opposite effects on the temperature profile of the system: 1) it reduces the heat loss through DSZ and therefore contributes to higher temperature, and 2) it reduces the average temperature of recirculation gases and therefore contributes to lower temperature. In the case of JEZ-1s' length, the second effect was dominant since the internal/middle zones were not affected by the heat loss, therefore lower carbon conversion was obtained (Figure 7-10.a) when the JEZ-1s' length was increased. However in the case of JEZ-2's length, the first effect was dominant which contributed to higher temperature and therefore more carbon conversion.

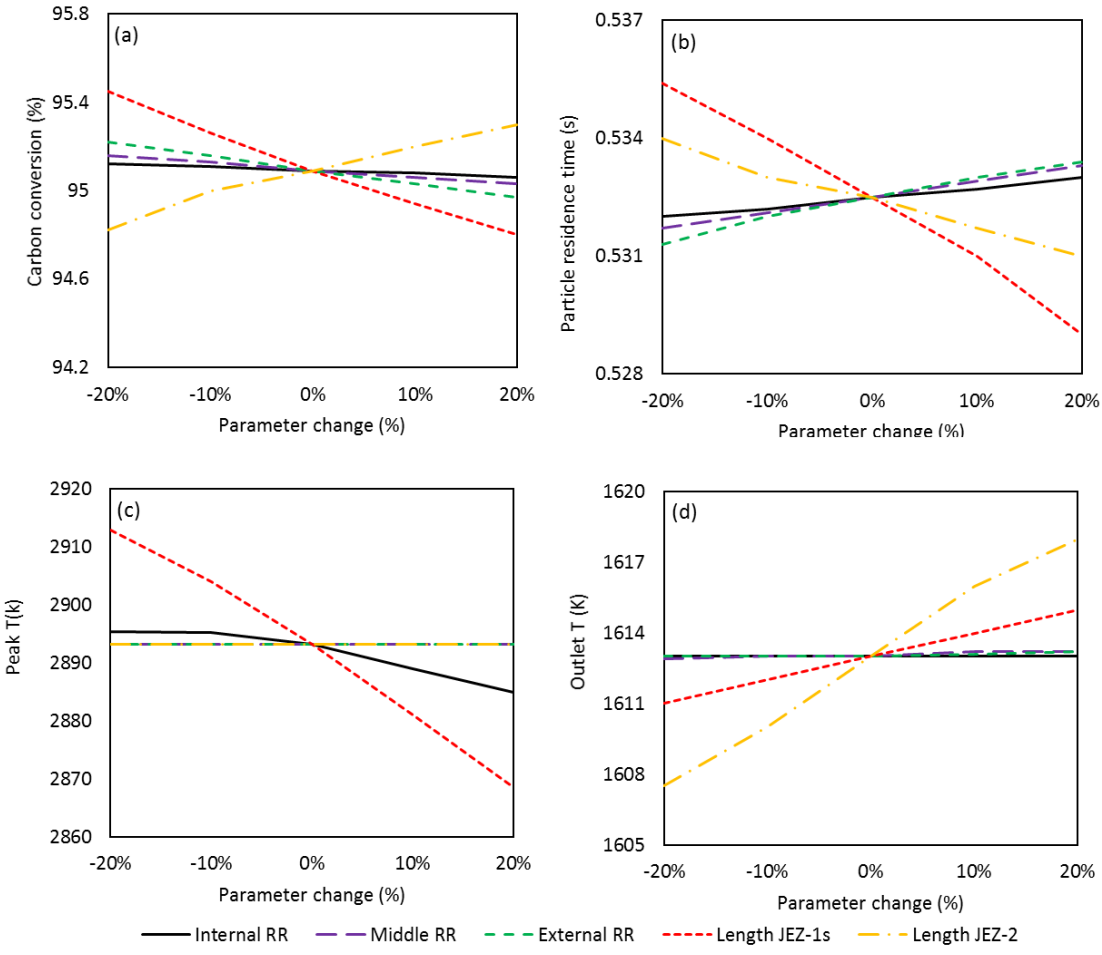

Figure 7-10. Results of sensitivity analyses on the reactor network parameters

In addition to determining the most influential model parameters, sensitivity analyses are useful to investigate the suitability of design and operation parameters on the performance of the system. In the

present work, the sensitivity to the oxygen, steam and nitrogen flowrates, the inlet temperature of oxidizing agents, the percentage of volatiles in the fuel, the thickness of nozzle layers, and the size of the fuel nozzles were considered. The effects of these design and operation parameters are presented in Figure 7-11 and Table 7-4. As seen in Figure 7-11.a, the oxygen/fuel ratio has the greatest impact on the carbon conversion. Moreover, the nitrogen/fuel ratio is the only parameter which was inversely proportional to the carbon conversion since a higher nitrogen/fuel ratio reduces the partial pressure of reacting species, and therefore the rate of gasification reactions. The residence time of particles was mostly affected by the nitrogen/fuel ratio and diameter of the feed nozzle (see Figure 7-11.b). Based on the results presented in Figure 7-11.c-d, in addition to the oxygen/fuel ratio, the inlet temperature of oxidizing agents and steam/fuel ratio were the other major parameters that affected the peak and outlet temperatures.

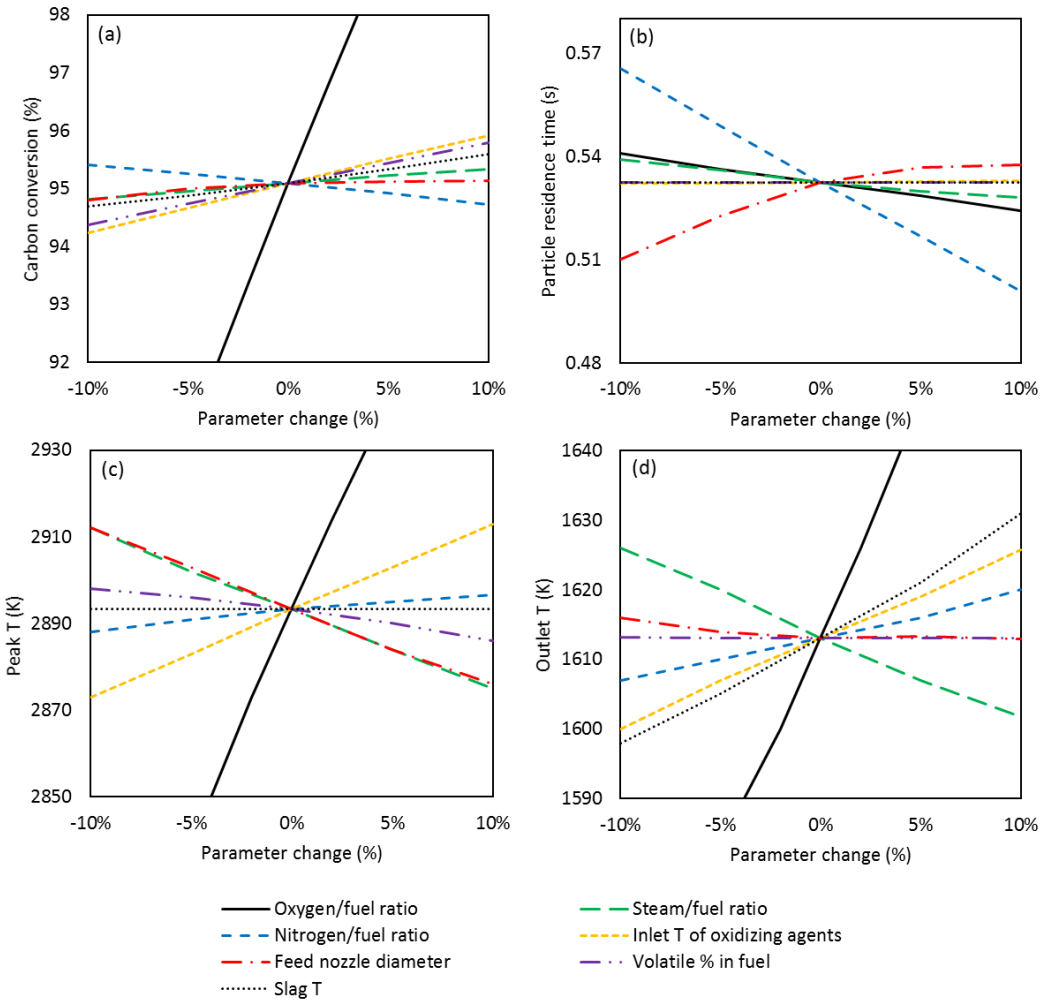

Figure 7-11. Sensitivity to design and operation parameters

One of the critical assumptions made in the ROM was the temperature of flowing slag. The sensitivity analysis presented in Figure 7-11, showed that increasing the slag temperature contributed to higher temperature profile since less heat was lost through the wall. Consequently higher temperature profile increased the carbon conversion. Since the changes in conversion and temperature were not significant, assuming a temperature which corresponds to slag viscosity of less than 25 pa.s is reasonable. The thickness of nozzle layers (λs) affect several reactor network parameters, i.e., four jet angles and the diameter of the JEZ-2. Therefore, univariate sensitivity analyses were not performed on the thicknesses. Instead, the effect of these parameters was examined in the three scenarios presented in Table 7-4.

Table 7-4. Results of sensitivity analysis for the thickness of nozzle layers

	Case 1	Case 2	Case 3
Internal nozzle, λ_1	0.3	0.35	0.4
Middle nozzle, λ_2	0.25	0.25	0.25
External nozzle, λ_3	0.3	0.25	0.2
Wall-space, λ_4	0.15	0.15	0.15
Carbon conversion %	95.1	94.9	94.7
Particle residence time (s)	0.53	0.52	0.50
Outlet T (K)	1613	1617	1622

As shown in this table, as the value of λ_1 increased, the value of λ_3 was reduced by the same amount, while λ_2 and the wall space thickness (λ_4) were kept constant. Such variation of parameters resulted in three scenarios which can be analyzed through the size of jet angles (θs). In case 1, the jet angle of the JEZ-1s increased in the radial domain, i.e., $\theta_{internal} < \theta_{middle} < \theta_{external}$. In case 2, the three nozzle layers have equivalent jet angles. In case 3, the jet angle of the JEZ-1s reduced in the radial domain. According to the results presented in Table 7-4, as the jet angle of nozzles in the external layer was decreased, the velocity of gases was increased which resulted in a lower particle residence time and carbon conversion. Note that since there are more nozzles in the external layer, λ_3 is more impactful on the results compared to λ_1. Overall, the results of the sensitivity analysis indicated the major outputs of the gasifier model did not change significantly by variation of λs.

7.6 Chapter summary

This chapter has evaluated the performance of a commercial-scale gasifier with a multi-element injector feed system by means of using a ROM. A reactor network consisting of 75 reactors is developed in the ROM to capture the streamlines of the multi-phase flow inside the gasifier with 36 feed nozzles. The results indicate that the ROM is able to predict the values reported for the carbon conversion and cold gas efficiency (CGE) at 69 bar in a reasonably low computational time, i.e. 17-30 min. The ROM was further used to evaluate the gasifier at lower pressures. According to the results, the proposed design parameters (nozzle size and inlet flowrates) were not suitable at 20 bar due to the high temperature surrounding the injectors, as well as high velocity of inlet gases which may increase the risk of damaging the injector and refractory. Furthermore, the adaptability of the gasifier was tested during two case-studies with non-uniform distribution of fuel among the nozzles. According to the scenarios, no significant change was observed in the carbon conversion when flow non-uniformity is considered among the nozzles. In addition, the measurements of flow and temperature may detect the presence of flow non-uniformity in the inlet, while the measurement of composition could not detect such effect. In the second scenario, plugging of six fuel injection tube was considered through failure of one of the flow splitters. The results illustrated that if the impinging orifices of the plugged nozzle continue to inject oxygen, a second peak temperature will be formed in the middle section of the gasifier which may increase the risk of damaging the wall. Nevertheless, if no oxygen is injected through the impinging orifices of the plugged nozzles, the fuel conversion and CGE will be reduced to 74% and 62%, respectively. Furthermore, the sensitivity analysis showed the suitability of the assumptions (such as geometric parameters and slag temperature) made in the ROM. It also revealed that oxygen/fuel ratio and the lengths of JEZ-1 and JEZ-2, are the most influential design and model parameters.

Chapter 8
Conclusions and Recommendations

The focus of this research is on the reduced order modeling of short-residence time entrained-flow gasifiers. The conservation equations and sub-models required to simulate gasification process is implemented inside a reactor network which captures the multi-phase flow characteristics of the system. The concluding remarks of this research is presented next, followed by recommendation statements for future work.

8.1 Applicability of reduced order models for gasification process

Reduced order models (ROMs) have been used to develop gasifier models over the past decade. The validation of the ROMs was often performed for a single operating condition. Therefore, the suitability of these models in predicting the gasifier's output in a range of operating condition was not investigated. Chapter 4 presents a comparison between the results of the ROM against the results of CFD simulation and experimental tests. It is determined that a systematically developed ROM with a fixed framework can predict the gasifier's behaviour over a wide range of operating condition, when the streamlines of multi-phase flow is captured via the reactor network. It was shown that the highest deviation between the results of the ROM and experimental tests was observed when the steam flowrate was set to zero. Such change in inlet flowrate results in a different pattern of streamline compare to the base-case condition used to develop the reactor network, and therefore reduces the accuracy of the ROM.

The average CPU time required by the ROM to compute the steady-state results for a single operating condition was approximately 4-5 minutes. Conducting the same simulation using CFD would require approximately 10 days; while the cost to perform an experimental test is estimated at $30,000 USD [12]. The computational benefits of the ROM makes possible to perform simulations and modeling analyses which are computationally expensive or even prohibitive for more other modelling approaches such as CFD. Uncertainty quantification with adequate number of samples was one of the analyses which was not available in the literature. In Chapter 5, this gap is addressed by using Monte Carlo sampling to assess the variability of gasifier's outputs in presence of uncertainty in the feed and model parameters. To increase the prediction capabilities of a ROM beyond its nominal operating condition, model parameters need to be updated by making changes in the inlet flowrates. The parameter estimation work presented in Chapter 5 is

an attempt towards this direction by proposing a semi-empirical correlation for the ROM's most influential parameter, i.e. recirculation ratio. The proposed correlation for recirculation ratio improved the predictions by 0.2-1.4 percentage points and 10-60 K in predicting carbon conversion and outlet temperature, respectively; compared to Thring and Newby method.

8.2 Assessment of short-residence time gasifiers

Development of a state-of-the-art gasification technology known as short-residence time gasifier is a significant contribution to make gasification-based power plants competitive with combustors. The initial assessments of this gasifier indicated substantial improvements in terms of system's availability and costs of electricity generation. The research performed in this study investigated the performance of the system in pilot-scale (1 TPD) and commercial-scale (1,500-3,000 TPD) through the development of ROMs. The ROMs considered various features of the gasification process such as fuel drying and devolatilization, chemical reactions, viscous fluid-solid interactions, pollutant formation, heat loss and slag formation. Prior to the assessment of gasifier's performance, the proposed ROM for a pilot-scale gasifier was validated as shown in Chapter 4. The steady-state results match the gas molar fraction and flowrate, temperature distribution, conversion and pollutant formation obtained from the experimental tests, CFD simulation and respective calculations. Accordingly, the pilot-scale gasifier is able to convert more than 99 % of the fuel's carbon in residence time of 0.4 seconds.

The validated model was then used to investigate the performance of the gasifier in several scenarios. In Chapter 5, it is determined that the recirculation ratio and oxygen flowrate have a significant effect on the gasifier's outputs (carbon conversion, H_2/CO ratio and temperature) compared to model geometry and kinetic parameters. Moreover, uncertainty quantification demonstrates significant variability in the conversion, peak temperature and steam percentage in the syngas; while the dry syngas composition does not seem to be significantly affected by the uncertainty in feed and model parameters. The results in Chapter 6 provides insight regarding the transient response and availability of the pilot-scale gasifier. In a load-following cycle with a fixed ratio of feed flowrates, the cold gas efficiency of the gasifier during reduced load increases by 4.6 percentage points. Moreover, the dynamic simulation of the gasifier in co-firing of 60:40 blended feed of petroleum coke and coal showed that the cold gas efficiency increase by 3.3 percentage points compared to firing of petroleum coke. To maintain the slag viscosity below 25 Pa.s and

avoid slag blockage in both cases, a minimum CaO mass percentage of 21% for load-following (respect to pet coke) and 20% for co-firing (respect to 60:40 blend of pet coke/coal) is required. In addition, the slag response demonstrated that the risk of slag blockage may be higher during load increments; thus, the system's temperature and fluxant flowrate must be accurately monitored during such events.

Chapter 7 evaluated the performance of a commercial-scale gasifier based on the design of short-residence time gasifier proposed by Gas Technology Institute. The results of the model for operating pressure of 69 bar meet the values of residence-time, conversion and cold gas efficiency reported for this gasifier. Although this data is not sufficient to validate the ROM, the defined set of process constraint for the system make sure that the results presented are within feasible limits. The ROM was further used to assess the effect of operating pressure on the performance of gasifier. Accordingly, the carbon conversion was reduced from 99.7% to 84.4%, when the operating pressure was decreased from 69 to 20 bar, due to a reduction in the particle's residence time. Furthermore, the gasifier was examined in scenarios with non-uniform distribution of fuel among the injection tubes. Based on the results, when the non-uniformity is evenly divided between the nozzles of each layer, no significant changes are observed in carbon conversion. However, the nozzle with lower fuel flowrate results in high temperature within certain sections of the gasifier which could create operational difficulties by damaging the injector and refractory layer. Also, noteworthy from Chapter 7 is the performance of gasifier during the plugging of nozzles. The results indicated that when during the failure of one of the splitters, no fuel is injected via 6 nozzles. If the corresponding oxygen/steam orifices of these nozzles continue to operate, a second peak temperature is created near the gasifier's wall which could damage the refractory. If these orifices do not inject any oxygen to the gasification chamber, the conversion is reduced to 74%.

8.3 Recommendations

The applicability of the ROM can be further increased by addition of other sub-models. Particularly, a sub-model for devolatization rate which increases the accuracy of the model in predicting the location of peak temperature. Moreover, it is recommended to assess the performance of gasifier in the presence of rest of the IGCC's unit operations. Low residence time of the gasifier and the interaction between process units may create critical scenarios that could affect the operability and controllability of

the IGCC plant. The easiest way to perform such analyses is through an automation link between the ROM and process simulators.

One of the key challenges faced by a gasifier is the identification of the sensors needed to maintain the dynamic operation within specifications. Due to the harsh conditions at which this process operates, standard measurement devices such as thermocouples cannot be used to monitor the temperature inside the gasifier unit. Hence, observability studies represent an attractive analysis that can be applied to identify suitable sensor locations for these systems under various scenarios. To date, studies that address this issue by considering the gasifier's dynamics are lacking in the literature.

There are three key variables that must be controlled in an entrained-flow gasifiers: syngas mass flowrate, H_2/CO ratio and temperature. The proposed control schemes are decentralized multi-loop controllers and model-based controllers are lacking in the literature. The implementation of model predictive controllers (MPC) for this gasification systems can provide substantial improvements in terms of close-loop settling time and integral squared error.

The proposed reactor network for the ROM of commercial-scale gasifier is based on heuristics and CFD simulation of a combustor. In addition, limited data was available to validate the model. As a result, the proposed ROM is based on assumptions that are not known with certainty. Although a sensitivity analysis was performed to examine the suitability of assumptions and identify the most important parameters that are required to obtain from higher order model. Performing CFD simulation of the commercial-scale gasifier would lead to a more accurate ROM that can be extended to dynamic mode to assess the transient response of the system. The recommended strategy is to use the results of the ROM as initial guesses for CFD simulation to reduced computational time and convergence difficulties of the CFD.

Letters of Copyright Permission

ELSEVIER LICENSE
TERMS AND CONDITIONS

This Agreement between Hossein Sahraei (You) and Elsevier (Elsevier) consists of your license details and the terms and conditions provided by Elsevier and Copyright Clearance Center.

License Number	3977150860211
License date	Oct 27, 2016
Licensed Content Publisher	Elsevier
Licensed Content Publication	Fuel
Licensed Content Title	Reduced order modeling of a short-residence time gasifier
Licensed Content Author	M. Hossein Sahraei,Marc A. Duchesne,Robert Yandon,Adrian Majeski,Robin W. Hughes,Luis A. Ricardez-Sandoval
Licensed Content Date	1 December 2015
Licensed Content Volume	161
Licensed Content Issue	n/a
Licensed Content Pages	11
Type of Use	reuse in a thesis/dissertation
Portion	full article
Format	both print and electronic
Are you the author of this Elsevier article?	Yes
Will you be translating?	No
Order reference number	
Title of your thesis/dissertation	Dynamic Reduced Order Modeling & Scale-up of an Entrained Flow Gasifier
Expected completion date	Oct 2016
Estimated size (number of pages)	110
Elsevier VAT number	GB 494 6272 12
Requestor Location	Waterloo, Canada
Customer VAT ID	ALHossein
Total	0.00 USD

ELSEVIER LICENSE
TERMS AND CONDITIONS

This Agreement between Hossein Sahraei (You) and Elsevier (Elsevier) consists of your license details and the terms and conditions provided by Elsevier and Copyright Clearance Center.

License Number	3977151441833
License date	Oct 27, 2016
Licensed Content Publisher	Elsevier
Licensed Content Publication	Fuel
Licensed Content Title	A survey on current advanced IGCC power plant technologies, sensors and control systems
Licensed Content Author	M. Hossein Sahraei,David McCalden,Robin Hughes,L.A. Ricardez-Sandoval
Licensed Content Date	1 December 2014
Licensed Content Volume	137
Licensed Content Issue	n/a
Licensed Content Pages	15
Type of Use	reuse in a thesis/dissertation
Portion	full article
Format	both print and electronic
Are you the author of this Elsevier article?	Yes
Will you be translating?	No
Order reference number	
Title of your thesis/dissertation	Dynamic Reduced Order Modeling & Scale-up of an Entrained Flow Gasifier
Expected completion date	Oct 2016
Estimated size (number of pages)	110
Elsevier VAT number	GB 494 6272 12
Requestor Location	Waterloo, Canada
Customer VAT ID	ALHossein
Total	0.00 USD

ELSEVIER LICENSE
TERMS AND CONDITIONS

This Agreement between Hossein Sahraei (You) and Elsevier (Elsevier) consists of your license details and the terms and conditions provided by Elsevier and Copyright Clearance Center.

License Number	3977160250681
License date	Oct 27, 2016
Licensed Content Publisher	Elsevier
Licensed Content Publication	International Journal of Greenhouse Gas Control
Licensed Content Title	Controllability and optimal scheduling of a CO2 capture plant using model predictive control
Licensed Content Author	M. Hossein Sahraei,L.A. Ricardez-Sandoval
Licensed Content Date	November 2014
Licensed Content Volume	30
Licensed Content Issue	n/a
Licensed Content Pages	14
Type of Use	reuse in a thesis/dissertation
Portion	full article
Format	both print and electronic
Are you the author of this Elsevier article?	Yes
Will you be translating?	No
Order reference number	
Title of your thesis/dissertation	Dynamic Reduced Order Modeling & Scale-up of an Entrained Flow Gasifier
Expected completion date	Oct 2016
Estimated size (number of pages)	110
Elsevier VAT number	GB 494 6272 12
Requestor Location	Waterloo, Canada
Customer VAT ID	ALHossein
Total	0.00 USD

References

[1] Exxon Mobil Corporation. The Outlook for Energy: A View to 2040. 2014, *<http://exxonmobil.com/energyoutlook> [cited 16.06.2015].*

[2] Banks B, Bigland-Pritchard M. SaskPower's carbon capture project: What risk? What reward?. Saskatchewan power corporation's carbon capture project, 2015.

[3] Buchan B, Cao C. Coalfired generation: proven and developing technologies. Office of market monitoring and strategic analysis florida public service commission; 2004..

[4] Rubin ES. The outlook for power plant CO2 capture. Erice International Seminar. 2009 <http://repository.cmu.edu/epp> [cited 16.06.2015].

[5] Christou C, Hadjipaschalis I, Poullikkas A. Assessment of integrated gasification combined cycle technology competitiveness. Renew Sust Energy Rev 2007;12:2459-2471.

[6] Monaghan RFD. Dynamic Reduced Order Modeling of Entrained Flow Gasifiers. PhD dissertation, MIT, 2010.

[7] Sahraei MH, McCalden D, Hughes R, Ricardez-Sandoval LA. A survey on current advanced IGCC power plant technologies, sensors and control systems. Fuel 2014;137:245–259.

[8] Pedersen LS, Breithauptb P, Dam-Johansen K, Weber R. Residence Time Distibutions in Confined Swirling Flames. Combust Sci Technol 1997;127(1):251-273.

[9] Talley P. Capitalizing on the emerging coal gasification market. Aspen Technology Webinar; 2007..

[10] Sahraei MH, Duchesne MA, Yandon R, Majeski A, Hughes RW, Ricardez-Sandoval LA. Reduced order modeling of a short-residence time gasifier. Fuel 2015;161:222-232.

[11] Sahraei MH, Yandon R, Duchesne MA, Hughes RW, Ricardez-Sandoval LA. Parametric analysis using a reactor network model for petroleum coke gasification. Energy Fuels 2015;29:7681-7688..

[12] Sahraei MH, Duchesne MA, Hughes RW, Ricardez-Sandoval LA. Experimental assessment, model validation and uncertainty quantification of a pilot-scale gasifier. Ind Eng Che Res 2016;55:6961-6970.

[13] Sahraei MH, Duchesne MA, Hughes RW, Ricardez-Sandoval LA. Dynamic reduced order modeling of an entrained-flow slagging gasifier using a new recirculation ratio correlation (Submitted for publication).

[14] Sahraei MH, Duchesne MA, Hughes RW, Ricardez-Sandoval LA. Reduced order modeling of a commercial-scale gasifier using multi-element injector feed system (Submitted for publication).

[15] Dairyland power cooporative. IGCC technology overview and Genoa site feasibility, 2008.

[16] Higman C., Reliability of IGCC power plants., *International freiberg conference on IGCC technologies, Freiberg (Sachsen); 2005. .*

[17] Monaghan RFD, Ghoniem AF. A dynamic reduced order model for simulating entrained flow gasifiers: Part I: Model development and description. Fuel 2012;91:61-80.

[18] Fusselman SP, Sprouse KM, Darby AK, Tennant J, Stiegel GJ. Pratt & Whitney rocketdyne/DOE advanced single-stage gasification development program. National Energy Technology Laboratory; 2007.

[19] IGCC state-of-the-art report. Department of Mech & Structural Eng & Material Science, University of Stavanger, Norway; 2010..

[20] Qi H, Zhao B. Cleaner combustion and sustainable world. Springer; 2013..

[21] Machowska H, Knapik E. Coal gasification using clean coal technology. CHEMIK 2011;65(10):946–953..

[22] National Energy Technology Laboratory, US department of energy., *<http://www.netl.doe.gov/research/coal/energy-systems/gasification/gasifipedia/ge> [cited 03.02.2014]..*

[23] Sprouse K, Widman F, Darby A. , Conceptual Design of an Ultra-Dense Phase Injector and Feed System., *Pratt & Whitney Rocketdyne Inc; 2006..*

[24] Lee S. Handbook of alternative fuel technology. Taylor & Francis Group; 2007.

[25] Hydrocarbon upgrading gasification program. Alberta innovates energy and environment solutions; 2011..

[26] Higman C,Van Der Burgt M. Gasification. Gulf Professional Publishing; 2008..

[27] Bell DA, Towler BF, Fan M. Coal gasification and its applications. Elsevier; 2011..

[28] Morehead H. Siemens gasification and IGCC update. Gasification technologies seminar, Washington; 2008..

[29] Visagie JP. Generic gasifier modelling: evaluation model by gasifier type. Master's dissertation, University of Pretoria, South Africa; 2007.

[30] Darby A. Gasification and dry solids pump status, Gasification technology council conference, Colorado, 2013.

[31] Chui EH, Majeski AJ, Lu DY, Hughes R, Gao H, McCalden DJ, Anthony EJ, Simulation of entrained flow coal gasification, *Energy Procedia 2009;1:503–509.*

[32] Xue Q, Fox RO, Multi-fluid CFD modeling of biomass gasification in polydisperse fluidized-bed gasifiers., *Powder Technology ,* 2014;254;:187–198.

[33] Slezak A, Kuhlman JM, Shadle LJ, Spenik J, Shi S. CFD simulation of entrained-flow coal gasification: Coal particle density/sizefraction effects. Powder Technology 2010;203:98-108.

[34] Vascellari M, Roberts DG, Hla SS, Harris DJ, Hasse C, From laboratory-scale experiments to industrial-scale CFD simulations of entrained flow coal gasification., *Fuel 2015.*

[35] Yong SZ, Ghoneim A, Modeling the slag layer in solid fuel gasification and combustion – Two-way coupling with CFD., *Fuel 2012;97:457-466.*

[36] Spliethoff H, Tremel A, Gasification kinetics during entrained flow gasification – Part III: Modelling and optimisation of entrained flow gasifiers, *Fuel 2013;107:170-182.*

[37] Aggarwal M, Balaji S, Ydstie BE. Invariant based modeling and control of multi-phase reactor systems.J Process Control 2011;21:1390–1406.

[38] Tan W, Lou G, Liang L. Partially decentralized control for ALSTOM gasifier. ISA Trans. 2011;50:397-408.

[39] Robinson PJ, Luyben WL. Simple dynamic gasifier model that runs in Aspen dynamics. Ind Eng Chem Res 2008;47:7784-7789.

[40] Gazzani M, Manzolini G, Macchi E, Ghoniem AF. Reduced order modeling of the Shell–Prenflo entrained flow gasifier. Fuel 2013:104;822–837.

[41] Lee HH, Lee JC, Joo YJ, Ohb M, Lee CH. Dynamic modeling of Shell entrained flow gasifier in an integrated gasification combined cycle process. Applied Energy 2014;131:425-440.

[42] Lee H, Lee H. Multiloop control strategies for a dry feeding gasifier in the integrated gasification combined cycle. Ind Eng Chem Res 2015;54:11113-11125.

[43] Monaghan RFD, Ghoniem AF. A dynamic reduced order model for simulating entrained flow gasifiers. Part II: Model validation and sensitivity analysis. Fuel 2012;94:280–297.

[44] Monaghan RFD, Ghoniem AF., Simulation of a commercial-scale entrained flow gasifier using a dynamic reduced order model., *Energy Fuels 2012;26:1089−1106.* .

[45] Gazzani M, Manzolini G, Macchi E, Ghoniem AF, Reduced order modeling of the Shell–Prenflo entrained flow gasifier, *Fuel ,* 2013:104;822–837.

[46] Yang Z, Wang Z, Wu Y, Zheng Li Z, Ni W, Use of a reactor network model in the design and operation of a new type of membrane wall entrained flow gasifier, *Energy Fuel,* 2013;27:6322−6332.

[47] Yang Z, Wang Z, Wu Y, Lu J, Li Z, Ni W. Dynamic model for an oxygen-staged slagging entrained flow gasifier. Energy Fuels 2011;25:3646-3656.

[48] Yang Z, Xue y, Wu Y, Wang Z, Li Z, Ni W. Modeling of an oxygen-staged membrane wall gasifier: effects ofsecondary oxygen. Chem Eng Process: Process Intensif 2013;74:131-141.

[49] Kong X, Weimin Zhong W, Du W, Qian F. Compartment modeling of coal gasification in an entrained flow gasifier: A study on the influence of operating conditions. Energy Convers Manage, 2014;82:202–211.

[50] Li C, Dai Z, Sun Z, Wang F. Modeling of an opposed multiburner gasifier with a reduced-order model. Ind Eng Chem Res 2013;52:5825-5834.

[51] Canmetenergy research service, [Cited 12.01.2015] <http://www.nrcan.gc.ca/sites/www.nrcan.gc.ca/files/canmetenergy/files/pubs/Gasification_eng.pdf>.

[52] Duchesne MA, Hughes RW, Lub DY, McCalden DJ, Anthony EJ, Macchi A, Fate of inorganic matter in entrained-flow slagging gasifiers: Pilot plant testing, *Fuel,* 2014;127:219–227.

[53] Duchesne MA, Hughes RW, Partitioning of inorganic elements in pilot-scale and demonstration-scale entrained-flow gasifiers, *Fuel,* 2014;127:219–227.

[54] Cousins A, Hughes RW, McCalden DJ, Lu DY, Anthony EJ, Waste classification of slag generated in a pilot-scale entrained-flow gasifier, *CCGP,* 2012;4:37-44.

[55] Kus F, Duchesne MA, Champagne S, Hughes RW, Lu D, Mehrani P, Macchi A, Dense-phase pneumatic conveying of pulverized fuel for gasification, *64th Canadian Chemical Engineering Conference, NIAGARA FALLS, ON 2014.*

[56] Stockman L, Turnbull D, Kretzmann S, Petroleum coke: the coal hiding in the tar sands, *Oil Change International,* 2013.

[57] Murthy BN, Sawarkar AN, Deshmukh NA, Mathew T, Joshi JB, Petroleum coke gasification: A review, *The Canadian Journal of Chemical Engineering ,* 2014;92:441–468.

[58] Beer JM, Chigier NA. Combustion Aerodynamics. London: Applied Science Publishers, Ltd; 1972.

[59] Niksa S, Kerstein AR, Flashchain theory for rapid coal devolatilization kinetics. 1. Formulation., Energy Fuels 1991;5:647–65.

[60] Solomon PR, Hamblen DG, Carangelo RM, Serio MA, Deshpande GV, General model of coal devolatilization., Energy Fuels 1988;2:405–22.

[61] Merrick D. Mathematical models of the thermal decomposition of coal: 1. The evolution of volatile matter. Fuel 1983;62:534-9.

[62] Lee HH, Lee JC, Joo YJ, Ohb M, Lee CH, Dynamic modeling of Shell entrained flow gasifier in an integrated gasification combined cycle process, *Applied Energy,* 2014;131:425–440.

[63] Arastoopour H, Gidaspow D, Vertical Pneumatic Conveying Using Four Hydrodynamic Models, *Ind Eng Chem Fundamentals 1970;18 (2):123-130.*

[64] White FM. Fluid Mechanics. Second Edition. New York (NY): McGraw-Hill; 1986..

[65] Mills AF. Heat Transfer, Second Edition. Upper Saddle River (NJ): Prentice Hall Inc.; 1999.

[66] Incropera FP, DeWitt DP, Fundamentals of Heat and Mass Transfe, Fifth Edition. New York (NY): John Wiley & Sons, Inc.; 2002..

[67] Ilyushechkin YA, Hla SS, Roberts DG, Kinaev NN. The effect of solids and phase compositions on viscosity behaviour and TCV of slags from Australian bituminous coals. J Non Cryst Solids 2011;357:893-902.

[68] Varga S, Frandsen FJ, Dam-Johansen K. Rheological properties of high-temperature melts of coal ashes and other silicates. Prog Energy Combust Sci 2001;27:237-429.

[69] Seggiani M. Modelling and simulation of time varying slag flow in a Prenflo entrained-flow gasifier. Fuel 1998;77(14):1611-1621.

[70] Sahraei MH, Farhadi F, Boozarjomehry RB, Analysis and interaction of exergy, environmental and economic in multi-objective optimization of BTX process based on evolutionary algorithm. Energy 2013;5:147-156.

[71] Li Z, Ierapetritou MG. Robust optimization for process scheduling under uncertainty. Ind Eng Chem Res 2008;47:4148-4157..

[72] Nease J, Adams II TA. Application of rolling horizon optimization to an integrated solid-oxide fuel cell and compressed air energy storage plant for zero-emissions peaking power under uncertainty. Comput Chem Eng 2014;65:203-219..

[73] Mehta S, Ricardez-Sandoval LA. Integration of design and control of dynamic systems under uncertainty: a new back-off approach. Ind Eng Chem Res 2016;55:485-498.

[74] Gel A, Chaudhari K, Turton R, Nicoletti P. Application of uncertainty quantification methods for coal devolatilization kinetics in gasifier modeling. Powder Technol 2014;265:66-75.

[75] Shastri Y, Diwekar U. Stochastic Modeling for Uncertainty Analysis and Multiobjective Optimization of IGCC System with Single-Stage Coal Gasification. Ind Eng Chem Res 2011;50:4879.

[76] Curran ET. An investigation of flame stability in a coaxial dump combustor. PhD dissertation, Air Force Institute of Technology 1979..

[77] Beer J, Chigier N. Combustion aerodynamics; Applied Science Publishers: London, 1972.

[78] Sahraei MH, Yandon R, Duchesne MA, Hughes RW, Ricardez-Sandoval LA. Parametric analysis using a reactor network model for petroleum coke gasification. Energy Fuels 2015;29:7681-7688.

[79] Henderson C. Increasing the flexibility of coal-fired power plants. IEA Clean Coal Centre 2014.

[80] Sahraei MH, Ricardez-Sandoval LA. Controllability and optimal scheduling of a CO2 capture plant using model predictive control. Int J Greenh Gas Control 2014;30:58-71.

[81] He Z, Sahraei MH, Ricardez-Sandoval LA. Flexible operation and simultaneous scheduling and control of a CO2 capture plant using model predictive control. Int J of Greenh Gas Control 2016;48:300-311.

[82] Kus F. Solid Fuel Pneumatic Conveying and its Injection Geometry in a Pressurized Entrained Flow Gasifier. MASc Thesis. University of Ottawa 2016.

[83] Myles P, Herron S. Impact of load following on power plant cost and performance: literature review and industry interviews. National Energy Technology Laboratory 2012.

[84] Superior Technical Ceramics. <http://www.ceramics.net/services/materials-engineering-expertise/mullite> [cited 18/05/2016].

[85] Comparison of pratt and whitney Rocketdyne IGCC and commercial IGCC performance, National Energy Technology Laboratory, 2006.

[86] Sprouse KM, Farhangi S, Matthews DR, Compact high efficiency gasifier, US patent no.: US 7547423B2, 2009.

[87] Sprouse k, Widman F, Darby A, Conceptual design of an ultra-dense phase injector and feed system, Pratt & Whitney Rocketdyne, Inc. 2006.

[88] Sprouse KM, Farhangi S, Matthews DR. Gasifier injector, European patent application no.: EP 1717295A1, 2006.

[89] Darby A. Pilot plant gasifier final test report hydrocarbon upgrading gasification program, Alberta energy research institute grant, 2011.

[90] Sahraei MH, Duchesne MA, Hughes RW, Ricardez-Sandoval LA. Dynamic reduced order modeling of an entrained-flow slagging gasifier using a new recirculation ratio correlation, Fuel (submitted).

[91] lyushechkin Y, Hla SS, Roberts DG, Kinaev NN. The effect of solids and phase compositions on viscosity behaviour and TCV of slags from Australian bituminous coals. J. Non. Cryst. Solids 2011;357:893-902..

[92] Higman C, van der Burgt M. Gasification, first ed., Elsevier Science USA, 2003.

[93] Hartung J, Darby A. Pratt & Whitney Rocketdyne (PWR) compact gasification system, Gasification technologies council conference, Washington, 2006.

[94] Sprouse KM, Matthews DR, Weber GF. Dry coal feed system and multi-element injector test report, Pratt & Whitney Rocketdyne, Inc. 2008.

[95] Jones WP Lindstedt RP, Global reaction schemes for hydrocarbon combustion., *Combustion and Flame 1988;73:233-249.*

[96] Kovacik GJ, Knill KJ, Numerical simulation of coal gasification reactors. American Society of Mechanical Engineers, Fuels and Combustion Technologies Division., *International joint power generation conference, Phoenix AZ.1994;101-106.*

[97] K.M. Sprouse, S, Farhangi, D.R. Matthews Gasifier injector, European patent application no.: EP 1717295A1, 2006.

[98] K.C. Mills, J.M Rhine, The measurement and estimation of the physical properties of slags formed during coal gasification: 2. Properties relevant to heat transfer, Fuel 68 (1989) 904.

Appendix A: Supplementary information for CFD simulation and experimental design

The description of CFD models and experimental design of petroleum-coke gasification tests performed by CanmetENERGY is presented in this section.

A.1 CFD simulation of CanmetENERGY's gasifier

A CFD model describing the behaviour of CanmetENERGY's entrained-flow gasifier was developed using the ANSYS® CFX® software (Version 16). The model geometry consists of a half-section of the gasifier and includes the sampling probe, a portion of the nozzle, and ends at the entrance to the quench section. Conjugate heat transfer is modeled through the innermost refractory layer and select parts of the nozzle. Beyond the inner layer, an estimated heat transfer coefficient is applied to represent the remaining insulating layers of the gasifier. The same coefficients have been implemented in the ROM to model heat transfer through the walls. This estimate takes into account temperature-dependent material properties, and includes radiation from the steel shell to the surroundings. The model uses the Reynolds-average Navier-Stokes with k-ε turbulence closure, the discrete transfer radiation model, composition-dependent gas properties, and Lagrangian particle tracking. The volatiles have been modeled in the CFD model as a single component, and the rate of devolatilization is modeled using a first-order Arrhenius rate equation. The char oxidation and gasification reactions are the same as those used in the ROM. For simplicity and numerical stability, the reaction of char with H_2 has been omitted and the inhibition of the char gasification reactions by CO and H_2 has been neglected.

The formation of NO and SO_2 is based only on the composition of char in order to balance the mass of the elements; gas phase reactions associated with these compounds were not implemented in the CFD model because of computational limitations. As the amount of sulfur is 6.1% of the dry-ash-free fuel, the difference in energy changes to form H_2S may explain some differences between CFD and ROM. The stoichiometry of the volatile oxidation reaction was obtained from PC Coal Lab®, but no reaction rate was available for

this matter. Thus, it is assumed that the volatile reaction was limited by turbulent mixing, using the Eddy Dissipation Model (EDM).

A.2 CFD simulation of combustor with multi-element injector

A preliminary study of high pressure combustion of slurry coal with multiple injection nozzles (with a design similar to GTI's compact gasifier) was conducted at CanmetENERGY to investigate particle residence time, coal reaction rates and the equipment size using the commercial CFD code ANSYS CFX 14.5. A full 3D simulation of cylindrical combustion vessel with a 1 m inner diameter and 10 m in length was performed. The computational grid used to represent the geometry was divided into an upper region (top 0.5 m) with 2,000,000 unstructured elements with a higher concentration of elements near the nozzles, and a lower region (remaining 9.5 m) with 200,000 structured elements. The two zones were coupled using a general grid interface able to conserve interface flux. Conservation equations of mass, momentum and energy was solved simultaneously. To simulate the combustion process, the CFD model implements sub-models for $k-\varepsilon$ closure, discrete transfer radiation model, Lagrangian particles tracking, heterogeneous and homogenous reactions, and coal devolatilization. Volatiles, once released from the coal, were modelled as a single component gas, however its oxidation produces six species: CO, CO_2, H_2, H_2O, NO and SO_2. Moreover, due to the high injected volume of slurry water, the excess oxygen and the available heat, the water gas shift reaction and H_2 oxidation were included in the model. Note that, the homogeneous gas phase reactions were modelled using a minimum rate approach, either eddy dissipation or finite rate chemistry.

Burner face cooling was achieved by specifying 20% of the total gas flow to be introduced through this face. This cooling flow rate together with the vessel diameter produced insufficient velocity leading to flow instability which will be further discussed in a later section. All injection boundary sites were modelled as walls with local mass sources instead of inlet boundaries to prevent the Lagrangian particles from exiting through these faces. The side walls were assumed to be covered by running slag therefore a set wall temperature of 1800 K was implemented. A constant wall emissivity of 0.83 was also implemented (0.83 is obtained for temperatures between 1070 and 1800 K).

A.3 Experimental design of petroleum coke gasification

Before testing, the gasifier was pre-heated overnight using natural gas and oxygen-enriched air. Once the desired temperature was attained, natural gas and oxygen injection were terminated. The reactor was then pressurized by injecting nitrogen. At the desired pressure, nitrogen injection was ceased. Fuel flow was then established, followed by a progressive ramping up of oxygen injection to obtain the desired temperature. Oxygen flow was adjusted to maintain a constant temperature at thermocouple TC4. Automation and data collection for the pilot gasifier facility was accomplished using an ABB Freelance 2000 distributed control system. The temperature profile within the gasifier was monitored using type B thermocouples protruding past the hot face and into the reaction chamber by ~5 mm. The locations of the thermocouples are indicated on Figure 6-4 as TC1 through TC4. A nitrogen-cooled gas sampling probe was inserted into the gasifier at the same elevation as TC4. Syngas was extracted through the probe to provide the syngas composition inside the reactor. Dried gas analysis was performed via gas chromatography capable of measuring CO, CO_2, CH_4, H_2, O_2, COS, H_2S and N_2 once every two minutes. On-line infrared carbon monoxide and carbon dioxide analyzers were used to validate syngas compositions generated by the gas chromatograph. Dry syngas flow exiting the reactor was estimated by performing a nitrogen mass balance based on the nitrogen injection flowrate and the dry syngas composition. Note that the nitrogen injection flowrate includes conveying gas and nitrogen in the petroleum coke. The dry syngas composition was obtained by gas chromatography with the dried syngas. Carbon conversion was estimated by performing a carbon mass balance with the injected fuel and dry syngas. The operating conditions of the experimental tests are presented in Table 2. As shown in this Table, these tests were conducted at different operating conditions, i.e., injected fuel flowrates vary from 41.2 to 52.3 kg/h, injected steam flowrates vary from 0 to 21.8 kg/h, and injected oxygen flowrates vary between 28.4 and 37.2 kg/h. A high operating pressure is often desired for these systems as it decreases the volume of the gasifier and reduces capital costs (larger reactor volume is not required) for a given throughput. Hence, the set of experimental tests was performed at 16 bar.

Appendix B

Supplementary information for physical properties

Gas phase

The physical properties of the gases have been calculated by using a thermodynamic package of a commercial process simulator, i.e. Soave-Redlich-Kwong (SRK) equation of state. Note that the simulator uses linear approximation to estimate the physical properties beyond the operating ranges of SRK.

Solid phase

The PC Coal Lab software has been used to calculate the physical properties of petroleum coke.

Liquid phase

The slag density has been calculated based on the ash's composition and partial molar volumes of the components. The specific heat capacity and conductivity of slag were taken from Seggiani [69]. Moreover, the model used by Seggiani was adopted for slag viscosity [69]. The results of this model were validated with experimental measurement of slag viscosity for petroleum coke.